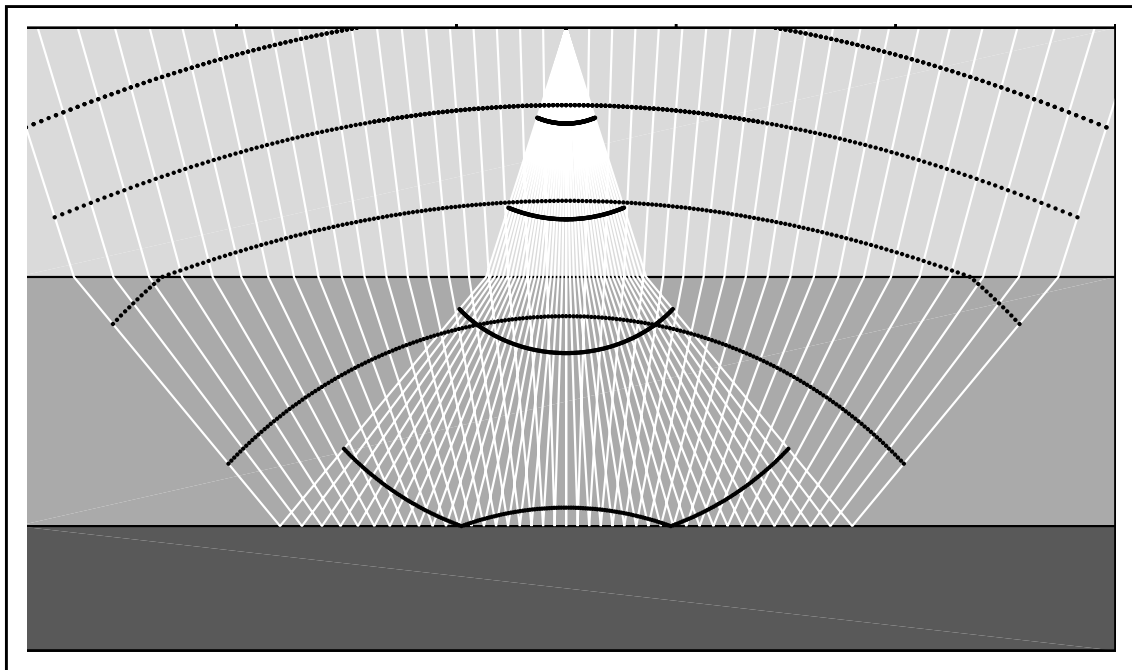


— Course Notes —

# Seismic Wavefields in Layered Isotropic Media

Ilya Tsvankin



**S**

Samizdat  
Press

— Course Notes —

# Seismic Wavefields in Layered Isotropic Media

Ilya Tsvankin

Center for Wave Phenomena  
Colorado School of Mines  
Golden, CO 80401  
ilya@dix.mines.edu

**S**

Samizdat Press, Golden • White River Junction

Published by the Samizdat Press

Center for Wave Phenomena  
Department of Geophysics  
Colorado School of Mines  
Golden, Colorado 80401



and  
New England Research  
76 Olcott Drive  
White River Junction, Vermont 05001



©Samizdat Press, 1995  
Release 1.0, October 30, 1995



Samizdat Press publications are available via FTP  
from [landau.mines.edu](http://landau.mines.edu) or 138.67.12.78.  
Permission is given to freely copy these documents.

# Contents

<b>1</b>	<b>Some basic facts from the theory of elasticity</b>	<b>1</b>
<b>2</b>	<b>Plane waves in 1-D isotropic media</b>	<b>5</b>
2.1	Homogeneous and evanescent plane waves . . . . .	5
2.2	Equations of motion for P-SV and SH-waves . . . . .	7
2.3	Boundary conditions . . . . .	8
2.4	Reflection and transmission at a fluid/fluid boundary . . . . .	10
2.5	Reflection at a free surface . . . . .	13
2.6	Reflection and transmission at a solid/solid boundary . . . . .	17
2.7	Plane waves in stratified media . . . . .	20
<b>3</b>	<b>Point-source radiation in fluid models</b>	<b>25</b>
3.1	Plane-wave decomposition of point-source radiation . . . . .	25
3.2	Integral solutions for scattering at a plane boundary . . . . .	30
3.3	Stationary-phase method for reflected wavefields . . . . .	30
3.3.1	Zero-order approximation of the method of stationary phase . . . . .	31
3.3.2	First-order approximation of SPM . . . . .	35
3.4	The method of steepest descent for the reflected wavefield . . . . .	38
3.4.1	Reflection from a low-velocity medium . . . . .	39
3.4.2	Reflection from a high-velocity medium: the head wave . . . . .	47
3.5	Properties of the head wave . . . . .	51
3.6	Asymptotic analysis of the transmitted wavefield . . . . .	59
3.6.1	Geometrical transmitted wave . . . . .	59
3.6.2	Inhomogeneous transmitted waves . . . . .	61
3.6.3	Transmission into a low-velocity medium: nongeometrical waves . . . . .	63
3.7	Numerical analysis of nongeometrical waves . . . . .	70
<b>4</b>	<b>Point-source radiation in elastic media</b>	<b>77</b>
4.1	Reflection/transmission of a spherical wave at a solid/solid boundary . . . . .	77
4.2	Analysis of the reflected/transmitted wavefield . . . . .	81
4.3	Nongeometrical waves in elastic media . . . . .	83
4.4	Wave phenomena due to additional terms of the ray series . . . . .	88
4.5	Comparison of modeling methods for stratified isotropic media . . . . .	93
4.6	Acknowledgments . . . . .	97

# Chapter 1

## Some basic facts from the theory of elasticity

The notes cover the second semester of a two-semester seismological course that the author teaches in the Department of Geophysics at the Colorado School of Mines. The first semester is devoted to the basics of elasticity, theory of seismic sources and plane-wave propagation in 1-D isotropic media. I begin with reviewing some relevant results from the first part of the course in Chapters 1 and 2.

We will be dealing with linear-elastic solids, and this means that each component of the stress tensor  $\tau_{ij}$  represents a linear combination of the components of the strain tensor  $e_{kl}$ :

$$\tau_{ij} = c_{ijkl}e_{kl}, \quad (1.0.1)$$

summation over repeated indices is implied. This is a modern version of Hooke's law that assumes a generally anisotropic linear-elastic medium. To describe nonlinear-elastic solids, we would have to add quadratic terms to the right-hand side of equation (1.0.1).

Due to the symmetry in the stress and strain tensors, we can switch the indices  $i$  and  $j$ ,  $k$  and  $l$  in the stiffness tensor  $c_{ijkl}$ :

$$c_{ijkl} = c_{jikl}$$

$$c_{ijkl} = c_{ijlk}$$

Also, from thermodynamic considerations

$$c_{ijkl} = c_{klij}$$

Due to these symmetries, we have “just” 21 independent elastic constants in the tensor  $c_{ijkl}$ .

For the strain tensor we have

$$e_{kl} = \frac{1}{2} \left( \frac{\partial u_k}{\partial x_l} + \frac{\partial u_l}{\partial x_k} \right). \quad (1.0.2)$$

Therefore, Hooke's law can be rewritten through the displacement components as

$$\tau_{ij} = c_{ijkl} \frac{\partial u_k}{\partial x_l}. \quad (1.0.3)$$

The equation of motion (wave equation) is given by (Aki and Richards, 1980)

$$\rho \frac{\partial^2 u_i}{\partial t^2} - \frac{\partial \tau_{ij}}{\partial x_j} = f_i,$$

where  $\vec{f}$  is the body force per unit volume.

Substituting Hooke's law (equation [1.0.3]) and assuming that the stiffness coefficients are either constant or vary slowly in space, we obtain the basic wave equation for the displacement vector:

$$\rho \frac{\partial^2 u_i}{\partial t^2} - c_{ijkl} \frac{\partial^2 u_k}{\partial x_j \partial x_l} = f_i. \quad (1.0.4)$$

If the medium is isotropic,  $c_{ijkl}$  becomes a fourth-order isotropic tensor:

$$c_{ijkl} = \lambda \delta_{ij} \delta_{kl} + \mu (\delta_{ik} \delta_{jl} + \delta_{il} \delta_{jk}), \quad (1.0.5)$$

$\lambda$  and  $\mu$  are the so-called Lamé constants.

Equations (1.0.4) and (1.0.5) make it possible to find the wave equation for homogeneous isotropic media:

$$\rho \frac{\partial^2 u_i}{\partial t^2} - (\lambda + \mu) \frac{\partial^2 u_j}{\partial x_i \partial x_j} - \mu \frac{\partial^2 u_i}{\partial x_j^2} = f_i. \quad (1.0.6)$$

At this point, we will introduce potentials in order to split this relatively complicated equation into two more simple equations for the two potential functions. Note that this technique does not work for a more complex wave equation (1.0.4) in anisotropic media. In this case, the wave equation can be solved directly by decomposing the displacement vector into Fourier integrals.

But for now,

$$\vec{u} = \nabla \phi + \nabla \times \vec{\psi} = \text{grad } \phi + \text{curl } \vec{\psi}, \quad (1.0.7)$$

where  $\phi$  and  $\vec{\psi}$  are the scalar and vector potentials, respectively. We will also require that

$$\text{div } \vec{\psi} = \nabla \cdot \vec{\psi} = 0. \quad (1.0.8)$$

Substituting equation (1.0.7) into the wave equation (1.0.6) and assuming that there are no sources ( $\vec{f} = 0$ ), we get two wave equations for the potentials:

$$\frac{\partial^2 \phi}{\partial t^2} = c^2 \nabla^2 \phi, \quad (1.0.9)$$

$$\frac{\partial^2 \vec{\psi}}{\partial t^2} = b^2 \nabla^2 \vec{\psi}, \quad (1.0.10)$$

$c = \sqrt{(\lambda + 2\mu)/\rho}$  is the P-wave velocity,  $b = \sqrt{\mu/\rho}$  is the S-wave velocity.

Aki and Richards (1980) show that we can always find potentials that satisfy equations (1.0.7)–(1.0.10). Therefore, instead of dealing with the original wave equation for the displacement vector, we can use the above equations for the potentials, which are much simpler. We should keep in mind that for solutions of equations (1.0.9) and (1.0.10) to form a solution of the wave equation (1.0.6), the vector potential must have a zero divergence (1.0.8). We will see the advantages of the potentials a little bit later, when we will consider wave propagation in 1-D isotropic elastic media.





# Chapter 2

## Plane waves in 1-D isotropic media

### 2.1 Homogeneous and evanescent plane waves

We have decomposed the wave equation into two equations for the potentials  $\phi$  and  $\vec{\psi}$ . The simplest solution of this equations, as we know, is a harmonic (steady-state) plane wave. Let us try a solution for the scalar potential in the form

$$\phi_{pl} = A_0 e^{i\omega(m_j x_j - t)}. \quad (2.1.1)$$

Clearly, the surfaces of constant phase  $m_j x_j - t = \text{const}$  are planes perpendicular to the slowness vector  $\vec{m} = \vec{k}/\omega$ ,  $\vec{k}$  is the wave vector.

Substituting the plane wave into the wave equation (1.0.9), we obtain

$$|\vec{m}|^2 = 1/c^2. \quad (2.1.2)$$

Now it is clear why we call  $\vec{m}$  the slowness vector. Introducing the unit vector  $\vec{n}$  perpendicular to the wavefront, we can now represent the plane wave as

$$\phi_{pl} = A_0 e^{i\omega(n_j x_j / c - t)}. \quad (2.1.3)$$

A plane wave is the simplest and most natural solution of the wave equation to be used in seismology. Also, it can be shown (Aki and Richards, 1980) that if we solve the wave equation by the method of separation of variables, we get a harmonic plane wave.

Here we assume that the components of the slowness and wave vectors are real. In this case we get a straightforward graphical representation of plane waves: they have a constant amplitude and a plane wavefront propagating in the direction determined by the slowness (or wave) vector.

However, we will see that in some cases we will have to deal with plane waves which have one or more complex components of the slowness vector. These waves are called inhomogeneous or evanescent. Two most important problems where the concept of inhomogeneous waves plays the central role are post-critical reflection-transmission of plane and spherical waves and decomposition of point-source radiation into plane waves.

If the components of the slowness vector are allowed to be complex, then

$$\phi_{pl} = A_0 e^{i\omega(m_j^r x_j - t) - \omega m_j^{im} x_j}. \quad (2.1.4)$$

This equation means that now the planes of constant phase are different from the planes of constant amplitude ( $m_j^{im} x_j = \text{const}$ ). We can show that the two planes are orthogonal to each other. Substituting the plane wave from equation (2.1.4 or 2.1.1) into the wave equation (1.0.9), we find

$$\Sigma m_j^2 = \Sigma (m_j^r + i m_j^{im})^2 = \frac{1}{c^2}. \quad (2.1.5)$$

If there is no attenuation in the medium, the P-wave velocity  $c$  is real, and the imaginary part of the left side of the equation should be zero:

$$\Sigma m_j^r m_j^{im} = 0, \quad (2.1.6)$$

and the two planes are perpendicular to each other. This is no longer the case when the medium is attenuative, and  $c$  is complex.

The next question to be answered is about the velocity of inhomogeneous waves. The time dependence is present only in the term  $i\omega(m_j^r x_j - t)$ , so the velocity is determined by the the absolute value of  $\vec{m}^r$ . From equation (2.1.5) we find

$$|\vec{m}^r|^2 = \frac{1}{c^2} + |\vec{m}^{im}|^2. \quad (2.1.7)$$

Therefore, the slowness of inhomogeneous plane waves is always larger than the slowness of conventional homogeneous waves, and the velocity of inhomogeneous waves would always be slower than the medium velocity  $c$ . This simple fact explains the velocity structure of two large classes of waves: surface waves and the so-called nongeometrical waves; we will talk about both classes in more detail later in the course.

Although I have not talked about boundary conditions yet, I would like to show how we can get inhomogeneous waves during reflection/transmission at a boundary. According to Snell's law, the projection of the slowness vector on the boundary is the same for all reflected/transmitted waves. If a homogeneous wave is incident in the plane  $[x_1, x_3]$  on a horizontal boundary  $x_3 = \text{const}$ , then

$$m_1 = \frac{\sin \theta}{V} = \text{const}, \quad (2.1.8)$$

$\theta$  is the incidence angle. The reflection/refraction angles  $\theta_r$  are given by

$$\sin \theta_r = \sin \theta \frac{V_r}{V}. \quad (2.1.9)$$

During reflection/transmission for  $\frac{V_r}{V} > 1$  it can happen that  $\sin \theta_r > 1$ , and the slowness vector becomes complex making the reflected/transmitted wave inhomogeneous. Conversely, inhomogeneous plane waves can be transformed into homogeneous ones if a wave is transmitted into a medium with lower velocity. It is noteworthy that inhomogeneous plane waves is an important component of wavefields not only in attenuative but also in purely elastic media.

I have used the P-wave potential in the above discussion. Evidently, inhomogeneous (evanescent) shear waves can be treated exactly the same way.

It is important to remember that inhomogeneous waves are unbounded and cannot be considered in full space. In the following we will use inhomogeneous waves in layered media or in halfspaces making sure that they decay away from the interfaces.

## 2.2 Equations of motion for P-SV and SH-waves

It looks like we do not gain much by using potentials instead of the displacement vector: while the equations became somewhat simpler, we have to handle four functions (the scalar potential plus 3 components of the vector potential) instead of the 3 components of the displacement vector. However, normally it is not necessary to introduce all 3 components of  $\vec{\psi}$ ; also, another advantage of potentials is that we can separate P and S-waves.

Let us consider 1-D isotropic media consisting of a stack of plane layers; the layers may in general be either liquid or solid. We will be looking at plane waves propagating in the vertical plane  $[x_1, x_3]$  perpendicular to the layering. Later in the text, we will refer to  $x_1$  as  $x$  and to  $x_3$  as  $z$ . It does not affect the generality of our treatment because the choice of the vertical plane is arbitrary. If we have a plane wave with an arbitrary direction of the wavefront normal, we just choose the vertical plane containing this normal. For P-waves, the polarization or displacement vector will always lie in the vertical plane. S-waves should be decomposed into the SV-waves polarized in the vertical plane and SH-waves polarized horizontally.

An important point here is that the displacements in the vertical plane and in the transverse horizontal direction are completely decoupled. Due to the symmetry of the model, a motion in the vertical plane cannot excite anything in the transverse horizontal direction and vice versa. This is actually true for any model in which the vertical plane is a plane of symmetry, not just for 1-D isotropic media.

If  $y(x_2)$ -direction is perpendicular to the vertical propagation plane, the wave equation (1.0.6) may be rewritten for horizontally polarized waves  $u_2(x, z)$  as

$$\frac{\partial^2 u_2}{\partial t^2} = b^2 \left( \frac{\partial^2 u_2}{\partial x^2} + \frac{\partial^2 u_2}{\partial z^2} \right). \quad (2.2.1)$$

This is exactly the acoustic wave equation for the pressure, the only difference being that the coefficient here is the shear-wave velocity  $b$ . We will see that the boundary conditions are also completely analogous to the acoustic case.

P- and SV-waves polarized in the vertical plane will be described by the potentials we introduced earlier. Since the motion is confined to the vertical plane, only one component of the vector potential is needed. The displacement due to the vector potential is given by  $\vec{u}^s = \text{curl} \vec{\psi}$ :

$$u_x^s = \frac{\partial \psi_z}{\partial y} - \frac{\partial \psi_y}{\partial z},$$

$$u_y^s = \frac{\partial \psi_x}{\partial z} - \frac{\partial \psi_z}{\partial x} = 0,$$

$$u_z^s = \frac{\partial \psi_y}{\partial x} - \frac{\partial \psi_x}{\partial y}.$$

Since  $u_y^s = 0$ , the only component of  $\vec{\psi}$  we need is  $\psi_y$  (we denote it just as  $\psi$ ). Note that since  $\frac{\partial \psi_y}{\partial y} = \frac{\partial \psi}{\partial y} = 0$ , the divergence of the vector potential is zero, as it should be.

The potentials satisfy the wave equations (1.0.9,1.0.10) given above; however, now we consider just one component of the vector potential, and both potentials are independent of  $y$ :

$$\frac{\partial^2 \phi}{\partial t^2} = c^2 \left( \frac{\partial^2 \phi}{\partial x^2} + \frac{\partial^2 \phi}{\partial z^2} \right), \quad (2.2.2)$$

$$\frac{\partial^2 \psi}{\partial t^2} = b^2 \left( \frac{\partial^2 \psi}{\partial x^2} + \frac{\partial^2 \psi}{\partial z^2} \right). \quad (2.2.3)$$

The displacement due to both potentials (1.0.7) in the vertical plane is

$$u_x = \frac{\partial \phi}{\partial x} - \frac{\partial \psi}{\partial z}, \quad (2.2.4)$$

$$u_z = \frac{\partial \phi}{\partial z} + \frac{\partial \psi}{\partial x}. \quad (2.2.5)$$

It is easy to show that the plane-wave vector potential produces a plane shear wave, while a scalar potential brings about a longitudinal (P-wave) motion.

## 2.3 Boundary conditions

To solve wave propagation problems in layered elastic media, we need to define the conditions at the interfaces between the layers. The type of boundary conditions has extremely important consequences in reflection-transmission problems. For example, the very existence of surface waves is dependent on the type of the interface. The Stoneley wave always exists at a fluid/solid boundary but almost never - at a solid/solid boundary. It turns out that the velocity and density ratios necessary for the Stoneley wave to propagate along a solid/solid boundary are seldom encountered in realistic Earth models.

The so-called kinematic conditions pertain to the displacement vector. For two solids in welded contact all three components of the displacement vector should be continuous. The stresses across a solid/solid boundary should also be continuous; the conditions on the stress tensor are usually called "dynamic." Therefore, at a solid/solid interface  $z = \text{const}$  we get the following boundary conditions:

$$[u_x] = [u_y] = [u_z] = 0, \quad (2.3.1)$$

$$[\tau_{zx}] = [\tau_{zy}] = [\tau_{zz}] = 0. \quad (2.3.2)$$

The brackets denote the difference in the stresses or displacements above and below the boundary.

The stress components can be expressed through displacement:

$$\tau_{zx} = \mu \left( \frac{\partial u_x}{\partial z} + \frac{\partial u_z}{\partial x} \right), \quad (2.3.3)$$

$$\tau_{zy} = \mu \frac{\partial u_y}{\partial z}, \quad (2.3.4)$$

$$\tau_{zz} = \lambda \left( \frac{\partial u_x}{\partial x} + \frac{\partial u_z}{\partial z} \right) + 2\mu \frac{\partial u_z}{\partial z}. \quad (2.3.5)$$

Equations (2.3.1-2.3.5) are quite general. Now let us rewrite them for the P-SV potentials describing wave propagation in the  $[x,z]$  plane and the SH-wave polarized in the  $y$  direction.

For the SH-wave, the situation is very simple: the only non-zero stress component is  $\tau_{zy}$ , and the boundary conditions are just

$$[u_y] = 0, \quad (2.3.6)$$

and

$$[\tau_{zy}] = \left[ \mu \frac{\partial u_y}{\partial z} \right] = 0. \quad (2.3.7)$$

Therefore, SH-wave propagation in 1-D elastic media is completely equivalent to the propagation of acoustic (pressure) waves in 1-D fluid media. The wave equation and boundary conditions for  $u_y$  are identical to those for the acoustic pressure, if we replace  $\mu$  by  $1/\rho$  and the velocity  $b$  by  $c$  (Brekhovskikh, 1980).

Expressing the stresses (2.3.3-2.3.5) through the potentials of P-SV waves using equations (2.2.4,2.2.5) yields

$$\phi : (\tau_{zx}, \tau_{zy}, \tau_{zz}) = \left( 2\mu \frac{\partial^2 \phi}{\partial x \partial z}, 0, \lambda \nabla^2 \phi + 2\mu \frac{\partial^2 \phi}{\partial z^2} \right), \quad (2.3.8)$$

$$\psi : (\tau_{zx}, \tau_{zy}, \tau_{zz}) = \left( \mu \left( \frac{\partial^2 \psi}{\partial x^2} - \frac{\partial^2 \psi}{\partial z^2} \right), 0, 2\mu \frac{\partial^2 \psi}{\partial z \partial x} \right). \quad (2.3.9)$$

The full set of the boundary conditions for P-SV waves at a solid/solid boundary now can be written as

$$[u_x] = \left[ \frac{\partial \phi}{\partial x} - \frac{\partial \psi}{\partial z} \right] = 0, \quad (2.3.10)$$

$$[u_z] = \left[ \frac{\partial \phi}{\partial z} + \frac{\partial \psi}{\partial x} \right] = 0, \quad (2.3.11)$$

$$[\tau_{zx}] = \left[ 2\mu \frac{\partial^2 \phi}{\partial x \partial z} + \mu \left( \frac{\partial^2 \psi}{\partial x^2} - \frac{\partial^2 \psi}{\partial z^2} \right) \right] = 0, \quad (2.3.12)$$

$$[\tau_{zz}] = [\lambda \nabla^2 \phi + 2\mu \left( \frac{\partial^2 \phi}{\partial z^2} + \frac{\partial^2 \psi}{\partial z \partial x} \right)] = 0. \quad (2.3.13)$$

If we replace one of the solids by a fluid, the normal displacement (perpendicular to the boundary) should remain continuous, while the tangential displacement (parallel to the boundary) becomes discontinuous because the fluid may slip along the solid. Thus, for P-SV waves at a fluid/solid boundary we can use only the last three conditions (2.3.11-2.3.13). Evidently, SV and SH-waves cannot propagate in the fluid at all.

For a fluid/fluid boundary ( $\mu = 0$ ), we have to deal with the potential  $\phi$  only. The only non-zero traction component is  $\tau_{zz}$ ; therefore, the two boundary conditions left are those on  $u_z$  and  $\tau_{zz}$ .

Finally, at a free surface of an elastic halfspace we cannot impose any conditions on the displacement vector but, clearly, the stresses should vanish completely. As a result, for P-SV waves at the free surface we are left just with the two last equations (2.3.12, 2.3.13).

The wave equations and boundary conditions are all we need to solve reflection/transmission problems in layered media.

## 2.4 Reflection and transmission at a fluid/fluid boundary

Below we will briefly consider reflection/transmission problems for plane waves at the boundaries described in the previous sections. The emphasis will be on the properties of the reflected and transmitted waves important in analysis of point-source radiation.

We start with the simplest case of a fluid/fluid boundary between the halfspaces with the acoustic velocities and densities  $c$  and  $\rho$  (incidence medium) and  $c_1$  and  $\rho_1$  (reflecting medium). A plane harmonic acoustic wave incident on the boundary  $z = 0$  from the halfspace  $z > 0$  is given by

$$\phi_{inc} = e^{ik(x \sin \theta - z \cos \theta) - i\omega t}. \quad (2.4.1)$$

$\theta$  is the incidence angle;  $k = \omega/c$ ; the factor  $e^{-i\omega t}$  will be omitted in the following. The reflected and transmitted (refracted) waves can be represented as

$$\phi_{refl} = V e^{ik(x \sin \theta_0 + z \cos \theta_0)}, \quad (2.4.2)$$

$$\phi_{tr} = W e^{ik_1(x \sin \theta_1 - z \cos \theta_1)}. \quad (2.4.3)$$

$V$  and  $W$  are the reflection and transmission coefficients, respectively; the signs of the components of the wave vector depend on the direction of wave propagation. If the boundary were located at  $z \neq 0$ , we would have to add the corresponding phase shift both to the reflected and transmitted waves.

As we found out above, there are two boundary conditions in this case:

$$[u_z] = 0,$$

$$[\tau_{zz}] = 0.$$

Using equations (2.3.11,2.3.13), the boundary conditions can be written as

$$\left[\frac{\partial\phi}{\partial z}\right] = 0, \quad (2.4.4)$$

$$[\lambda\nabla^2\phi] = \left[\rho\frac{\partial^2\phi}{\partial t^2}\right] = 0. \quad (2.4.5)$$

Substituting expressions (2.4.1 - 2.4.3) into the first boundary condition (2.4.4) and setting  $z = 0$ , we find

$$-ik \cos \theta e^{ikx \sin \theta} + ik \cos \theta_0 V e^{ikx \sin \theta_0} = -ik_1 \cos \theta_1 W e^{ik_1 x \sin \theta_1}. \quad (2.4.6)$$

Since this equation should be satisfied at all  $x$ , the phase functions should be identical, and

$$\sin \theta = \sin \theta_0, \quad (2.4.7)$$

$$\frac{\sin \theta}{c} = \frac{\sin \theta_1}{c_1}. \quad (2.4.8)$$

This is Snell's law that is valid not just for this particular problem, but for all other types of boundaries as well. In order to satisfy boundary conditions, the horizontal slownesses of all waves taking part in the reflection/transmission process should be the same. The horizontal slowness is often called the ray parameter; from Snell's law it is clear that the ray parameter is preserved during the plane-wave propagation in 1-D media. Snell's law is valid for anisotropic media as well; however, the velocities in equation (2.4.8) are themselves functions of incidence and refraction angles.

Equation (2.4.6) now becomes

$$k \cos \theta (1 - V) = k_1 \cos \theta_1 W. \quad (2.4.9)$$

The second boundary condition (2.4.5) takes the form

$$\rho(1 + V) = \rho_1 W. \quad (2.4.10)$$

Solving equations (2.4.9,2.4.10) for the reflection and transmission coefficients, we get

$$V = \frac{c_1 \rho_1 \cos \theta - c \rho \cos \theta_1}{c_1 \rho_1 \cos \theta + c \rho \cos \theta_1}, \quad (2.4.11)$$

$$W = \frac{\rho}{\rho_1} (1 + V) = \frac{2c_1\rho \cos \theta}{c_1\rho_1 \cos \theta + c\rho \cos \theta_1}. \quad (2.4.12)$$

These are the coefficients for the potential function. For the z-component of the displacement vector, the reflection coefficient changes sign but keeps the same absolute value, while the transmission coefficient changes to

$$W_u = \frac{2c\rho \cos \theta_1}{c_1\rho_1 \cos \theta + c\rho \cos \theta_1}. \quad (2.4.13)$$

Usually, acoustic problems are solved for pressure rather than potential or displacement. In this case, the transmission coefficients would have a slightly different form but this difference is immaterial for our purposes.

At normal incidence, the reflection coefficient reduces to the fractional difference between the acoustic impedances of the two media:

$$V = \frac{c_1\rho_1 - c\rho}{c_1\rho_1 + c\rho}. \quad (2.4.14)$$

Now we will discuss reflection and transmission in the case when one or more waves become inhomogeneous. From Snell's law,

$$\sin \theta_1 = \sin \theta \frac{c_1}{c}, \quad (2.4.15)$$

and for  $c_1 > c$  and  $\sin \theta > c/c_1$  the refraction angle  $\theta_1$  becomes complex.  $\theta_{cr} = \sin^{-1}(c/c_1)$  is called the critical angle. Thus, if the reflecting medium has a higher velocity, at post-critical incidence angles the transmitted wave becomes inhomogeneous:

$$\cos \theta_1 = i\sqrt{\sin^2 \theta_1 - 1}. \quad (2.4.16)$$

The sign in equation (2.4.16) is chosen to keep the amplitude of the transmitted wave finite in the halfspace  $z < 0$ . The transmitted wave then becomes

$$\phi_{tr} = W e^{ik_1 x \sin \theta_1 + k_1 z |\cos \theta_1|}. \quad (2.4.17)$$

This is an inhomogeneous wave of the type we discussed above. It propagates in the x-direction with the velocity  $c_{hor} = c_1/\sin \theta_1$ , which is smaller than the medium velocity  $c_1$ , and exponentially decays in the vertical (z) direction away from the boundary. Inhomogeneous waves of this type play an important role in analysis of point-source radiation.

The reflection coefficient at post-critical incidence is

$$V = \frac{c_1\rho_1 \cos \theta - ic\rho |\cos \theta_1|}{c_1\rho_1 \cos \theta + ic\rho |\cos \theta_1|}. \quad (2.4.18)$$

The absolute value of  $V$  at post-critical incidence angles is unity, and we get what is sometimes called the total internal reflection.



Let us now make one more step forward and let both angles be complex. It is not clear why the incidence angle becomes complex but we will see that these complex angles are necessary to describe inhomogeneous plane waves contained in any plane-wave decomposition of point-source radiation. Now we consider an incident wave of the form

$$\phi = e^{ikx \sin \theta - kz |\cos \theta|}, \quad (2.4.19)$$

$\sin \theta > 1$ ,  $|\cos \theta| = \sqrt{\sin^2 \theta - 1}$ .

If the reflecting medium has a higher velocity, both angles are complex, and the reflection coefficient is again real:

$$V = \frac{c_1 \rho_1 |\cos \theta| - c \rho |\cos \theta_1|}{c_1 \rho_1 |\cos \theta| + c \rho |\cos \theta_1|}. \quad (2.4.20)$$

In principle, at a certain complex angle, the reflection coefficient may go to infinity, and this angle would correspond to the horizontal velocity of the surface wave. We will discuss this effect in more detail for a more classical model of the free surface of an elastic medium.

An important special case is the refraction of inhomogeneous waves into a low-velocity medium  $c_1 < c$ . From Snell's law (2.4.15) it is clear that for a certain range of complex angles  $\theta$  the refraction angle is real i.e., if  $1 < \sin \theta < c/c_1$ ,  $\sin \theta_1 < 1$ . This means that inhomogeneous plane waves can be converted into conventional homogeneous ones during the transmission into a low-velocity medium.

## 2.5 Reflection at a free surface

Essentially the same approach as above works for all kinds of boundaries. However, the behavior of the reflection/transmission coefficients strongly depends on the character of the boundary conditions. For a more complicated case of point source radiation, the boundary conditions and the velocity ratios determine the number and types of surface and nongeometrical waves generated during the reflection/transmission process.

Our next model will be the free surface of an elastic halfspace. Either a P or SV-wave is incident on the surface from the halfspace  $z > 0$  with the P- and S-velocities of  $c$  and  $b$  respectively. The full system of potentials for the incident P-wave can be written as

$$\phi = e^{ik(x \sin \theta - z \cos \theta)} + V_{pp} e^{ik(x \sin \theta + z \cos \theta)}, \quad (2.5.1)$$

$$\psi = V_{ps} e^{ik_s(x \sin \theta_s + z \cos \theta_s)}. \quad (2.5.2)$$

The boundary conditions in this case are

$$\tau_{xz} = 0, \quad \tau_{zz} = 0.$$

Expressing the stresses using equations (2.3.12, 2.3.13), we get two equations to be solved for the reflection ( $V_{pp}$ ) and conversion ( $V_{ps}$ ) coefficients. Denoting the vertical

component of the wave vector for the reflected waves by  $\alpha = k \cos \theta$  (for P-waves) and  $\beta = k_s \cos \theta_s$  for (S-waves), we find

$$V_{pp} = \frac{\alpha\beta - q^2}{\alpha\beta + q^2}, \quad (2.5.3)$$

where  $q = [\xi^2 - (k_s^2/2)]/\xi$ ,  $\xi = k \sin \theta = k_s \sin \theta_s$  is the horizontal component of the wave vector which remains the same for all reflected/converted waves.

The conversion coefficient is given by

$$V_{ps} = \frac{2\alpha q}{\alpha\beta + q^2}. \quad (2.5.4)$$

If the S-wave is incident on the free surface, the corresponding expressions are

$$V_{ss} = V_{pp}, \quad (2.5.5)$$

$$V_{sp} = \frac{-2\beta q}{\alpha\beta + q^2}. \quad (2.5.6)$$

At normal incidence,  $\xi = 0$ ,  $q = \infty$ , and the reflection coefficients are

$$V_{pp} = V_{ss} = -1. \quad (2.5.7)$$

We should remember that the above formulas are for the potentials rather than the displacements. For normal incidence, the P-wave displacement is

$$u_z(P) = -ike^{-ikz} + ikV_{pp}e^{ikz}. \quad (2.5.8)$$

Thus, the reflection coefficient for the displacement has the opposite sign compared to the coefficient for the potential. This means that for normal incidence the P-wave amplitude at the free surface doubles rather than goes to zero. The same thing happens with the SV-wave amplitude: although the SS reflection coefficient in potentials at normal incidence is equal to -1, the total displacement is twice the displacement of the incident wave.

Both conversion coefficients ( $V_{ps}$  and  $V_{sp}$ ) for normal incidence are zero, so the P-wave does not excite shear reflection and vice versa. On the other hand, at some horizontal slowness it may happen that  $\alpha\beta = q^2$ , and the P-wave at the surface transforms entirely into the shear wave without exciting a P-reflection, while the incident SV-wave goes entirely into the P-wave.

If the SV-wave is incident at post-critical angles  $\sin \theta_s > b/c$ , the reflected P-wave becomes inhomogeneous with

$$\phi_{refl} = V_{sp} e^{i\xi x - z|\alpha|} \quad (2.5.9)$$

with  $\alpha = ik\sqrt{\sin^2 \theta - 1}$ ; the SS reflection coefficient is  $|V_{ss}| = 1$ .

We have already discussed this situation when we considered post-critical incidence of an acoustic wave on a fluid/fluid boundary. The SP reflection from the free surface

at post-critical incidence propagates horizontally at velocities smaller than the P-wave velocity  $c$  and decays exponentially away from the boundary. The horizontal velocity of the inhomogeneous SP-wave is

$$V_{hor} = \frac{c}{\sin \theta} = \frac{b}{\sin \theta_s}. \quad (2.5.10)$$

From equation (2.5.10) (essentially, Snell's law) one can see that  $V_{hor}$  for the inhomogeneous wave changes from the P-wave velocity  $c$  for  $\sin \theta_s = b/c$  to the S-wave velocity  $b$  for  $\sin \theta_s = 1$ .

We will see that the distorting influence of the inhomogeneous SP reflection on the S-wave polarization has unpleasant consequences in polarization shear-wave analysis in anisotropic media.

One subtle point about inhomogeneous waves is the phase shifts caused by the complexity of the wave vector. When one of the reflected/converted waves is inhomogeneous, the reflection/conversion coefficients become complex but they seem to be independent of frequency. However, it turns out that that the phase shifts in the inhomogeneous waves change sign in accordance with the sign of frequency. Let us get back to equation (2.5.9). The displacements of the inhomogeneous SP-wave can be written as:

$$u_x = \sin \theta V_{sp} e^{ikx \sin \theta - z|k \cos \theta|}, \quad (2.5.11)$$

$$u_z = \cos \theta V_{sp} e^{ikx \sin \theta - z|k \cos \theta|}, \quad (2.5.12)$$

$\cos \theta = i\sqrt{\sin^2 \theta - 1}$ , if  $\omega > 0$ . We omit the factor  $ik$  that would appear during the formal differentiation of equation (2.5.9) assuming that the displacement components of the incident wave are real. It is more appropriate to consider  $V_{sp}$  in the above formulas as the conversion coefficient for displacements but the difference is not important in terms of the discussion below.

There are two phase shifts in expressions (2.5.11,2.5.12) we have to distinguish between. First, since  $\cos \theta$  is imaginary, there is a phase shift of  $\pi/2$  between the vertical and horizontal components of the displacement vector. As a result, the particle motion of the inhomogeneous wave will be elliptical rather than linear. To show this explicitly, we take the real parts of the vertical and horizontal displacements:

$$u_x^{re} = \sin \theta |V_{sp}| e^{-z|k \cos \theta|} \cos \phi(t), \quad (2.5.13)$$

$$u_z^{re} = \sqrt{\sin^2 \theta - 1} |V_{sp}| e^{-z|k \cos \theta|} [-\sin \phi(t)], \quad (2.5.14)$$

$\phi(t) = kx \sin \theta + \Phi_v - \omega t$ ,  $\Phi_v$  is the phase of the conversion coefficient. Now it is clear that

$$(u_x^{re})^2/l^2 + (u_z^{re})^2/m^2 = 1,$$

$$l^2 = \sin^2 \theta (|V_{sp}| e^{-z|k \cos \theta|})^2,$$

$$m^2 = (\sin^2 \theta - 1) (|V_{sp}| e^{-z|k \cos \theta|})^2,$$

and the particle motion represents an ellipse in the  $[x,z]$  plane.

In order to find out whether the motion is prograde (clockwise with the axis  $z$  pointing down) or retrograde, it is convenient to examine the point where  $\phi(t) = 2\pi n$ ,  $n$  is an integer. At this point,  $u_x^{re}$  is positive and reaches its maximum, while  $u_z^{re} = 0$ . It is clear from equations (2.5.13,2.5.14) that with increasing time  $u_z^{re}$  becomes positive, and this means that the particle moves down, in the prograde fashion.

Second, both displacement components have phase shifts with respect to conventional homogeneous waves due to the complexity of  $\cos \theta$  and the conversion coefficient  $V_{sp}$ . We have chosen the sign for the P-wave vertical wavenumber assuming that the frequency is positive. If it is negative, then in order to assure that the inhomogeneous SP wave decays away from the boundary, we have to set  $\cos \theta = -i\sqrt{\sin^2 \theta - 1}$ . This will give us the same expressions (2.5.11,2.5.12) for the displacement but the sign of the phase of the conversion coefficient (2.5.6) is now different. Indeed, if  $\omega < 0$ ,  $\beta$  and  $q$  change sign, while  $\alpha = \frac{i\omega}{c} \cos \theta$  remains the same. Also, the phase shift due to  $\cos \theta$  in equation (2.5.12) becomes  $-\pi/2$  instead of  $\pi/2$ . Thus, the phase shifts in the displacements (2.5.11,2.5.12), being the same for all positive frequencies or all negative frequencies, change the sign when we switch from positive to negative frequency.

Although a curved wavefront rather than a plane wave is needed to excite a surface wave, we can already show how to get the velocity of the Rayleigh wave from the boundary conditions. It turns out that it is possible to satisfy the boundary conditions just by using the waves propagating away from the surface, with no incident wave at all. Denoting the amplitudes of the outgoing potentials as  $A_p$  and  $A_s$ , we get from the boundary conditions

$$\beta A_s = q A_p,$$

$$q A_s = -\alpha A_p,$$

and the equations are simultaneously solved if

$$\alpha \beta = -q^2. \tag{2.5.15}$$

All three quantities in equation (2.5.15) depend on the horizontal slowness or the horizontal component of the wave vector  $\xi$ . Solving equation (2.5.15) gives the horizontal velocity of the Rayleigh wave, which turns out to be somewhat smaller than the S-wave velocity  $b$ .

Let us describe several important properties of the Rayleigh wave. First, the Rayleigh root of equation (2.5.15) and, consequently, the Rayleigh wave at the free surface always exists. Since  $q$  is real (in the absence of attenuation),  $\alpha$  and  $\beta$  are imaginary, i.e., both waves propagating from the boundary are inhomogeneous, exponentially decaying in the vertical direction.

Second, the Rayleigh wave is not dispersive in an unbounded non-attenuating half-space i.e., its velocity is independent of frequency. However, the Rayleigh wave becomes dispersive in the presence of layering.

Third, the P- and SV-components of the Rayleigh wave have different degrees of amplitude decay. The potentials in the Rayleigh wave can be written as

$$\phi = A_p e^{i\xi x - z\sqrt{\xi^2 - k^2}}, \quad (2.5.16)$$

$$\psi = A_s e^{i\xi x - z\sqrt{\xi^2 - k_s^2}}, \quad (2.5.17)$$

$\xi$  is the horizontal wavenumber of the Rayleigh wave at a certain frequency. Since  $k < k_s$ , the rate of decay away from the surface is higher for the P-component than for the SV-component, and the latter dominates the Rayleigh wave's displacement when  $z$  increases.

Fourth, the motion in the Rayleigh wave at the surface is retrograde elliptical, although both components (P, SV) have prograde trajectories. At a certain depth, the motion in the Rayleigh wave degenerates into a vertical line and at greater depths becomes prograde.

Derivation of the formulas for the displacement components of the Rayleigh wave and analysis of the particle motion is left out as an exercise for the students.

By definition, surface waves in the plane-wave domain exist without an incident wave. Therefore, an alternative way to derive the velocity of the Rayleigh wave is to set the denominator of the reflection coefficient to zero, which leads to the same equation (2.5.15).

It is clear that the incident wave corresponding to the Rayleigh root would be unbounded since its amplitude would increase exponentially away from the surface. In reality, the Rayleigh wave is excited by seismic sources, and its amplitude decreases between the source and the surface as well as away from the surface to a receiver (if the receiver is buried).

## 2.6 Reflection and transmission at a solid/solid boundary

This is the most important model in seismological applications. The solutions are quite straightforward and, in principle, not much different from the ones discussed above. However, the reflection/transmission process is more difficult to analyze due to a more complex algebra.

We consider a P-wave incident on a solid/solid boundary from the halfspace  $z > 0$  with the P-wave velocity  $c$ , S-wave velocity  $b$ , and density  $\rho$ . The parameters of the reflecting medium will have subscript "1." Using the same notation as in the previous problem, the potentials in the incidence medium can be written as (the horizontal slowness term and the factor  $e^{-i\omega t}$  are omitted):

$$\phi = e^{-i\alpha z} + V_{pp} e^{i\alpha z}, \quad (2.6.1)$$

$$\psi = V_{ps} e^{i\beta z}. \quad (2.6.2)$$

The potentials in the second medium are

$$\phi_1 = W_{pp} e^{-i\alpha_1 z}, \quad (2.6.3)$$

$$\psi_1 = W_{ps} e^{i\beta_1 z}. \quad (2.6.4)$$

According to the boundary conditions (2.3.10-2.3.13), two components of the displacement vector and two traction components should be continuous at the interface. Substituting equations (2.6.1-2.6.4) into (2.3.10-2.3.13), we arrive at a system of four linear simultaneous equations. The solution is quite straightforward but algebraically involved; the final results in different notations can be found in a number of papers and books, including Brekhovskikh (1980) and Aki and Richards (1980). Using Brekhovskikh's notation,

$$V_{pp} \Delta = A_1^2 - \beta A_2^2/\alpha + (\alpha_1/\beta_1)(B_1^2 - \beta B_2^2/\alpha) + m(\beta_1/\beta - \alpha_1/\alpha)(k_{s1}^4/4\xi^4), \quad (2.6.5)$$

where

$$\Delta = A_1^2 + \beta A_2^2/\alpha + (\alpha_1/\beta_1)(B_1^2 + \beta B_2^2/\alpha) + m(\beta_1/\beta + \alpha_1/\alpha)(k_{s1}^4/4\xi^4), \quad (2.6.6)$$

$$A_1 = n^2 - mq_1/\xi,$$

$$A_2 = (n^2 q - mq_1)/\beta,$$

$$B_1 = (n^2 - m)\beta_1/\xi,$$

$$B_2 = (\beta_1/\beta)(n^2 q/\xi - m),$$

$$q_1 = [\xi^2 - (k_{s1}^2/2)]/\xi,$$

$$n \equiv b/b_1, \quad m \equiv \rho_1/\rho.$$

The other coefficients are given by

$$(-\Delta/2) V_{ps} = A_1 A_2 + (\alpha_1/\beta_1) B_1 B_2, \quad (2.6.7)$$

$$\Delta W_{pp} = (k_{s1}^2/\xi^2) (A_1 - B_2), \quad (2.6.8)$$

$$\Delta W_{ps} = (k_{s1}^2/\xi^2) (A_2 + \alpha_1 B_1/\beta_1). \quad (2.6.9)$$

Since there are four possible waves incident on the boundary from both halfspaces, there is a total of 16 reflection/transmission coefficients. However, it is not necessary to solve the four simultaneous equations arising from boundary conditions anew for each incident wave. If we substitute all 4 possible waves into the boundary conditions, it turns out that the 16 reflection/transmission coefficients can be gathered into the so-called *scattering matrix*  $S$ :

$$S = \begin{pmatrix} \dot{P}\dot{P} & \dot{S}\dot{P} & \dot{P}\dot{P} & \dot{S}\dot{P} \\ \dot{P}\dot{S} & \dot{S}\dot{S} & \dot{P}\dot{S} & \dot{S}\dot{S} \\ \dot{P}\dot{P} & \dot{S}\dot{P} & \dot{P}\dot{P} & \dot{S}\dot{P} \\ \dot{P}\dot{S} & \dot{S}\dot{S} & \dot{P}\dot{S} & \dot{S}\dot{S} \end{pmatrix} = M^{-1}N. \quad (2.6.10)$$

The first letter in the elements of the scattering matrix denotes the incident wave, the second one - the reflected/transmitted wave. An acute accent ( $\dot{P}$ ) stands for an upgoing wave, a grave accent ( $\grave{P}$ ) denotes a downgoing wave.  $M$  and  $N$  are 4x4 matrices with the elements depending on the horizontal slowness and elastic parameters (for explicit expressions of  $M$  and  $N$  see Aki and Richards, 1980).

The formula of the most practical importance in seismology is the one for the PP reflection coefficient  $V_{pp}$  (2.6.5). At normal incidence,  $V_{pp}$  reduces to the fractional difference in the acoustic impedances across the boundary, i.e., to the reflection coefficient at a fluid/fluid boundary (2.4.11). However, the angular behavior of the reflection coefficient strongly depends on the ratio of S-wave velocities in both media, and this fact has serious implications in the so-called amplitude-versus-offset (AVO) analysis - one of the few methods capable of direct detection of hydrocarbon reservoirs.

There is a number of critical angles corresponding to a solid/solid interface. If, for instance, the SV-wave is incident on the boundary from the low-velocity medium ( $b < b_1 < c < c_1$ ), the critical angles are

$$\theta_1 = \sin^{-1}(b/c_1), \quad (2.6.11)$$

$$\theta_2 = \sin^{-1}(b/c), \quad (2.6.12)$$

$$\theta_3 = \sin^{-1}(b/b_1). \quad (2.6.13)$$

If the incidence angle  $\theta$  is larger than the smallest critical angle  $\theta_1$ , the transmitted SP wave becomes inhomogeneous. At large incidence angles, exceeding all three critical angles, both transmitted waves and the the SP reflection are inhomogeneous, and only the SS reflection is a homogeneous plane wave. The inhomogeneous reflected/transmitted waves have essentially the same properties considered above for the models of a fluid/fluid boundary and a free surface. For instance, the horizontal velocity of the transmitted SP inhomogeneous wave may become as low as  $b$  compared to the minimum horizontal velocity of  $c_1$  for the conventional homogeneous SP-wave. The slower the inhomogeneous wave becomes, the faster is the amplitude decay away from the boundary.

The condition for the existence of a surface wave (it is called the Stoneley wave) at a solid/solid boundary is  $\Delta = 0$ . Unlike the case of a free surface or fluid/solid boundary, this surface wave does not exist for all sets of elastic parameters (Sezawa and Kanai, 1939; Ginzburg and Strick, 1958). More than that, it cannot exist for ratios of velocities and densities typical for seismic reflectors in the Earth; essentially, the medium with higher velocities should have a smaller density for the Stoneley wave to be excited.

## 2.7 Plane waves in stratified media

Suppose that the model we are dealing with consists not just of a single boundary but of a stack of plane layers. If we are interested in a specific wave type (say, transmitted PPSP wave) or several wave types, it is sufficient to multiply the appropriate reflection/transmission coefficients and take into account the appropriate phase shifts. Let us add one more boundary to the model of a solid/solid interface discussed above and consider a P-wave reflected from a plane layer. As before, we will omit the horizontal phase term. Parameters of the incidence medium will be denoted by index 1, of the layer - by 2, of the underlying medium - by 3. The wave transmitted through the layer's top can be written as (equation [2.6.3])

$$\dot{\phi} = W_{12} e^{-i\alpha_2 z}, \quad (2.7.1)$$

with  $W_{12}$  is the transmission coefficient given by equation (2.6.8). If the thickness of the layer is denoted by  $d$ , the layer's bottom would correspond to  $z = -d$ . The P-wave reflected from the bottom is then

$$\dot{\phi} = W_{12} V_{23} e^{i\alpha_2(z+2d)}. \quad (2.7.2)$$

$V_{23}$  is the PP-reflection coefficient from the layer's bottom as given by equation (2.6.5). The phase of the reflected plane wave is chosen to satisfy the boundary conditions; since the incident wave has a phase shift of  $\alpha_2 d$  at  $z = -d$ , all reflected/transmitted waves should contain the same phase term at the boundary. The sign of the phase in equation (2.7.2) ensures that the reflected waves propagates upwards, in the positive  $z$ -direction.

When the reflected wave gets back to the layer's top, its phase becomes  $2\alpha_2 d$ . After the transmission back into the first medium, the primary P-reflection is

$$\phi_{pr} = W_{12} V_{23} W_{21} e^{i(\alpha_1 z + 2\alpha_2 d)}. \quad (2.7.3)$$

Repeating this derivation for the first multiple inside the layer, we obtain

$$\phi_{m1} = W_{12} V_{23} V_{21} V_{23} W_{21} e^{i(\alpha_1 z + 4\alpha_2 d)}. \quad (2.7.4)$$

Summing up all P-reflections including the reflection from the top yields

$$\phi_{refl} = e^{i\alpha_1 z} (V_{12} + W_{12} V_{23} W_{21} e^{2i\alpha_2 d} + W_{12} V_{23}^2 V_{21} W_{21} e^{4i\alpha_2 d} + \dots). \quad (2.7.5)$$

It is an infinite geometrical progression with the sum

$$\phi_{refl} = e^{i\alpha_1 z} \left( V_{12} + \frac{W_{12} V_{23} W_{21} e^{2i\alpha_1 d}}{1 - V_{23} V_{21} e^{2i\alpha_1 d}} \right). \quad (2.7.6)$$

Equation (2.7.6) gives the complete solution for the acoustic case, when there is no P-S conversion. The method outlined above will still work in elastic media if we are interested just in certain wave types (say, in pure P-waves or a specific conversion, like PPSPS-wave), especially if the model is relatively simple. Note that the above expressions



for plane waves provide a basis for ray-theory treatment of body waves. An important advantage of the techniques based on summation of elementary waves is an easy decomposition of the wavefield into individual wave types.

However, often we would like to get the full reflection and transmission response of a layered model including all kinds of multiple reflections and conversions. In this case, the simple summation approach is ineffective, and we have to use the so-called matrix propagators. I will describe the simplest version of the matrix technique due to Thomson (1950). There have been many improvements upon the original Thomson's work, especially in connection with the development of the reflectivity method; most of them are summarized by B.L.N. Kennett (1983). After Kennett's book had been published, the matrix-propagator method was extended to anisotropic media but the essence of it remains unchanged.

Let a plane P-wave be incident on a stack of elastic layers. We place the origin of the coordinate system on the top of the first layer. The potentials of the upgoing and downgoing waves in the upper halfspace are

$$\phi_1 = (\dot{\phi}_1 e^{-i\alpha_1 z} + \acute{\phi}_1 e^{i\alpha_1 z}) e^{i\xi x}, \quad (2.7.7)$$

$$\psi_1 = (\dot{\psi}_1 e^{-i\beta_1 z} + \acute{\psi}_1 e^{i\beta_1 z}) e^{i\xi x}. \quad (2.7.8)$$

If the potentials are given by equations (2.7.7,2.7.8), the vertical displacement, according to equation (2.2.5), becomes (index 1 and the horizontal slowness term are omitted):

$$u_z = i\alpha \cos(\alpha z)(\acute{\phi} - \dot{\phi}) - \alpha \sin(\alpha z)(\dot{\phi} + \acute{\phi}) + i\xi \cos(\beta z)(\acute{\psi} + \dot{\psi}) + \xi \sin(\beta z)(\dot{\psi} - \acute{\psi}). \quad (2.7.9)$$

From equation (2.7.9) we see that  $u_z$  is a linear combination of the sums and differences of the potential coefficients for P and SV-waves. It is straightforward to show that the horizontal displacement  $u_x$  (equation [2.2.4]) and the components of the stress tensor  $\tau_{xz}$  and  $\tau_{zz}$  (equations [2.3.3],[2.3.5]) are also linear combinations of the same quantities  $\acute{\phi} + \dot{\phi}$ ,  $\acute{\phi} - \dot{\phi}$ ,  $\acute{\psi} + \dot{\psi}$ ,  $\dot{\psi} - \acute{\psi}$ . We can write these relations for the upper halfspace in the matrix form as

$$\begin{pmatrix} u_z^{(1)} \\ u_x^{(1)} \\ \tau_{zz}^{(1)} \\ \tau_{xz}^{(1)} \end{pmatrix} = P(\xi, c_1, b_1, \rho_1, z) \begin{pmatrix} \acute{\phi}_1 + \dot{\phi}_1 \\ \acute{\phi}_1 - \dot{\phi}_1 \\ \acute{\psi}_1 + \dot{\psi}_1 \\ \dot{\psi}_1 - \acute{\psi}_1 \end{pmatrix}, \quad (2.7.10)$$

where  $P$  is a 4x4 matrix dependent on the incidence angle, medium parameters, and the vertical coordinate.

The displacement-stress vector at the first boundary is given by equation (2.7.10) with  $P = P(\xi, c_1, b_1, \rho_1, 0)$ . The potentials in the first layer (below the boundary) can be written in the same form as in equations (2.7.7,2.7.8), only the vertical components of the wave vector would be different. Clearly, the same relationship as (2.7.10) between the displacement-stress vector and the potential coefficients is valid in the first layer:

$$\begin{pmatrix} u_z^{(2)} \\ u_x^{(2)} \\ \tau_{zz}^{(2)} \\ \tau_{xz}^{(2)} \end{pmatrix} = P(\xi, c_2, b_2, \rho_2, z) \begin{pmatrix} \acute{\phi}_2 + \grave{\phi}_2 \\ \acute{\phi}_2 - \grave{\phi}_2 \\ \acute{\psi}_2 + \grave{\psi}_2 \\ \acute{\psi}_2 - \grave{\psi}_2 \end{pmatrix}, \quad (2.7.11)$$

Since all four components of the stress-displacement vector remain continuous across the boundary, the left columns in equations (2.7.10,2.7.11) are identical at  $z = 0$ . Therefore,

$$P(\xi, c_1, b_1, \rho_1, 0) \begin{pmatrix} \acute{\phi}_1 + \grave{\phi}_1 \\ \acute{\phi}_1 - \grave{\phi}_1 \\ \acute{\psi}_1 + \grave{\psi}_1 \\ \acute{\psi}_1 - \grave{\psi}_1 \end{pmatrix} = P(\xi, c_2, b_2, \rho_2, 0) \begin{pmatrix} \acute{\phi}_2 + \grave{\phi}_2 \\ \acute{\phi}_2 - \grave{\phi}_2 \\ \acute{\psi}_2 + \grave{\psi}_2 \\ \acute{\psi}_2 - \grave{\psi}_2 \end{pmatrix}, \quad (2.7.12)$$

so

$$\begin{pmatrix} \acute{\phi}_2 + \grave{\phi}_2 \\ \acute{\phi}_2 - \grave{\phi}_2 \\ \acute{\psi}_2 + \grave{\psi}_2 \\ \acute{\psi}_2 - \grave{\psi}_2 \end{pmatrix} = P^{-1}(\xi, c_2, b_2, \rho_2, 0) P(\xi, c_1, b_1, \rho_1, 0) \begin{pmatrix} \acute{\phi}_1 + \grave{\phi}_1 \\ \acute{\phi}_1 - \grave{\phi}_1 \\ \acute{\psi}_1 + \grave{\psi}_1 \\ \acute{\psi}_1 - \grave{\psi}_1 \end{pmatrix}. \quad (2.7.13)$$

Essentially, we have transmitted the potentials through the top of the first layer. Equation (2.7.13) can be used to find the reflection and transmission coefficients at a solid/solid boundary discussed above. However, in a layered medium we lack equations to find the potentials on both sides of the boundary. Physically this means that we cannot find the potentials inside the layer by using the boundary conditions only at the layer's top.

The displacement-stress vector at the bottom of the layer ( $z = -d$ ) is given by

$$\begin{pmatrix} u_z^{(2)}(-d) \\ u_x^{(2)}(-d) \\ \tau_{zz}^{(2)}(-d) \\ \tau_{xz}^{(2)}(-d) \end{pmatrix} = P(\xi, c_2, b_2, \rho_2, -d) \begin{pmatrix} \acute{\phi}_2 + \grave{\phi}_2 \\ \acute{\phi}_2 - \grave{\phi}_2 \\ \acute{\psi}_2 + \grave{\psi}_2 \\ \acute{\psi}_2 - \grave{\psi}_2 \end{pmatrix}. \quad (2.7.14)$$

Using the relation between the potentials in the incidence medium and the layer (2.7.13), we get

$$\begin{pmatrix} u_z^{(2)}(-d) \\ u_x^{(2)}(-d) \\ \tau_{zz}^{(2)}(-d) \\ \tau_{xz}^{(2)}(-d) \end{pmatrix} = P_{\Sigma_2} \begin{pmatrix} \acute{\phi}_1 + \grave{\phi}_1 \\ \acute{\phi}_1 - \grave{\phi}_1 \\ \acute{\psi}_1 + \grave{\psi}_1 \\ \acute{\psi}_1 - \grave{\psi}_1 \end{pmatrix}, \quad (2.7.15)$$

where

$$P_{\Sigma_2} = P(\xi, c_2, b_2, \rho_2, -d) P^{-1}(\xi, c_2, b_2, \rho_2, 0) P(\xi, c_1, b_1, \rho_1, 0)$$

Note that we can now move the origin of our coordinate system to the bottom of the first layer since it does not change the displacement-stress vector. Continuing this procedure down to the last,  $(n - 1) - th$  boundary, we find the relation between the potentials in the upper and lower halfspaces:

$$\begin{pmatrix} \phi^n + \dot{\phi}^n \\ \phi^n - \dot{\phi}^n \\ \psi^n + \dot{\psi}^n \\ \psi^n - \dot{\psi}^n \end{pmatrix} = P_\Sigma \begin{pmatrix} \phi_1 + \dot{\phi}_1 \\ \phi_1 - \dot{\phi}_1 \\ \psi_1 + \dot{\psi}_1 \\ \psi_1 - \dot{\psi}_1 \end{pmatrix}, \quad (2.7.16)$$

where  $P_\Sigma$  is the product of the propagator matrices for the whole stack of layers:

$$P_\Sigma = \begin{matrix} P^{-1}(\xi, c_n, b_n, \rho_n, 0) P(\xi, c_{n-1}, b_{n-1}, \rho_{n-1}, -d) \\ P^{-1}(\xi, c_{n-1}, b_{n-1}, \rho_{n-1}, 0) \dots P(\xi, c_1, b_1, \rho_1, 0). \end{matrix} \quad (2.7.17)$$

Essentially, we have reduced the reflection-transmission problem for a multilayered medium to the problem for a single boundary we have already considered. However, the potentials in the upper and lower halfspaces are now related by a product of matrix propagators corresponding to all individual layers. Since we consider the incident P-wave,  $\dot{\phi}_1 = 1, \dot{\psi}_1 = 0$ ; also, there are no upgoing waves in the lower halfspace, and  $\phi^n = \dot{\psi}^n = 0$ . Therefore,

$$\begin{pmatrix} \dot{\phi}^n \\ -\dot{\phi}^n \\ \dot{\psi}^n \\ -\dot{\psi}^n \end{pmatrix} = P_\Sigma \begin{pmatrix} \phi_1 + 1 \\ \phi_1 - 1 \\ \psi_1 \\ \psi_1 \end{pmatrix}, \quad (2.7.18)$$

All we have to do is to solve these four simultaneous equations for two reflected and two transmitted waves, thus getting the reflection and transmission responses of the layered medium. The reflection and transmission coefficients for the incident SV-wave can be obtained exactly the same way.

One of the reasons why this approach is attractive is that the matrix propagators can be easily inverted. Although the matrix-propagator approach is straightforward in principle, it suffers from some numerical problems, such as the loss of accuracy due to the exponential terms in the propagator matrices. This and some other problems of matrix propagators are discussed in Kind (1976) and Kennett (1983), among others.



# Chapter 3

## Point-source radiation in fluid models

### 3.1 Plane-wave decomposition of point-source radiation

First, we will decompose point-source radiation into plane and cylindrical waves and then solve the reflection/transmission problem for a spherical wave at a fluid/fluid boundary. This will enable us to establish many important concepts to be used in more complicated reflection/transmission problems for realistic models consisting of solid layers.

Let us consider the wave equation for the P-wave potential  $\phi$  (1.0.9) with a point source at the origin of the Cartesian coordinate system:

$$\frac{\partial^2 \phi}{\partial t^2} - c^2 \nabla^2 \phi = 4\pi c^2 f(t) \delta(\vec{x}). \quad (3.1.1)$$

For the time being, the source will be a harmonic oscillator with  $f(t) = e^{-i\omega t}$ . This means that we will get solutions for a fixed frequency; the corresponding solutions in the time domain can be obtained by applying a Fourier transform to a particular source pulse.

Equation (3.1.1) describes a small (compared to the predominant wavelength) sphere oscillating in a fluid or an explosive (spherically-symmetric) source in a solid.

Since the medium is isotropic and the source is spherically-symmetric, the solution of equation (3.1.1) should also be spherically-symmetric, determined just by  $R = \sqrt{x^2 + y^2 + z^2}$ . The form of the spherically-symmetric solution of the wave equation is well-known (Aki and Richards, 1980):

$$\phi(\vec{x}, t) = \frac{1}{R} e^{i(kR - \omega t)}. \quad (3.1.2)$$

It is easy to verify that the spherical wave (3.1.2) satisfies the wave equation at  $R \neq 0$ . A rigorous proof that the potential (3.1.2) gives the required singularity at the source point can be found in Aki and Richards (1980). Below we will outline an alternative way to prove that the solution of the wave equation (3.1.1) is represented by (3.1.2). If the

coefficient  $4\pi c^2$  is not added to the right-hand side of the wave equation, it appears in the expression for the spherical wave.

The spherical wave propagates away from the source with the velocity  $c$  and decays as  $1/R$ ; the amplitude depends only on the distance from the source. Our task now is to represent the spherical solution (3.1.2) in the way that will make it easy for us to solve reflection-transmission problems in stratified media. Since we already know reflection/transmission coefficients for plane waves, we will decompose point-source radiation into plane waves and, later on, into the so-called cylindrical waves.

Let us represent the solution of equation (3.1.1) as a triple Fourier transform :

$$\phi(\vec{x}, t) = \frac{e^{-i\omega t}}{(2\pi)^3} \int_{-\infty}^{\infty} \int_{-\infty}^{\infty} \int_{-\infty}^{\infty} \tilde{\phi}(\vec{k}, \omega) e^{i(k_x x + k_y y + k_z z)} d\vec{k}, \quad (3.1.3)$$

$$d\vec{k} = dk_x dk_y dk_z.$$

Similarly,

$$\delta(\vec{x}) = \frac{1}{(2\pi)^3} \int_{-\infty}^{\infty} e^{i(k_x x + k_y y + k_z z)} d\vec{k}. \quad (3.1.4)$$

Substituting equations (3.1.3, 3.1.4) into the wave equation (3.1.1), we get

$$\tilde{\phi}(\vec{k}, \omega) = \frac{4\pi c^2}{k^2 c^2 - \omega^2}. \quad (3.1.5)$$

Now we have found the integral kernel in equation (3.1.3), and it is possible to prove by direct integration of (3.1.3) that the spherical wave's potential is given by equation (3.1.2):

$$\frac{1}{R} e^{i(kR - \omega t)} = \frac{e^{-i\omega t}}{2\pi^2} \int_{-\infty}^{\infty} \frac{e^{i(k_x x + k_y y + k_z z)}}{k^2 - \frac{\omega^2}{c^2}} d\vec{k}, \quad (3.1.6)$$

Although it looks like we have already decomposed the spherical wave into plane waves, we are not there yet: the plane waves under the integral (3.1.6) do not satisfy the wave equation (although their sum does). Actually the waves which comply with the wave equation cause singularities in the integrand. The simplest way to reduce the spherical wave to a sum of plane-wave solutions of the wave equation is to carry out integration over one of the wavenumbers. Since we wish to use the result in solving reflection-transmission problems at horizontal boundaries, we will integrate over the vertical wavenumber  $k_z$ .

We carry out the integration over  $k_z$  by extending the integral to the complex plane and apply residue theory. If  $z > 0$ , we have to use a semicircle in the upper half-plane, so that  $ik_z z$  decays for  $k_z = i\infty$ . If  $z < 0$ , the semicircle should lie in the lower half-plane. Now we have to find the poles within the semicircles.

The integrand has poles at the vertical wavenumbers  $k_z^2 = \frac{\omega^2}{c^2} - k_x^2 - k_y^2$ . Apparently, the poles can lie on the real axis of  $k_z$  i.e., on the integration path. To avoid this situation, we introduce small attenuation, making the velocity  $c$  complex. For positive frequencies,  $Im(1/c) > 0$  for the spherical wave (3.1.2) to decay away from the source. This trick adds a positive imaginary part to  $k_z^2$  and moves the poles from the real axis to the first and third quadrants.

The poles corresponding to negative values of  $\frac{\omega^2}{c^2} - k_x^2 - k_y^2$  lie on the imaginary axis. By introducing small attenuation, we also move these poles to the first and third quadrants.

If  $z > 0$ , we have to pick up the residue in the upper half-space (i.e., in the first quadrant). The direction of the integration path is positive, and

$$\phi = 2\pi i \operatorname{Res}[Im k_z > 0] = \frac{e^{-i\omega t}}{2\pi} \int_{-\infty}^{\infty} \int_{-\infty}^{\infty} \frac{i}{k_z} e^{i(k_x x + k_y y + k_z z)} dk_x dk_y, \quad (3.1.7)$$

where  $k_z = (\frac{\omega^2}{c^2} - k_x^2 - k_y^2)^{1/2}$ , and the square root is chosen so that  $Re k_z > 0$ ,  $Im k_z > 0$ . Similarly, for  $z < 0$

$$\phi = -2\pi i \operatorname{Res}[Im k_z < 0] = \frac{e^{-i\omega t}}{2\pi} \int_{-\infty}^{\infty} \int_{-\infty}^{\infty} \frac{-i}{k_z} e^{i(k_x x + k_y y + k_z z)} dk_x dk_y, \quad (3.1.8)$$

where  $k_z = (\frac{\omega^2}{c^2} - k_x^2 - k_y^2)^{1/2}$ , but the square root is chosen so that  $Re k_z < 0$ .

The physical meaning of this difference in signs of  $k_z$  is that the waves are going away from the source: for  $z > 0$  they are propagating in the positive  $z$ -direction, for  $z < 0$  - in the negative  $z$ -direction. Equations (3.1.7,3.1.8) can be written together as the so-called Weyl integral:

$$\frac{1}{R} e^{ikR} = \frac{i}{2\pi} \int_{-\infty}^{\infty} \int_{-\infty}^{\infty} \frac{e^{i(k_x x + k_y y + k_z |z|)}}{k_z} dk_x dk_y. \quad (3.1.9)$$

The sign of  $k_z$  in equation (3.1.9) is chosen so that  $Re k_z > 0$ . Now we have reached our goal: the field of a point source is decomposed into plane waves which satisfy the wave equation. We already know how to solve reflection/transmission problems for an elementary plane wave from integral (3.1.9).

Plane waves comprising point-source radiation propagate in all directions because the integration is carried out over all possible  $k_x, k_y$ . More than that, in addition to conventional homogeneous waves, the Weyl integral (3.1.9) contains inhomogeneous plane waves decaying in the vertical direction. The inhomogeneous waves are due to the poles near the imaginary axis on the complex  $k_z$ -plane picked up during the integration over  $k_z$ .

It is useful to replace the horizontal wavenumbers with the angles which determine the direction of propagation of elementary plane waves (Figure 3.1).

We denote

$$k_x = k \sin \theta \cos \phi, \quad k_y = k \sin \theta \sin \phi, \quad k_z = k \cos \theta.$$

The area element in polar coordinates is

$$dk_x dk_y = k_r dk_r d\phi,$$

where  $k_r = \sqrt{k_x^2 + k_y^2} = k \sin \theta$ . Hence,

$$dk_x dk_y = k^2 \sin \theta \cos \theta d\theta d\phi.$$

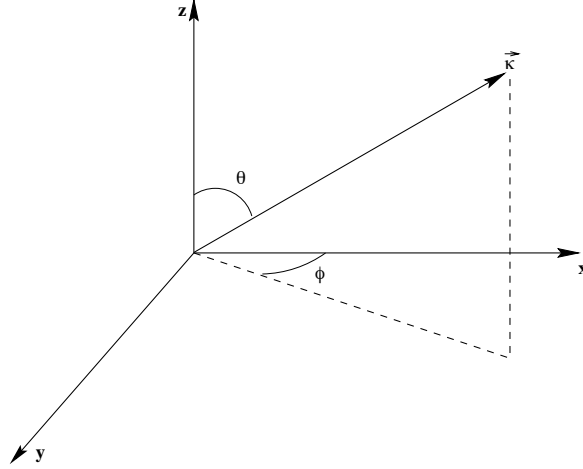


Figure 3.1: The angles used in the plane-wave decomposition of point-source radiation.

Then

$$\frac{1}{R} e^{ikR} = \frac{ik}{2\pi} \int_0^{\pi/2-i\infty} \int_0^{2\pi} e^{i(k_x x + k_y y + k_z |z|)} \sin \theta d\theta d\phi. \quad (3.1.10)$$

The limits of the integration over  $\theta$  (Figure 3.2) need to be explained. When  $k_r > k$ , then  $\sin \theta > 1$ , and the integrand becomes an inhomogeneous wave. Clearly, for  $k < k_r < \infty$  the angle  $\theta$  should be complex. To cover the range  $k \geq k_r < \infty$ , we represent  $\theta$  as  $\theta = \pi/2 - ia$ , where  $a$  is real and non-negative. Then,  $\sin \theta = \cosh a$ , and  $\cos \theta = i \sinh a$ . For the integration over  $\theta$ , the path lies on the real axis up to  $\theta = \pi/2$ , and then turns down into the complex plane parallel to the imaginary axis. The part of the integration path on the real axis corresponds to homogeneous plane waves, the part parallel to the imaginary axis picks up inhomogeneous plane waves.

Inhomogeneous waves decay in the vertical direction as  $e^{-k \sinh a |z|}$  and propagate in the horizontal direction with the velocity  $v_{hor} = c / \sin \theta = c / \cosh a$ , which is smaller than the medium velocity  $c$ . The smaller the velocity of an inhomogeneous wave, the faster is the amplitude decay in the vertical direction. We have analyzed inhomogeneous waves of this type when we considered reflection/transmission problems for plane waves.

Why do we need inhomogeneous waves in the plane-wave decomposition of the point-source radiation? From equation (3.1.10) it is clear that it is impossible to get the required singularity at  $x = y = z = 0$  by superposition of homogeneous plane waves only since the integral has finite limits. By including inhomogeneous waves, we make the field at the source infinite. If  $z \neq 0$ , the integral becomes finite because of the attenuating factor for inhomogeneous waves. When  $x \neq 0$  or  $y \neq 0$ , the finite value of the field is ensured by the oscillations of the integrand (interference of inhomogeneous waves with different phases).

Our model (a homogeneous medium) is axially symmetric, and we can take advantage of the symmetry to reduce the double integral (3.1.10) to a single integral over horizontal slowness. Substituting the expressions for the horizontal components of the wave vector



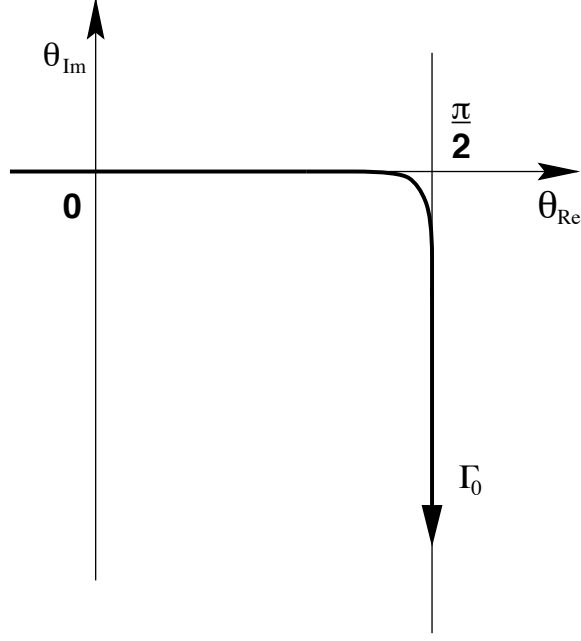


Figure 3.2: The path of integration in the decomposition of point-source radiation into plane and cylindrical waves.

yields

$$\frac{1}{R} e^{ikR} = \frac{ik}{2\pi} \int_0^{\pi/2-i\infty} \int_0^{2\pi} e^{i[k_r r \cos(\phi-\alpha) + k_z |z|]} \sin \theta \, d\theta d\phi, \quad (3.1.11)$$

where we used  $x = r \cos \alpha$ ,  $y = r \sin \alpha$ .

The dependence on the azimuthal angle  $\phi$  is limited to the term  $\cos(\phi - \alpha)$ . Using an integral expression for the zero-order Bessel function

$$J_0(x) = \frac{1}{2\pi} \int_0^{2\pi} e^{ix \cos t} dt, \quad (3.1.12)$$

we arrive at the so-called Sommerfeld integral:

$$\frac{1}{R} e^{ikR} = ik \int_0^{\pi/2-i\infty} e^{ik|z| \cos \theta} J_0(kr \sin \theta) \sin \theta \, d\theta. \quad (3.1.13)$$

As before,  $Re k_z (Re \cos \theta) > 0$ . Instead of the plane waves in the Weyl integral, the elementary components of the Sommerfeld integral are the so-called “cylindrical” waves with a separate dependence on  $r$  and  $z$ . Note that wavefronts of “cylindrical” waves from the Sommerfeld’s integral are not cylinders. We will see that integral (3.1.13) is very convenient in solving reflection/transmission problems at plane boundaries. Although, unlike the Weyl integral, it does not formally contain plane waves, boundary problems for cylindrical waves can still be handled using plane-wave reflection/transmission coefficients. As the Weyl integral (3.1.10), decomposition (3.1.13) contains inhomogeneous waves corresponding to complex values of  $\theta$ .

## 3.2 Integral solutions for scattering at a plane boundary

Suppose a point source is located at distance  $z_0$  above a plane interface  $z = 0$ . The pressure or potential of the spherical wave radiated by the source may be decomposed into plane or cylindrical waves as discussed in the previous section. Let us start with the Weyl integral over plane waves (3.1.10). The field of the incident wave is given by

$$\phi_{inc} = \frac{ik}{2\pi} \int_0^{\pi/2-i\infty} \int_0^{2\pi} e^{i[k_x x + k_y y + k_z(z_0-z)]} \sin \theta d\theta d\phi. \quad (3.2.1)$$

Since we are dealing with a linear problem, each elementary plane wave under the integral (3.2.1) can be treated separately. Taking into account the vertical phase shift, the reflected plane wave can be written as

$$\phi_{refl}^{pl} = V(\theta) e^{i[k_x x + k_y y + k_z(z+z_0)]}. \quad (3.2.2)$$

Integrating over the reflected plane waves, we get

$$\phi_{refl} = \frac{ik}{2\pi} \int_0^{\pi/2-i\infty} \int_0^{2\pi} V(\theta) e^{i[k_x x + k_y y + k_z(z+z_0)]} \sin \theta d\theta d\phi. \quad (3.2.3)$$

Applying formula (3.1.12) for the Bessel function, we find

$$\phi_{refl} = ik \int_0^{\pi/2-i\infty} V(\theta) e^{ik(z+z_0) \cos \theta} J_0(kr \sin \theta) \sin \theta d\theta. \quad (3.2.4)$$

This expression is very similar to the Sommerfeld integral, only the vertical phase term corresponds to the reflected wave and the plane-wave amplitude contains the reflection coefficient. It turns out that we can apply plane-wave reflection/transmission coefficients directly to the cylindrical waves comprising the Sommerfeld integral because the horizontal phase term remains unchanged during reflection or transmission at a horizontal boundary.

The transmitted wave, obtained in the same way, is

$$\phi_{tr} = ik \int_0^{\pi/2-i\infty} W(\theta) e^{i(kz_0 \cos \theta - k_1 z \cos \theta_1)} J_0(kr \sin \theta) \sin \theta d\theta, \quad (3.2.5)$$

where  $W(\theta)$  is the transmission coefficient,  $k_1$  is the wavenumber in the second medium ( $z < 0$ ).

Although the formal solution of the reflection/transmission problem is now obtained, the properties of the reflected and transmitted waves are hidden in the integrals (3.2.4,3.2.5). Below we study the wavefields on both sides of the boundary by performing asymptotic analysis of the integral solutions.

## 3.3 Stationary-phase method for reflected wavefields

We will use two asymptotic techniques designed for integrals of oscillatory functions: the stationary phase method and saddle-point integration. The idea of both methods

is essentially the same: if the integrand contains an exponential function with a large parameter, the value of the integral is determined just by one or several relatively short parts of the integration path.

Wave integrals (3.2.4,3.2.5) are well-suited for the application of these asymptotic methods if the receiver is relatively far from the source (compared to the predominant wavelength). Since in the far field the terms  $kz_0$ ,  $kz$  and/or  $kr$  are large, the integrand is a rapidly oscillating function. In the near field the situation is different:  $kz_0$  and  $kr$  are relatively small, and the integrand may not oscillate rapidly enough for the asymptotic techniques to be accurate.

The stationary-phase method (SPM) and saddle-point integration are ideologically related to ray theory. Like the ray method, asymptotic techniques for analysis of wave integrals provide high-frequency approximations valid in the far field. We will see that, for instance, the geometrical-seismics solution can be directly obtained from the zero-order approximation of the SPM.

We start out with the stationary-phase method that is more straightforward mathematically although, in general, is less powerful than the saddle-point integration technique. SPM is practically ignored in major textbooks (Aki and Richards, 1980; Brekhovskikh, 1980), so the reader will have to rely mostly on these notes and a paper by Fuchs (1971).

SPM, unlike saddle-point integration, does not require any distortions of the integration path. The goal of this technique is to find the points where the phase of the integrand does not change rapidly (stationary points) and reduce the integral to the contributions of the immediate vicinity of these points.

### 3.3.1 Zero-order approximation of the method of stationary phase

First, we apply the SPM to the potential of the reflected field (3.2.4). It is convenient to use an asymptotic representation of Bessel function  $J_0(x)$  valid for large arguments  $x$ :

$$J_0(x) \approx \sqrt{\frac{2}{\pi x}} \cos(x - \pi/4) = \sqrt{\frac{1}{2\pi x}} [e^{i(x-\pi/4)} + e^{-i(x-\pi/4)}]. \quad (3.3.1)$$

In a more accurate representation, the Bessel function is decomposed into the sine and cosine functions with coefficients in the form of infinite series in inverse powers of  $x$ . However, formula (3.2.4) is sufficient for our purpose of studying the reflected/transmitted waves in the far field.

Substituting formula (3.3.1) into the integral for the reflected wave (3.2.4) yields

$$\begin{aligned} \phi_{refl} = & i\sqrt{\frac{k}{2\pi}} \int_0^{\pi/2-i\infty} \frac{V(\theta)}{\sqrt{r \sin \theta}} \{e^{i[k(z+z_0) \cos \theta + kr \sin \theta - \pi/4]} \\ & + e^{i[k(z+z_0) \cos \theta - kr \sin \theta + \pi/4]}\} \sin \theta d\theta. \end{aligned} \quad (3.3.2)$$

The initial integral can be now divided into two integrals with different phase functions. Except for the exponentials, the integrands contain only slowly varying functions - the

reflection coefficient  $V(\theta)$  and  $\sin \theta$ . Therefore, the oscillations of the exponential terms are supposed to cancel the integral everywhere except for a certain vicinity of the points of stationary phase. As we will see later, the assumption about the slow variation in  $V(\theta)$  is not valid near the critical angle but at this time we will ignore this complication. The variant of the stationary phase method taking into account only the phase of the exponential function is sometimes called the zero-order approximation of the SPM (Fuchs, 1971).

The stationary-phase condition can be written as

$$\frac{d\Phi}{d\theta} = 0, \quad (3.3.3)$$

$\Phi$  is the phase of the integrand.

Applying (3.3.3) to the first phase term in equation (3.3.2) we find

$$\frac{d\Phi_1}{d\theta} = k[-(z + z_0) \sin \theta + r \cos \theta] = 0. \quad (3.3.4)$$

Note that we apply the SPM to the part of the integration path corresponding to homogeneous plane waves ( $0 < \theta < \pi/2$ ) and, therefore,  $\cos \theta$  is real.

From equation (3.3.4) the stationary point is

$$\theta_{st} = \tan^{-1} \frac{r}{z + z_0}. \quad (3.3.5)$$

We recall that  $\theta$  is the incidence angle of an elementary plane wave from the plane-wave decomposition of point-source radiation. The SPM enabled us to single out the plane wave that makes the most prominent contribution to the reflected wavefield. As expected, this wave corresponds to the geometrical ray reflected in accordance with Snell's law.

It is easy to verify that the second exponential function in equation (3.3.2) does not generate any stationary phase points on the integration path. Indeed, the stationary-phase equation for the second exponential

$$\frac{d\Phi_2}{d\theta} = k[-(z + z_0) \sin \theta - r \cos \theta] = 0 \quad (3.3.6)$$

does not have solutions for  $0 < \theta < \pi/2$ .

The second exponential corresponds to the waves coming towards the source (the so-called in-going waves) in the horizontal direction. These waves are contained both in the plane-wave and cylindrical-wave decompositions of point-source radiation. It is clear from simple physical considerations that only out-going waves should contribute to the incident and, consequently, reflected wavefields. While we have eliminated the vertically in-going waves during the integration over  $k_z$ , the horizontally in-going waves have been retained under the integral. Thus, the stationary-phase technique makes it possible to discriminate between in-going and out-going waves.

The next step is to find the amplitude of the geometrical reflection by evaluating the contribution of the stationary point (3.3.5) to the integral. We expand the phase  $\Phi = \Phi_1$

into a Taylor series at the stationary point taking into account that the first derivative of  $\Phi$  is zero:

$$\Phi(\theta) = \Phi(\theta_{st}) + \frac{1}{2} \frac{d^2\Phi}{d\theta^2} (\theta - \theta_{st})^2. \quad (3.3.7)$$

By substituting  $y = \theta - \theta_{st}$ , the integral for the reflected wave near the stationary point can be represented as

$$I = \int_{-b}^d S(y) e^{i\Phi(y)} dy, \quad (3.3.8)$$

where  $S(y)$  is a slowly varying function,  $b$  and  $d$  are small and positive. In accordance with the SPM methodology, we substitute expansion (3.3.7) into (3.3.8) and take  $S(\theta_{st})$  out of the integral assuming that the variations in  $S(\theta)$  near  $\theta_{st}$ . The contribution of the stationary point  $\theta_{st}$  ( $y = 0$ ) then becomes

$$I\{\theta_{st}\} = S(\theta_{st}) \int_{-b}^d e^{i[\Phi(\theta_{st}) + \frac{1}{2} \frac{d^2\Phi}{d\theta^2} y^2]} dy. \quad (3.3.9)$$

Then we formally extend the limits of integration to infinity because the oscillations of the integrand will cancel the contribution of any other part of the integration path except for a certain vicinity of the stationary point:

$$I\{\theta_{st}\} = S(\theta_{st}) e^{i\Phi(\theta_{st})} \int_{-\infty}^{\infty} e^{\frac{i}{2} \frac{d^2\Phi}{d\theta^2} \theta^2} d\theta. \quad (3.3.10)$$

The remaining integral reduces to the so-called Fresnel's integral (it is assumed that  $\frac{d^2\Phi}{d\theta^2} < 0$ ):

$$\int_{-\infty}^{\infty} e^{\frac{i}{2} \frac{d^2\Phi}{d\theta^2} \theta^2} d\theta = \sqrt{\frac{2\pi}{\left| \frac{d^2\Phi}{d\theta^2} \right|}} e^{-i\pi/4}. \quad (3.3.11)$$

For the contribution of the stationary point (3.3.10) we now have

$$I\{\theta_{st}\} = S(\theta_{st}) e^{i\Phi(\theta_{st})} \sqrt{\frac{2\pi}{\left| \frac{d^2\Phi}{d\theta^2} \right|}} e^{-i\pi/4}. \quad (3.3.12)$$

Now we apply general SPM formula (3.3.12) to calculate the contribution of the geometrical stationary point to integral (3.3.2). According to equation (3.3.4), the second derivative of the phase function in (3.3.2) is given by

$$\frac{d^2\Phi}{d\theta^2} = k[-(z + z_0) \cos \theta - r \sin \theta].$$

At the stationary point  $\theta_{st}$  (3.3.5),

$$\frac{d^2\Phi}{d\theta^2}(\theta_{st}) = -k[(z + z_0)^2/R + r^2/R] = -kR, \quad (3.3.13)$$

$$R = \sqrt{(z + z_0)^2 + r^2}.$$

Using equations (3.3.2,3.3.12,3.3.13), we find the following contribution of the geometrical stationary point to the reflected wave:

$$\phi_{refl} = i\sqrt{\frac{k}{2\pi}} \frac{V(\theta_{st}) \sin \theta_{st}}{\sqrt{r \sin \theta_{st}}} e^{i(kR - \pi/4)} \sqrt{\frac{2\pi}{kR}} e^{-i\pi/4}.$$

After simple algebra, the specular (geometrical) reflection takes the form

$$\phi_{refl} = V(\theta_{st}) \frac{e^{ikR}}{R}. \quad (3.3.14)$$

We obtained a well-known geometrical seismics approximation valid for the reflected P-wave potential both in fluid and solid models. The amplitude of the reflected wave is determined by the spherical divergence along the geometrical raypath and the plane-wave reflection coefficient. This means that the zero-order stationary phase approximation is equivalent to geometrical seismics; the geometrical solution is valid at source-receiver distances large compared to the predominant wavelength.

It is important to find out when the geometrical-seismics solution (3.3.14) becomes inaccurate. In our derivation we ignored the higher-order terms in the asymptotic expression for the Bessel function  $J_0$  and in the Taylor series expansion of the phase function. Brekhovskikh (1980) shows that the neglected terms depend on the derivatives of the reflection coefficient with respect to the angle  $\theta$ . Therefore, the geometrical seismics is exact for perfectly reflecting interfaces  $V = \pm 1$  or for boundaries between the media with the same velocity. In the latter case, the reflection coefficient is equal to the fractional difference between the densities and does not depend on the angle of incidence. Although the correction to geometrical seismics is supposed to become negligible for large source-receiver distances, it cannot be ignored when the wavefield in the geometrical-seismics approximation is small. For instance, when the source and receiver are close to the interface, the angle of incidence approaches  $90^\circ$  and the reflection coefficient  $V \approx -1$ . As a result, the direct and reflected wave cancel each other, and the additional terms become the principal component of the wavefield.

The corrections discussed above affect the amplitude and waveform but not the travel-time of the reflected wave. Later in the course we will see that the geometrical seismics and ray theory as a whole cannot account for a number of distinct arrivals generated when the source or receiver are located near the interface.

The above analysis has been done for the part of the integration path corresponding to homogeneous incident waves with real  $\cos \theta$  ( $0 < \theta < \pi/2$ ). In the part corresponding to inhomogeneous waves  $\cos \theta$  is imaginary and the phase function contains only  $kr \sin \theta = kr \cosh a$ ,  $\theta = \pi/2 - ia$ . The derivative of the phase function is  $\Phi' = kr \sinh a$ , and it seems that there is a stationary point at  $a = 0$  ( $\theta = \pi/2$ ). However, if the limit of  $\Phi$  is taken for  $\theta \rightarrow \pi/2$ ,  $\theta < \pi/2$ , it gives (in accordance with equation [3.3.4])  $\Phi'(\pi/2) = -k(z + z_0) \neq 0$ . This means that the first derivative of the phase function at  $\theta = \pi/2$  is discontinuous, and the SPM methodology cannot be applied at this point. The same result can be obtained if we use the horizontal slowness (ray parameter) as an independent variable instead of  $\theta$ .

Later on, we will find out that inhomogeneous reflected waves do contribute to the wavefield near the boundary if the incidence medium has a higher velocity. These waves are coupled to the nongeometrical components of the transmitted wavefield, and we will study them after examining the transmission problem. In order to single out nongeometrical reflected waves, we have to apply the so-called first-order approximation of the stationary-phase method and take the phase of the reflection coefficient into account.

### 3.3.2 First-order approximation of SPM

Although an asymptotic expression for the reflected wave has been derived, we have not been able to get a complete solution in the far field. We should have obtained the head wave in the post-critical domain but there are no more stationary points in the zero-order SPM approximation, even when the velocity in the reflecting medium is higher than in the incidence medium. The simplicity of the zero-order approximation is the main advantage of the application of the SPM to wave integrals. While in the case of the acoustic reflection the SPM has not provided us with more information than geometrical seismics, its application to the transmitted wave is much more productive. Below we will show that the zero-order SPM makes it possible to describe the so-called pseudospherical wave that belongs to the class of nongeometrical waves.

In order to include the head wave into the solution, we have to use the so-called first-order approximation of the SPM. Suppose the reflecting medium has a higher velocity than the incidence medium ( $c_1 > c$ ). Then in the post-critical domain  $\theta_{cr} < \theta < \pi/2$ ,  $\theta_{cr} = \sin^{-1}(c/c_1)$ , the reflection coefficient becomes complex, and its phase should be included in SPM treatment.

The reflection coefficient (2.4.11) can be rewritten at post-critical incidence as

$$V(\theta) = \frac{\sigma \cos \theta - i \sqrt{\sin^2 \theta - n^2}}{\sigma \cos \theta + i \sqrt{\sin^2 \theta - n^2}}, \quad (3.3.15)$$

$$\sigma = \rho_1/\rho, \quad n = c/c_1.$$

The phase of  $V(\theta)$  is given by

$$\Phi_v = -2 \tan^{-1} \left( \frac{\sqrt{\sin^2 \theta - n^2}}{\sigma \cos \theta} \right). \quad (3.3.16)$$

The total phase of the integrand in (3.3.2) for  $\theta_{cr} < \theta < \pi/2$  is (only the first exponential is taken into account)

$$\Phi(\theta) = k(z + z_0) \cos \theta + kr \sin \theta - \pi/4 + \Phi_v(\theta). \quad (3.3.17)$$

Differentiating  $\Phi(\theta)$  yields

$$\Phi'(\theta) = -k(z + z_0) \sin \theta + kr \cos \theta + \Phi'_v(\theta), \quad (3.3.18)$$

with

$$\Phi'_v(\theta) = \frac{-2\sigma \sin \theta (1 - n^2)}{[(\sigma^2 - 1) \cos^2 \theta + (1 - n^2)] \sqrt{\sin^2 \theta - n^2}}. \quad (3.3.19)$$

The stationary-phase equation  $\Phi'(\theta) = 0$  now is

$$r = (z + z_0) \tan \theta + \frac{A \tan \theta}{k \sqrt{\sin^2 \theta - n^2}}, \quad (3.3.20)$$

$$A = \frac{2\sigma (1 - n^2)}{(\sigma^2 - 1) \cos^2 \theta + (1 - n^2)}. \quad (3.3.21)$$

When the frequency is high enough, the influence of  $\Phi'_v$  is small everywhere except for a small vicinity of the critical angle  $\theta_{cr} = \sin^{-1} n$ . Near the critical angle  $\Phi'_v$  becomes infinite and introduces a second stationary phase point corresponding to the head wave.

Assuming  $\cos^2 \theta \approx 1 - n^2$  near  $\theta_{cr} = \sin^{-1} n$ , the coefficient  $A$  can be substantially simplified:

$$A \approx \frac{2\sigma (1 - n^2)}{(\sigma^2 - 1)(1 - n^2) + (1 - n^2)} = \frac{2}{\sigma}. \quad (3.3.22)$$

The stationary-phase equation (3.3.20) then becomes

$$r = (z + z_0) \tan \theta + \frac{2 \tan \theta}{k \sigma \sqrt{\sin^2 \theta - n^2}}, \quad (3.3.23)$$

The easiest way to analyze the solutions of equation (3.3.23) is to plot the right part of the equation. Figure 3.3 reproduced from Fuchs (1971) shows the determination of the stationary phase points for a solid/solid boundary. Though the model used by Fuchs is different from ours, the structure of the stationary phase equation for fluid/fluid and solid/solid interfaces is essentially the same.

Without the contribution of the phase of the reflection coefficient, equation (3.3.23) has just one solution for the geometrical (specular) reflection ( $\tan \theta = r/(z + z_0)$ ) discussed above. Since the term due to the reflection coefficient is positive, the curve showing the right part of (3.3.23) as a function of angle lies above the curve  $(z + z_0) \tan \theta$ . Due to the term  $\sqrt{\sin^2 \theta - n^2}$  in the denominator of  $\Phi'_v$ , the right-hand side of equation (3.3.23) goes to infinity at the critical angle.

For sufficiently large offsets  $r$  equation (3.3.23) has two solutions, one corresponding to the head wave (it is close to the critical angle  $\theta_{cr}$ ) and another to the reflected wave. The second stationary point is close to the angle of the geometrical reflection  $\theta = \tan^{-1} \frac{r}{z+z_0}$ .

Assuming that the stationary point for the head wave is at  $\theta = \theta_{cr}$ , the traveltime of the head wave is given by

$$t_h = \frac{\Phi(\theta_{cr})}{\omega}. \quad (3.3.24)$$

Ignoring the frequency-independent terms in the expression for  $\Phi(\theta)$  (3.3.17) (they will result only in the distortion of the pulse shape), we obtain



# Determination of Stationary Phases

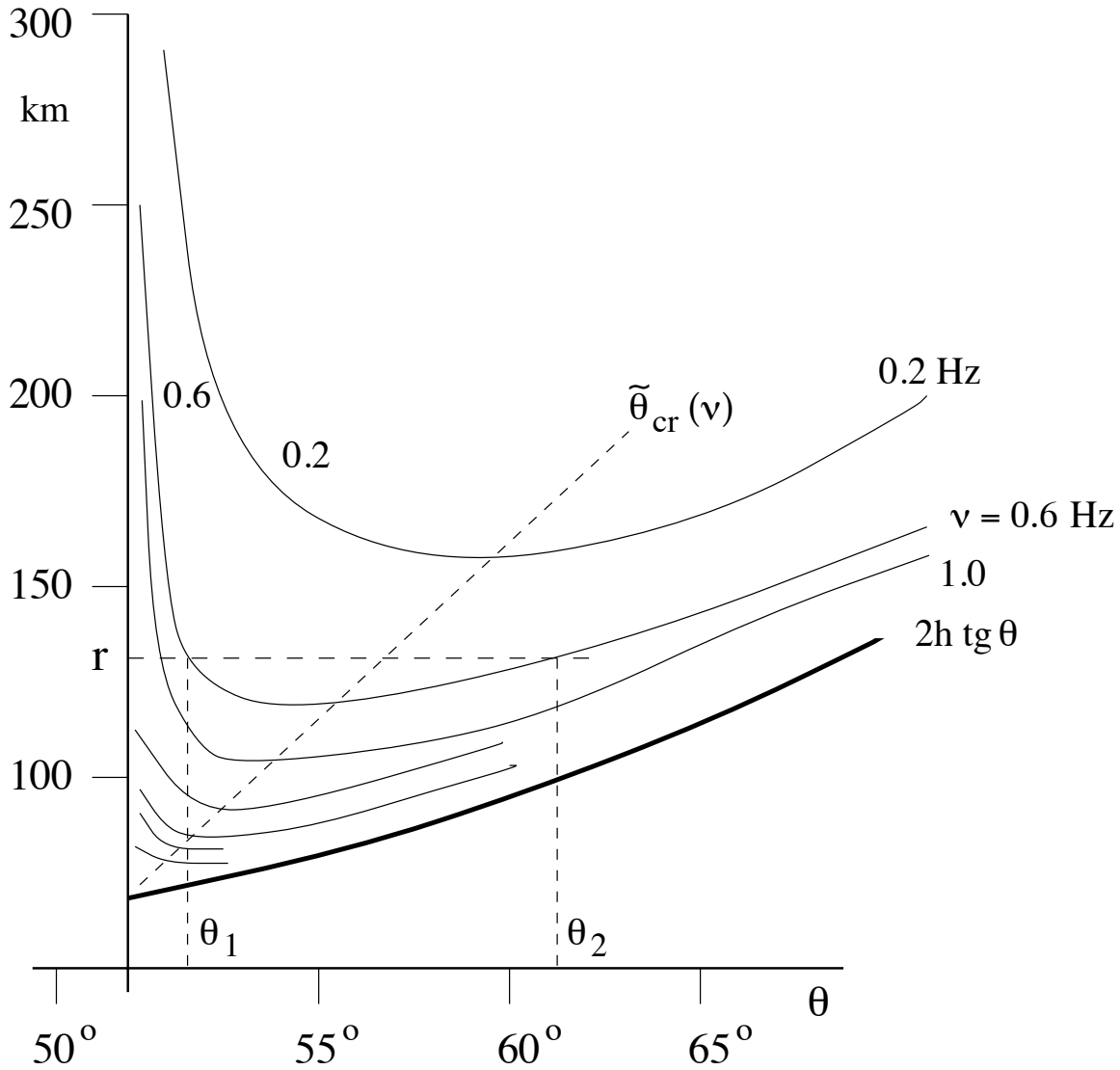


Figure 3.3: Graphic solution of the stationary-phase equation for the head wave and post-critical reflection at a solid/solid boundary (after Fuchs, 1971).  $\tilde{\theta}_{cr}$  is the frequency-dependent critical angle (the curves are calculated for different frequencies  $\nu$  with a step of 0.4 Hz). The  $P$ -wave velocity changes across the boundary from 6.4 km/s to 8.2 km/s;  $h=(z+z_0)/2=30\text{km}$ .

$$t_h = r/c_1 + (z + z_0) \cos \theta_{cr}/c. \quad (3.3.25)$$

The traveltime  $t_h$  may be also represented as

$$t_h = L/c_1 + (z + z_0)/(c \cos \theta_{cr}), \quad (3.3.26)$$

$L = r - (z + z_0) \tan \theta_{cr}$  is the path traveled by the head wave along the boundary with the velocity in the second medium  $c_1$ . Formulas (3.3.25,3.3.26) show that the head wave has a plane wavefront and propagates away from the boundary at the critical angle  $\theta_{cr}$ .

The most striking feature of the obtained solution is the frequency dependence of the critical angle and critical offset  $r_{cr}$ . With decreasing frequency, both the critical angle and critical offset increase making the velocity of the head wave frequency-dependent. Indeed, the horizontal velocity of the head wave at the critical distance is given by  $c/\sin \theta_{cr}$ ; for smaller frequencies,  $\sin \theta_{cr}$  is higher than  $n = c/c_1$ , leading to a decrease in the head-wave's velocity. At large  $r$ , the velocity of the head wave becomes less dependent on frequency.

It is interesting that at low frequencies there is a range of offsets (below the frequency-dependent critical distance  $r$ ) without any stationary points at all. Also note that the stationary point for the reflected wave deviates from the geometrical-seismics value with decreasing frequency. However, we should remember that the stationary phase method is accurate only at high frequencies, and all dependencies on frequency obtained by the SPM should be regarded with a certain caution.

The main problem in the stationary-phase treatment outlined above is that it properly accounts only for post-critical incidence angles. As we will see later from exact numerical results, sub-critical angles also make a significant contribution to the head wave. Unfortunately, even the first-order approximation of the SPM cannot produce any additional stationary points in the sub-critical domain because the phase of the reflection coefficient at sub-critical incidence is zero. While the reflection coefficient  $V(\theta)$  at sub-critical angles ( $\theta < \sin^{-1} n$ ) is real and does not change the phase of the integrand, a rapid variation in  $V(\theta)$  in the immediate vicinity of the critical angle makes the SPM approach inaccurate. Therefore, we will not seek a complete first-order SPM solution for the amplitude of the head wave; the properties of the head wave will be discussed in more detail in the next section, after application of saddle-point integration.

Despite the above problem with the stationary phase method, it should be emphasized that it enabled us to single out both principal components of the wavefield: the reflected and head waves. Later on, we will apply the SPM to the integral for the transmitted wave.

### 3.4 The method of steepest descent for the reflected wavefield

Now we will proceed with the analysis of the reflected wave by means of saddle-point integration. This section is based on the material from chapter 6 in the book by Aki

and Richards (1980); however, we'll correct several mistakes and fill in some gaps in the explanations.

The saddle-point method is designed to evaluate integrals of the type

$$I(x) = \int_c F(\xi) e^{xf(\xi)} d\xi, \quad (3.4.1)$$

where  $x$  is assumed to be large and positive, and  $f$  is an analytic complex function.

The idea of the method is to distort the integration path so that it would go through the saddle point of the function  $f(\xi)$  along the steepest descent path of  $Re f$ . Since the value of the integral is mostly determined by  $e^{xRe f(\xi)}$ , only a small part of the new integration path near the maximum (saddle point) of  $Re f$  makes the principal contribution to the integral. Since  $f(\xi)$  is analytic, contours of  $Re f = const$  and  $Im f = const$  are orthogonal to each other (Figure 3.4).

Therefore, the steepest descent path for the function  $Re f$  would be a line of constant phase ( $Im f = const$ ). One can see that the stationary phase and saddle-point integration methods have a lot in common: in both cases the integral is reduced to the contribution of a relatively short part of the path where the phase of the integral is stationary. The complexities of saddle-point integration are mostly associated with taking a proper care of the poles and branch cuts of the integrand affected by the transformation of the integration path.

Using the ray parameter  $p = \sin\theta/c$  in the integral expression for the reflected wave (3.2.4), we find

$$\phi_{refl} = i\omega \int_0^\infty V(p) \frac{p}{\zeta} e^{i\omega\zeta(z+z_0)} J_0(\omega pr) dp, \quad (3.4.2)$$

$\zeta = \sqrt{1/c^2 - p^2}$  is the vertical slowness; we recall that  $\zeta$  lies in the first quadrant  $Re \zeta \geq 0$ ,  $Im \zeta \geq 0$ .

### 3.4.1 Reflection from a low-velocity medium

We first assume that the incidence medium has a higher velocity:  $c > c_1$ . In order to make the integration path symmetric with respect to the origin, the Bessel function should be replaced with the Hankel function  $H_0^{(1)}$ :

$$J_0(x) = \frac{1}{2} [H_0^{(1)}(x) - H_0^{(1)}(-x)]. \quad (3.4.3)$$

Substituting equation (3.4.3) into (3.4.2) and noting that

$$\int_0^\infty -V(p) \frac{p}{\zeta} H_0^{(1)}(-\omega pr) dp = \int_{-\infty}^0 V(p) \frac{p}{\zeta} H_0^{(1)}(\omega pr) dp, \quad (3.4.4)$$

we obtain

$$\phi_{refl} = \frac{i\omega}{2} \int_{-\infty}^\infty V(p) \frac{p}{\zeta} e^{i\omega\zeta(z+z_0)} H_0^{(1)}(\omega pr) dp. \quad (3.4.5)$$

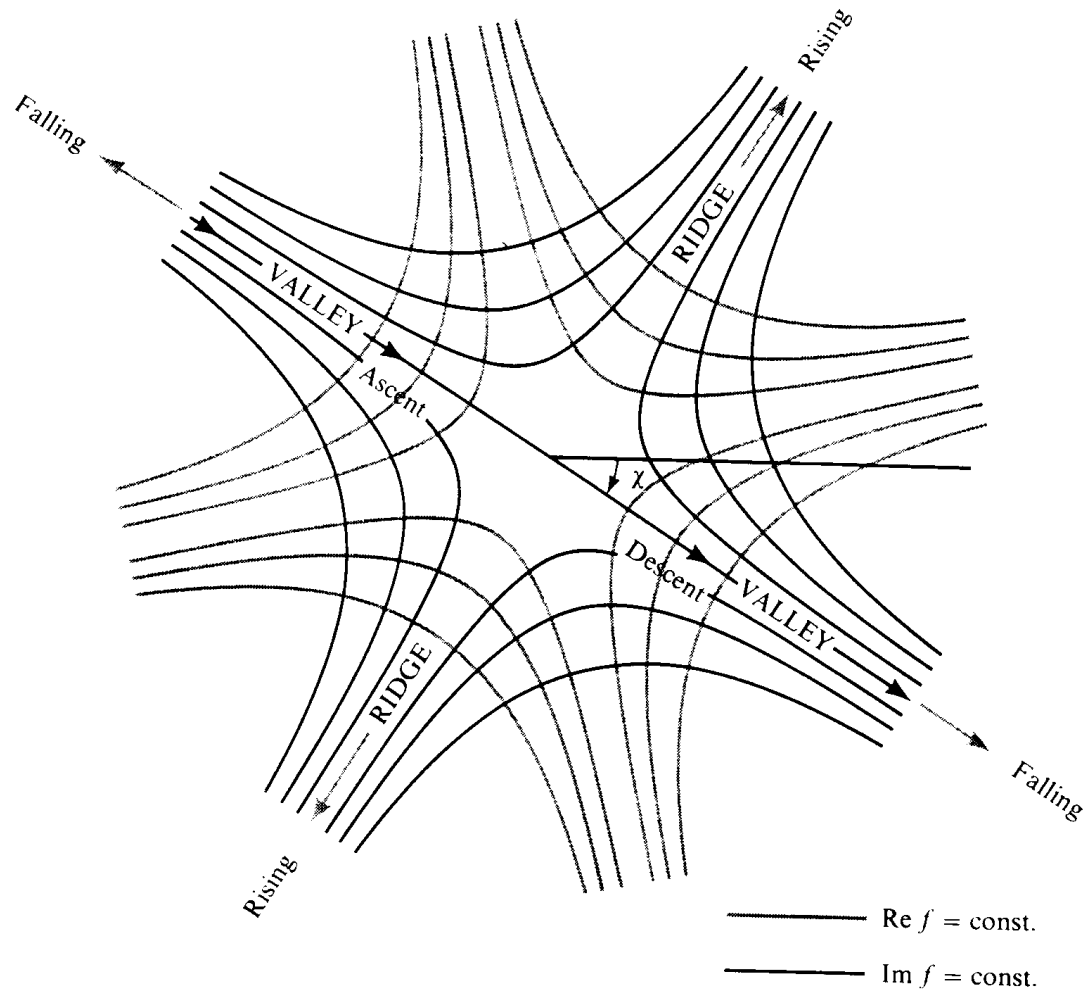


Figure 3.4: Structure of an analytic function  $f$  near its saddle point (after Aki and Richards, 1980). The steepest-descent path is inclined at  $-45^\circ$  to the positive direction of the  $x$ -axis.

Then we assume that the horizontal source-receiver distance is large compared to the wavelength, and replace the Hankel function with its asymptotic representation:

$$H_0^{(1)}(\omega pr) = \sqrt{\frac{2}{\pi\omega pr}} e^{i(\omega pr - \pi/4)}. \quad (3.4.6)$$

Clearly, the approximation (3.4.6) cannot be used near  $p = 0$  but we will avoid this point after deforming the integration path. The reflected wave becomes

$$\phi_{refl} = \sqrt{\frac{\omega}{2\pi r}} e^{i\pi/4} \int_{-\infty}^{\infty} V(p) \frac{p^{1/2}}{\zeta} e^{i\omega[pr + \zeta(z+z_0)]} dp. \quad (3.4.7)$$

Now we are ready for saddle-point integration. Before actually deforming the integration path, it is necessary to determine what sign of the square root in  $\zeta$  should be chosen. In the complex  $p$ -plane  $\zeta$  is double-valued, and it is convenient to make it a single-valued analytic function of  $p$  by means of some reasonable convention. Usually the complex  $p$ -plane is replaced by two planes, or Riemann sheets, on which  $\zeta$  is unambiguously determined. On the so-called top sheet,  $Im \zeta > 0$ , on the bottom sheet  $Im \zeta < 0$ ; the sheets are connected along branch cuts on which  $Im \zeta = 0$ . The points on the branch cuts where  $\zeta = 0$  ( $p = \pm 1/c$ ) are called branch points.

An alternative way of introducing branch cuts is discussed by Bleistein (1984). One should keep in mind that branch cuts represent just a convenient way to keep track of the signs of double-valued functions in the complex plane. While the branch points are strictly fixed, there is some flexibility in devising branch cuts for any particular problem.

Let us find the position of the branch cuts on the complex  $p$ -plane. For the imaginary part of  $\zeta$  to be zero,  $1/c^2 - p^2$  should be real, and  $1/c^2 - p^2 \geq 0$ . Therefore,

$$1/c^2 - (Re p)^2 + (Im p)^2 - 2i(Re p)(Im p) \geq 0. \quad (3.4.8)$$

We have seen that the imaginary part of  $1/c^2$  is small and positive (or zero, if there is no attenuation). Thus,

$$(Re p)(Im p) = \epsilon, \quad \epsilon \geq 0. \quad (3.4.9)$$

This determines the branch cuts as hyperbolas in the first and third quadrants. We have to make sure that on the cuts  $\zeta^2$  is nonnegative, or

$$(Re p)^2 \leq Re(1/c^2) + (Im p)^2. \quad (3.4.10)$$

When  $c$  is real, the conditions (3.4.9,3.4.10) are satisfied on the whole imaginary axis and on the part of the real axis between the branch points  $-1/c$  and  $1/c$  (Figure 3.5). In an attenuative medium, the branch cuts move into hyperbolas in the first and third quadrants limited by the branch points located close to the points  $p = 1/c$  and  $p = -1/c$ .

The same structure of the branch cuts is valid for the vertical slowness in the reflecting medium  $\zeta_1$ , the only difference being that the branch points are at  $p = \pm 1/c_1$ . We will see that the relative position of the branch points is extremely important in the evaluation of the integral for the reflected wave.

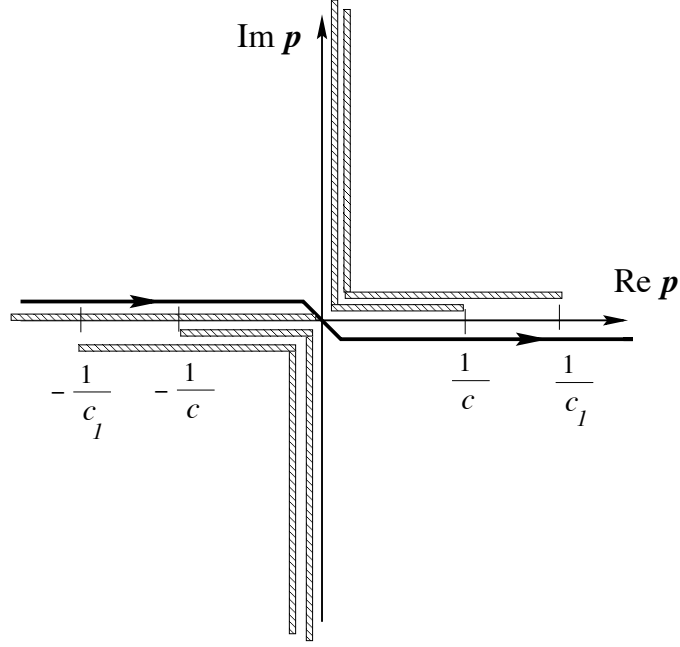


Figure 3.5: Branch cuts for the vertical slownesses on the complex  $p$ -plane.

The analysis of the branch cuts shows that (assuming small attenuation) our integration path lies above the branch cuts in the left half-space ( $\text{Re } p < 0$ ), and below the branch cuts in the right half-space. We also have a branch point for  $p^{1/2}$  on the integration path, but we will avoid it while moving towards the path of steepest descent.

At the saddle point, the real part of the exponential function  $xf(\xi)$  (see equation [3.4.1]) reaches its maximum, while the imaginary part is stationary. Therefore, the first derivative of  $xf(\xi)$  at the saddle point is zero. In our case,  $x = \omega$ ,  $\xi = p$ , and

$$f(p) = i [pr + \zeta(z + z_0)], \quad (3.4.11)$$

and

$$f'(p) = i [r - p(z + z_0)/\zeta], \quad (3.4.12)$$

$$f''(p) = -i(z + z_0)/(c^2\zeta^3). \quad (3.4.13)$$

The saddle point is determined by  $f'(p) = 0$ :

$$r = p(z + z_0)/\zeta; \quad \tan \theta = \frac{r}{z + z_0}. \quad (3.4.14)$$

Therefore, the saddle point lies on the real axis to the left of both branch cuts (if  $c > c_1$ ). This saddle point corresponds to the same geometrical reflection we have previously obtained by the stationary phase method. Our task now is to find the steepest descent path from the saddle point.



asymptote in the second quadrant makes the same angle (equal to the incidence angle of the geometrical reflection) with the negative  $p$ -axis. Note that the asymptotes cross the imaginary  $p$ -axis at different points away from the origin.

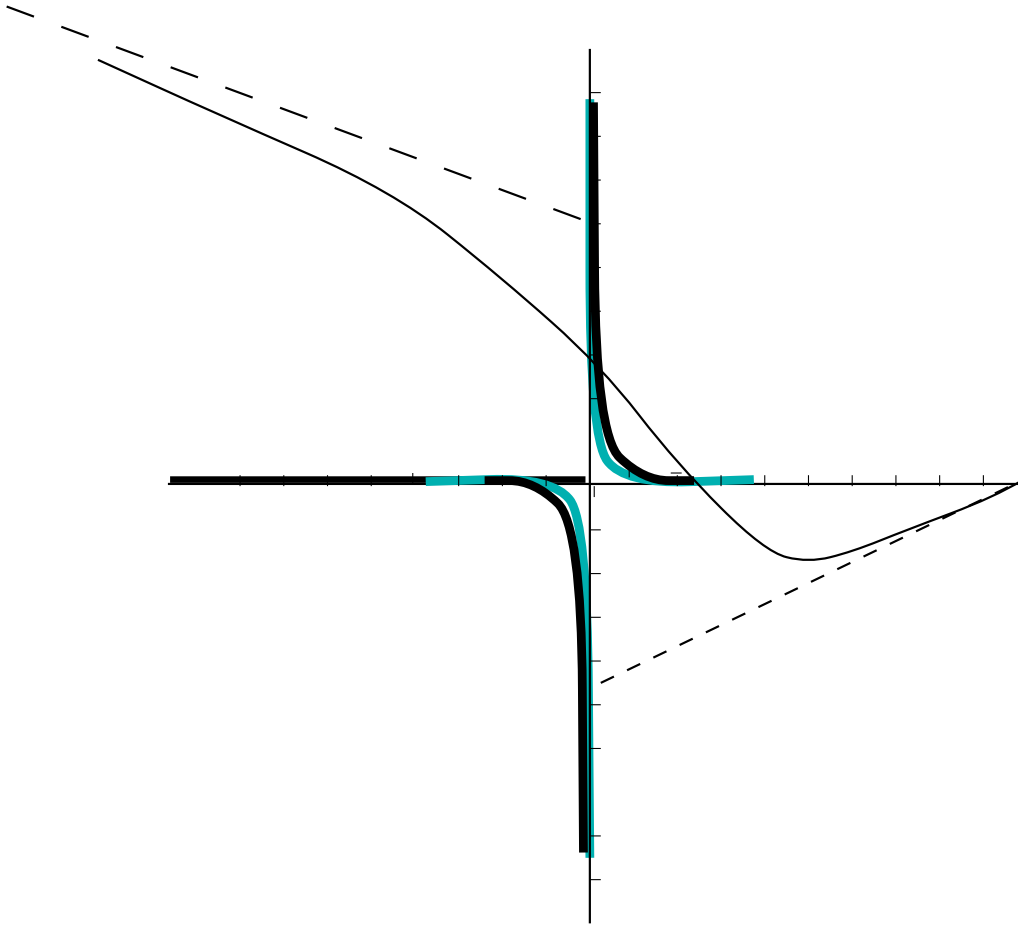


Figure 3.7: The asymptotes of the steepest-descent path for the reflected wave.

One subtlety here is associated with the transition from the top to the bottom Riemann sheet at the intersection of the path with the imaginary  $p$ -axis. This transition is necessary to preserve the continuity of  $\zeta$  and  $\zeta_1$  (and the integrand) on the integration path. Indeed, in the first quadrant near the imaginary axis (assuming real  $c$ )

$$\zeta \approx \sqrt{1/c^2 + (Im p)^2 - 2i(Im p)|Re p|},$$

while in the second quadrant

$$\zeta \approx \sqrt{1/c^2 + (Im p)^2 + 2i(Im p)|Re p|}.$$

If we require that  $Im \zeta > 0$ , the real part of  $\zeta$  will change sign at the branch cut near the imaginary axis. The integration path returns to the top Riemann sheet ( $Im \zeta > 0$ ) at the saddle point ensuring an exponential decay of the integrand at the arcs at  $Re p = \pm\infty$ .



Most importantly, we have not touched the branch points or poles during the transformation. In addition to the pole  $\zeta = 0$  (it is also a branch point), the poles may be associated with the reflection coefficient  $V$  (2.4.11). It is easy to verify that there are no poles of  $V(p)$  on the original integration path, and the poles in the complex plane are not affected during the transformation of the path. Physically, this means that there are no surface waves in this model.

With increasing geometrical incidence angle (the case of  $r \gg z + z_0$ ), the steepest-descent path tilts closer to the imaginary axis, thus causing some interference with the branch points. The contributions of the branch points correspond to inhomogeneous reflected waves coupled to nongeometrical transmitted waves. These waves will be examined later on, in the section devoted to the transmitted wavefield.

Therefore, the integral reduces to the contribution of a certain vicinity of the saddle point. The methodology of evaluating the contribution of the saddle point is essentially the same as in the stationary phase method. The function  $f(p)$  is expanded into a Taylor series near the saddle point:

$$f(p) = f(p_s) + \frac{1}{2} f''(p_s)(p - p_s)^2 + \dots \quad (3.4.16)$$

On the integration path the difference  $f(p) - f(p_s)$  or, in other words, the term containing  $f''(p_s)$  is real and negative (see equation [3.4.15]), causing an exponential decay of the integrand away from the saddle point. The degree of the decay depends on how large the parameters  $\omega r$  and  $\omega(z + z_0)$  are.

Since the integration is carried out only in the vicinity of the saddle point, the slowly varying terms can be taken out of the integral while series (3.4.16) can be truncated after the second term:

$$\phi_{refl} = \sqrt{\frac{\omega}{2\pi r}} V(p_s) \frac{p_s^{1/2}}{\zeta(p_s)} e^{i\pi/4} e^{i\omega R/c} \int_C e^{\frac{1}{2}\omega f''(p_s)(p-p_s)^2} dp, \quad (3.4.17)$$

where  $C$  covers a vicinity of the saddle point on the integration path. Let us do the derivation of the saddle-point contribution carefully because the saddle-point formula given in Aki and Richards (Box 6.3) is in error and does not lead to the desired result.

First, note that the integrand and the integration path are symmetric with respect to the stationary point, so we will examine the part of the path to the right of  $p_s$ . Introducing a new variable  $y = |p - p_s|$ ,  $p - p_s = ye^{i\chi}$ , where  $\chi$  is the angle between the path and the positive direction of the  $x$ -axis, the integral from equation (3.4.17) can be represented as

$$I = 2 \int_0^b e^{\frac{1}{2}\omega f''(p_s)y^2 e^{2i\chi}} e^{i\chi} dy, \quad (3.4.18)$$

$b$  is real and positive.

Since we have established that  $f''(p_s) e^{2i\chi}$  is a negative real number, it is convenient to change variables once again:

$$v = \sqrt{-\omega f''(p_s) e^{2i\chi}} y. \quad (3.4.19)$$

Then integral (3.4.18) becomes

$$I = 2 \frac{e^{i\chi}}{\sqrt{-\omega f''(p_s) e^{2i\chi}}} \int_0^d e^{-v^2/2} dv, \quad (3.4.20)$$

$$d = b \sqrt{-\omega f''(p_s) e^{2i\chi}}.$$

We have arrived at the well-known normal probability integral:

$$\int_{-d}^d e^{-v^2/2} dv = \sqrt{2\pi} \left(1 - \sqrt{\frac{2}{\pi}} \frac{e^{-d^2/2}}{d} + \dots\right) \quad (3.4.21)$$

Unlike the SPM, saddle point integration does not require the limits of the integral to be formally extended to  $\pm\infty$ . The exponential decay of the integrand allows the limits to remain finite, and we get the asymptotic result by retaining only the first term of the series (3.4.21) under the assumption of a large parameter in the exponential. Substituting equation (3.4.21) into (3.4.20) yields

$$I = \frac{e^{i\chi} \sqrt{2\pi}}{\sqrt{-\omega f''(p_s) e^{2i\chi}}}. \quad (3.4.22)$$

Using equation (3.4.13) for the second derivative of  $f$  and recalling that  $\chi = -45^\circ$ , we get

$$I = \frac{e^{-i\pi/4} \sqrt{2\pi(z+z_0)^2}}{\sqrt{\omega cR^3}}. \quad (3.4.23)$$

Substituting this result into the expression for the reflected wave (3.4.17) gives

$$\phi_{refl} = V(p_s) e^{ikR} \sqrt{\frac{\omega}{2\pi r}} \frac{p_s^{1/2}}{\zeta(p_s)} e^{i\pi/4} \frac{e^{-i\pi/4} \sqrt{2\pi(z+z_0)^2}}{\sqrt{\omega cR^3}} = V(p_s) \frac{e^{ikR}}{R}. \quad (3.4.24)$$

Thus, we have obtained the same geometrical-seismics solution, this time by means of saddle-point integration. Among the approximations made during the derivation, the crudest one is perhaps the replacement of the integrand with the quadratic Taylor series and using the asymptotic expression for the probability integral. Depending on the value of the large parameter in the exponential, our integration path may extend relatively far from the saddle point making it necessary to add more terms to the expansion of  $f(p)$ . This leads to the so-called wavefront expansions, which are more accurate than the geometrical-seismics expression. An even higher accuracy may be achieved by numerical integration over the transformed path with the exact computation of  $f(p)$ . This also eliminates the error due to another approximation - a fixed angle between the integration path and the real axis.

Another, often more acceptable approximation is the one for the Hankel function; it is sometimes used in more accurate integration methods as well.

### 3.4.2 Reflection from a high-velocity medium: the head wave

Now let us consider the case when the source is located in the low-velocity medium ( $c < c_1$ ). Then the branch points near or on the real axis will be interchanged, and the point  $p = 1/c_1$  will be to the left of  $p = 1/c$ . If the saddle point  $p_s$  belongs to the interval  $0 < p_s < 1/c_1$ , the analysis discussed above is entirely valid. The integration path is the same, and the integral is reduced to the contribution of a vicinity of the saddle point. In the end, we get the same geometrical-seismics solution (3.4.24) as for the case  $c > c_1$ , and the reflection coefficient  $V(p_s)$  remains real. For the saddle point to satisfy  $0 < p_s < 1/c_1$ , the receiver should lie in the so-called “subcritical” region corresponding to subcritical incidence angles  $\sin \theta < \sin \theta_{cr} = c/c_1$ .

Problems arise when the receiver is in the postcritical region  $\sin \theta > \sin \theta_{cr}$ , and the saddle point is located between the branch points:  $1/c_1 \leq p_s \leq 1/c$ . While geometrically the steepest descent path remains the same, now it lies on the lower Riemann sheet  $Im \zeta_1 < 0$  near the saddle point. As a result, the value of  $\zeta_1$  contained in the reflection coefficient at the saddle point would have the wrong sign.

Since the branch cut for  $\zeta_1$  ends at  $p = 1/c_1$ , there is no way to return to the top Riemann sheet for  $\zeta_1$  above the saddle point as we did in the previous case. On the other hand, as shown above, it is impossible to stay on the same Riemann sheet while crossing the branch cut if we are to preserve the continuity of the integrand. The solution for a new integration path is shown in Figure 3.8. The idea is to cross the branch cut for  $\zeta_1$  twice, thus making the integrand continuous.

The path starts on the top Riemann sheet (for both vertical slownesses) in the second quadrant and follows along the branch cut for  $\zeta_1$  into the first quadrant. Then it crosses the cut into the lower Riemann sheet  $Im \zeta_1 < 0$  ( $Im \zeta > 0$  as before) into the second quadrant and turns into the steepest descent path. The path crosses both branch cuts and returns to the first quadrant where  $Im \zeta < 0$ ,  $Im \zeta_1 > 0$ . At the saddle point the path returns to the top Riemann sheet for  $\zeta$ , where  $Im \zeta > 0$ ,  $Im \zeta_1 > 0$ . This path allows us to keep the correct signs of both vertical slownesses near the saddle point and on the ends of the real axis and, at the same time, preserve the continuity of the integrand.

If the frequency is large enough for the integrand to become negligibly small at the intersection of the steepest-descent path with the imaginary axis (point  $F'$ ), it is possible to avoid the lower Riemann sheet for  $\zeta_1$  altogether by embarking on the steepest-descent path at  $F'$  after moving up along the imaginary axis. However, in general we have to continue the path along the imaginary axis up to point  $D$  where the integrand becomes negligible. By doing this, we allow the oscillations of the integrand to cancel the contribution of the path along the imaginary axis.

The distortion of the path in the second quadrant (from  $A$  to  $B$  to  $C$ ) is designed to demonstrate that the part of the original path from  $A$  to  $C$  contributes nothing. Another way to prove this is to apply the stationary phase method and show that there are no stationary points for  $p < 0$ . In fact, we have done this before by decomposing the Bessel function into two exponents and proving that the exponent containing the term  $(-kr \sin \theta)$  ( $p < 0$ ) does not produce stationary points. Physically, negative  $p$  correspond to nonphysical waves propagating towards the source in the horizontal direction.

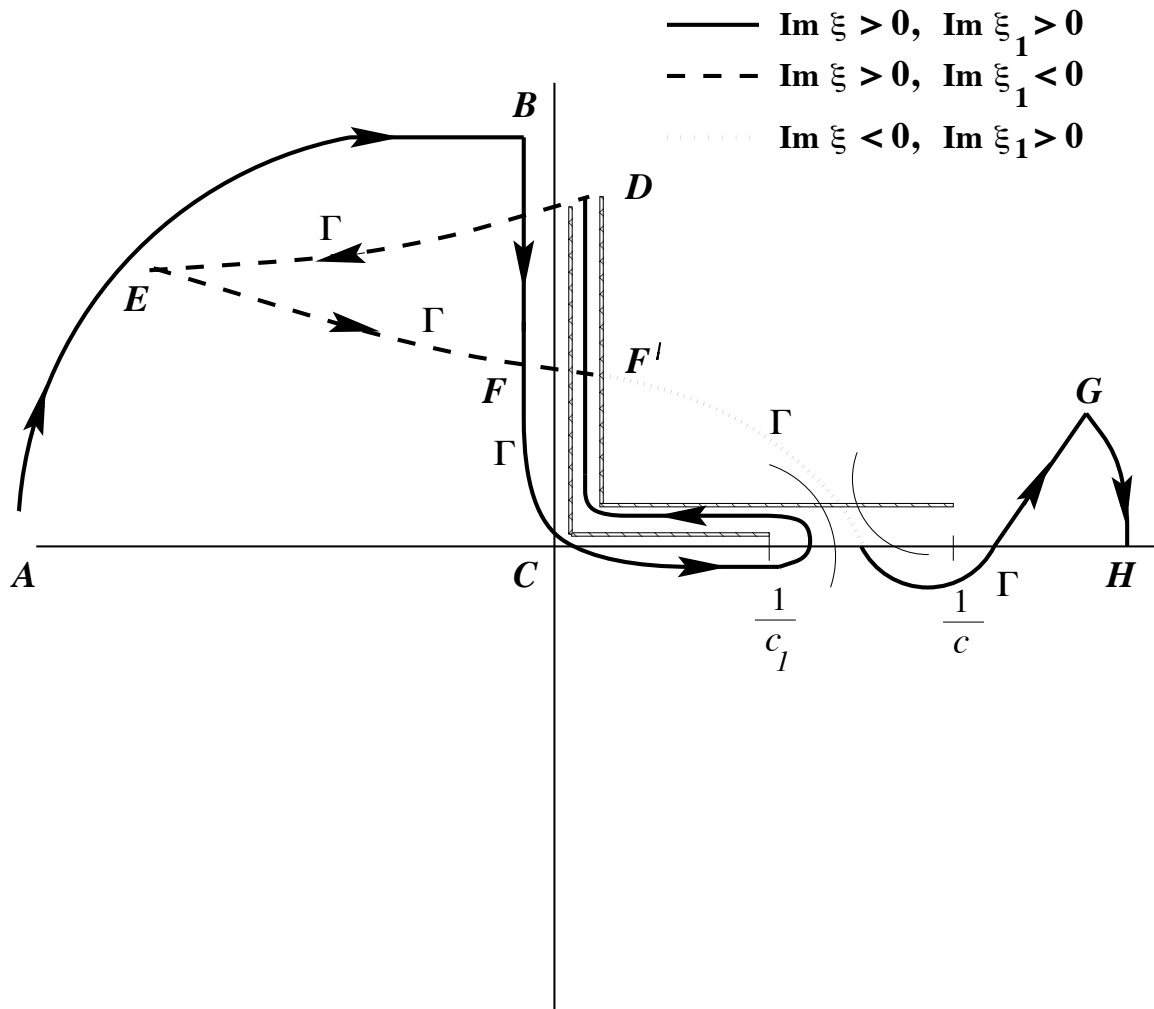


Figure 3.8: The steepest-descent integration path for the case when the receiver is in the post-critical domain (after Aki and Richards, 1980).

Now our task is to find out which parts of the path make the principal contributions to the integral. Arc AB does not contribute anything because the integrand is negligibly small for large negative  $p$  due to the exponential term ( $Im \zeta > 0$ ). The same is true for arc GH in the first quadrant. Away from real axis the integrand becomes small because the integrand contains the term  $e^{-\omega Im(p)r}$ . Assuming that  $\omega$  is very large we neglect the integral along the imaginary axis. Therefore, in addition to the contribution of the saddle point, we have to take into account the integral around the branch cut near the real axis.

The saddle-point integration along the steepest-descent path leads to the same expression for the geometrical reflection discussed above. However, while the reflection coefficient for sub-critical angles is real, it becomes complex in the post-critical domain. The frequency-independent phase shift in the reflection coefficient distorts the shape of the reflected wave making it different from the shape of the incident wave.

The most interesting effect in the post-critical domain is the generation of the so-called head wave associated with the integral around the branch cut. It is important that the sign of the real part of  $\zeta_1$  changes when the integration path turns around the branch point and goes above the branch cut. Below the cut, on the original integration path,  $Im \zeta_1 > 0$  and  $Re \zeta_1 > 0$ . Above the cut,

$$\zeta_1 \approx \sqrt{1/c_1^2 - (Re p)^2 - 2i Re p Im p}$$

Since the path stays on the upper Riemann sheet with  $Im \zeta_1 > 0$ , above the cut we have to choose the root with  $Re \zeta_1 < 0$ . This means that  $\cos \theta_1$  in the reflection coefficient (2.4.11) will be also negative.

Using equation (3.4.7) for the reflected wave, the integral below the branch cut can be represented as

$$\phi^{(1)} = \sqrt{\frac{\omega}{2\pi r}} e^{i\pi/4} \int_0^{1/c_1} V(p) \frac{p^{1/2}}{\zeta} e^{i\omega [pr + \zeta(z+z_0)]} dp, \quad (3.4.25)$$

$$V^{(1)} = \frac{c_1 \rho_1 \cos \theta - c \rho \cos \theta_1}{c_1 \rho_1 \cos \theta + c \rho \cos \theta_1}. \quad (3.4.26)$$

The integral above the cut has the opposite sign and the reflection coefficient is different:

$$\phi^{(2)} = -\sqrt{\frac{\omega}{2\pi r}} e^{i\pi/4} \int_0^{1/c_1} V(p) \frac{p^{1/2}}{\zeta} e^{i\omega [pr + \zeta(z+z_0)]} dp, \quad (3.4.27)$$

$$V^{(2)} = \frac{c_1 \rho_1 \cos \theta + c \rho \cos \theta_1}{c_1 \rho_1 \cos \theta - c \rho \cos \theta_1}. \quad (3.4.28)$$

The integrand between  $p = 0$  and  $p = 1/c_1$  is oscillatory, and in keeping with the stationary phase methodology, the main contribution is made by a certain vicinity of the point where the phase changes most slowly. There are no stationary phase points  $f'(p) = 0$  between  $p = 0$  and  $p = 1/c_1$  because the only stationary point corresponds to the geometrical reflection (it is the saddle point). However, the minimum of  $f'(p)$  is

reached at the branch point  $p = 1/c_1$ . Expanding the exponent function near the branch point, we get

$$f(p) = f(1/c_1) + f'(1/c_1)(p - 1/c_1). \quad (3.4.29)$$

The terms of the second and higher order have been ignored. The phase term at the branch point is

$$f(1/c_1) = i[r/c_1 + (z + z_0)\sqrt{1/c^2 - 1/c_1^2}] = i[r/c_1 + (z + z_0)\cos\theta_{cr}/c] = i t_h \quad (3.4.30)$$

describes the traveltime of the head wave  $t_h$  that we obtained earlier in equation (3.3.25) by the stationary phase method.

The first derivative of the phase function at the branch point is given by

$$f'(1/c_1) = i \left[ r - \frac{(z + z_0)c}{c_1\sqrt{1 - c^2/c_1^2}} \right] = i L, \quad (3.4.31)$$

$L$  is the distance traveled by the head wave along the boundary.

In order to find an approximation for the reflection coefficient near the branch point, we represent  $\cos\theta_1 = c_1\sqrt{1/c_1^2 - p^2} \approx \sqrt{2c_1}\sqrt{1/c_1 - p}$ , and  $V(p)$  near the branch point below the cut (3.4.26) becomes

$$V^{(1)} = \frac{1 - x}{1 + x} \approx 1 - 2x.$$

$$x = \frac{c\rho\cos\theta_1}{c_1\rho_1\cos\theta} \approx \frac{c\rho\sqrt{2c_1}\sqrt{1/c_1 - p}}{c_1\rho_1\sqrt{1 - c^2/c_1^2}}.$$

In the same fashion, the reflection coefficient above the cut (3.4.28) is

$$V^{(2)} = \frac{1 + x}{1 - x} \approx 1 + 2x.$$

The integrals above and below the cut (3.4.25,3.4.27) contain the constant part of the reflection coefficients  $V^{(1)} = V^{(2)} = 1$  and, therefore, cancel each other; only the variable part  $\pm 2x$  contributes to the final result. After taking the slowly varying terms out of the integral, we obtain the following approximation for the total integral around the branch cut:

$$\phi_{head} = \phi^{(1)} + \phi^{(2)} = -4\sqrt{\frac{\omega}{2\pi r}} e^{i\pi/4 + i\omega t_h} \frac{c\rho\sqrt{2c_1}}{c_1\rho_1\sqrt{1 - c^2/c_1^2}} \frac{c\sqrt{1/c_1}}{\sqrt{1 - c^2/c_1^2}} I(L), \quad (3.4.32)$$

$$I(L) = \int_0^{1/c_1} \sqrt{1/c_1 - p} e^{i\omega L(p - 1/c_1)} dp. \quad (3.4.33)$$

After some small algebra,

$$\phi_{head} = -4 \sqrt{\frac{\omega}{\pi r}} e^{i\pi/4 + i\omega t_h} \frac{c^2 \rho}{c_1 \rho_1 (1 - c^2/c_1^2)} I(L). \quad (3.4.34)$$

In order to evaluate integral (3.4.33), it is convenient to substitute  $iy^2 = p - 1/c_1$ . Then  $dp = 2iy dy$  and

$$I(L) = -2 e^{i\pi/4} \int_0^{\frac{e^{i\pi/4}}{\sqrt{c_1}}} y^2 e^{-\omega L y^2} dy. \quad (3.4.35)$$

We assume that the path of integration over  $y$  lies in the first quadrant at  $45^\circ$  to the real axis. While choosing the sign for  $y$  it is necessary to make sure that  $\sqrt{1/c_1 - p}$  remains positive. Recalling that  $\omega$  is supposed to be large, we formally extend the integration path to infinity. The integrand in (3.4.35) is an analytic function that does not have poles between the path of integration and the real axis. Therefore, the integral over a closed path including the path of integration and returning to the origin along the real axis will give zero. This means that the integration along the  $45^\circ$  line in the first quadrant in (3.4.35) may be replaced with integration along the real axis.

Using

$$\int_0^\infty y^2 e^{-\omega L y^2} dy = \frac{\sqrt{\pi}}{4(\omega L)^{3/2}},$$

we get for  $I(L)$ :

$$I(L) = -e^{i\pi/4} \frac{\sqrt{\pi}}{2(\omega L)^{3/2}}, \quad (3.4.36)$$

Substituting equation (3.4.36) into (3.4.34) yields

$$\phi_{head} = \frac{i}{\omega} \frac{2c^2 \rho}{c_1 \rho_1 (1 - c^2/c_1^2)} \frac{e^{i\omega t_h}}{r^{1/2} L^{3/2}}. \quad (3.4.37)$$

This is an asymptotic expression for the head wave valid everywhere except for some vicinity of the critical ray  $\theta = \theta_{cr}$  for which  $L = 0$ .

### 3.5 Properties of the head wave

Before analyzing asymptotic formula (3.4.37), let us consider some physical aspects of the generation of the head wave. At post-critical incidence, the horizontal velocity of the incident, reflected and transmitted waves is smaller than the velocity  $c_1$  in the reflecting medium, while the head wave propagates along the boundary with the constant velocity  $c_1$ . Therefore, the head wave travels along the boundary ahead of the wavefront of the incident wave.

This means that at the critical angle the reflected/transmitted waves split up into two groups which propagate along the boundary independently of each other (Figure 3.9). The

transmitted wave whose wavefront at the critical incidence angle is perpendicular to the boundary, splits from the incidence wave and continues to travel along the boundary with the velocity  $c_1$ . While sliding along the boundary, this wave radiates the head wave back into the low-velocity medium. The wavefront of the head wave in the incidence plane is a straight line tangential to the wavefront of the reflected wave at the critical ray. Due to the axial symmetry of the problem, the wavefront of the head wave is conical in space.

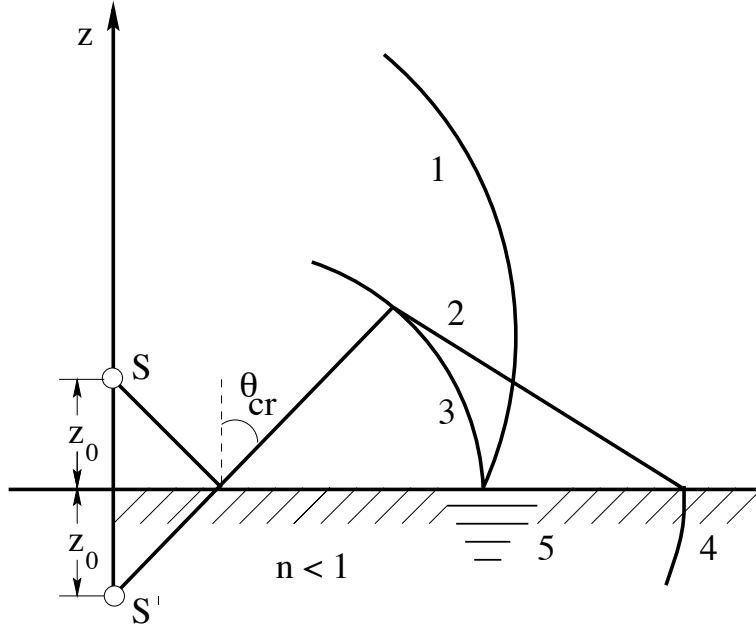


Figure 3.9: Wavefronts of the reflected/transmitted waves at a fluid/fluid boundary (after Brekhovskikh, 1980). 1 - Direct (incident) wave; 2 - head wave; 3 - reflected wave; 4 - transmitted homogeneous wave; 5 - transmitted inhomogeneous (evanescent) wave.

The second group that propagates along the boundary behind the first one, is represented by the incident, reflected and transmitted wave. The horizontal velocity of the incident wave at post-critical angles is smaller than  $c_1$ , and the transmitted wave is inhomogeneous, exponentially decaying away from the boundary.

Asymptotic formula (3.4.37) enables us to understand some basic features of the head wave. First, the amplitude decay with distance is given by the factor  $r^{-1/2}L^{-3/2}$ . For large  $r$  this factor becomes just  $r^{-2}$ , which means that the head wave decays with horizontal offset much more rapidly than the incident or reflected wave. Such a rapid decay is explained by the loss of energy due to the radiation into the low-velocity medium during the head-wave propagation along the boundary. It is interesting that the amplitude of the head wave even increases if the source and/or receiver are moved away from the boundary while the horizontal distance between them is kept constant. In this case,  $r = const$ , but  $L$  (the path traveled by the head wave along the boundary) becomes smaller leading to a higher head-wave amplitude. Although this amplitude behavior seems unusual, it can be easily understood by recalling that the energy loss of the head wave is mostly associated with the path along the boundary.



According to expression (3.4.37), in the vicinity of the critical ray the head wave decays with  $r$  even more rapidly than  $r^{-2}$ . At the critical ray itself  $L = 0$ , and the asymptotic formula (3.4.37) is no longer valid. Brekhovskikh (1980) derives a more accurate asymptotic expression for the head wave in the near-critical area by making more elaborate expansions of the integrands in branch-cut integrals similar to (3.4.25) and (3.4.27).

Furthermore, the geometrical-seismics formula (3.4.24) for the reflected wave is also inaccurate near the critical ray. Although the expression (3.4.24) remains finite at the critical ray, some of the expansions used to derive it become divergent. One of the main assumptions made during the steepest-descent integration is that the reflection coefficient is a slowly-varying function of the horizontal slowness near the saddle point. This assumption breaks down near the critical ray where  $dV/d\theta$  is infinite.

The shapes of both the post-critical reflection and head wave are different from the shape of the incident wave. Close to the critical ray, these two waves interfere with each other giving rise to a complicated waveform that is very sensitive to the traveltimes and shapes of both arrivals. Therefore, in spite of the existence of asymptotic solutions for the critical ray and its vicinity (Brekhovskikh, 1980), it is preferable to use more exact numerical methods in this area.

The solution (3.4.37) is obtained in the frequency domain. The factor  $e^{i\omega t_h}$  is responsible for the traveltime of the head wave; it will cause a shift of  $t_h$  in the time domain. If the rest of the formula were real and did not depend on frequency, the shape of the head and incident wave would be identical. However, the asymptotic formula (3.4.37) contains the term  $i/\omega$  which corresponds to integration in the time domain. Therefore, the shape of the head wave is determined by the integral of the incident wave, and the spectrum of the head wave is shifted towards low frequencies with respect to the spectrum of the source pulse. However, we should remember that the above analysis is based on asymptotic methods. Exact numerical results discussed below give a more accurate description of the properties of the head wave.

The most straightforward way to study the properties of the head wave is to evaluate the exact integral (3.2.4) for the reflected wave. The results below are obtained by direct numerical integration of (3.2.4) for the model of a fluid/solid boundary. In this case, the integral expression remains the same but the reflection coefficient has a different form. Integration around the branch cut yields an asymptotic formula for the head wave very similar to expression (3.4.37), with the same phase term and dependencies on  $r$ ,  $L$ , and  $\omega$ ; only the constant coefficient containing elastic parameters is different.

The plots in Figure 3.10 are generated by calculating the contributions of sub-critical and post-critical incidence angles separately. The upper plot is the contribution of  $\theta < \sin^{-1}(c/c_1)$  obtained by numerical integration of (3.2.4) from  $\theta = 0$  to  $\theta = \sin^{-1}(c/c_1)$  and subsequent application of the inverse Fourier transform. The middle plot is the result of the same operation for post-critical incidence angles  $\sin^{-1}(c/c_1) < \theta < \pi/2$ . The plot on the bottom is the total seismogram that would be recorded by a real receiver. The influence of inhomogeneous waves is negligible because the source is far away from the boundary.

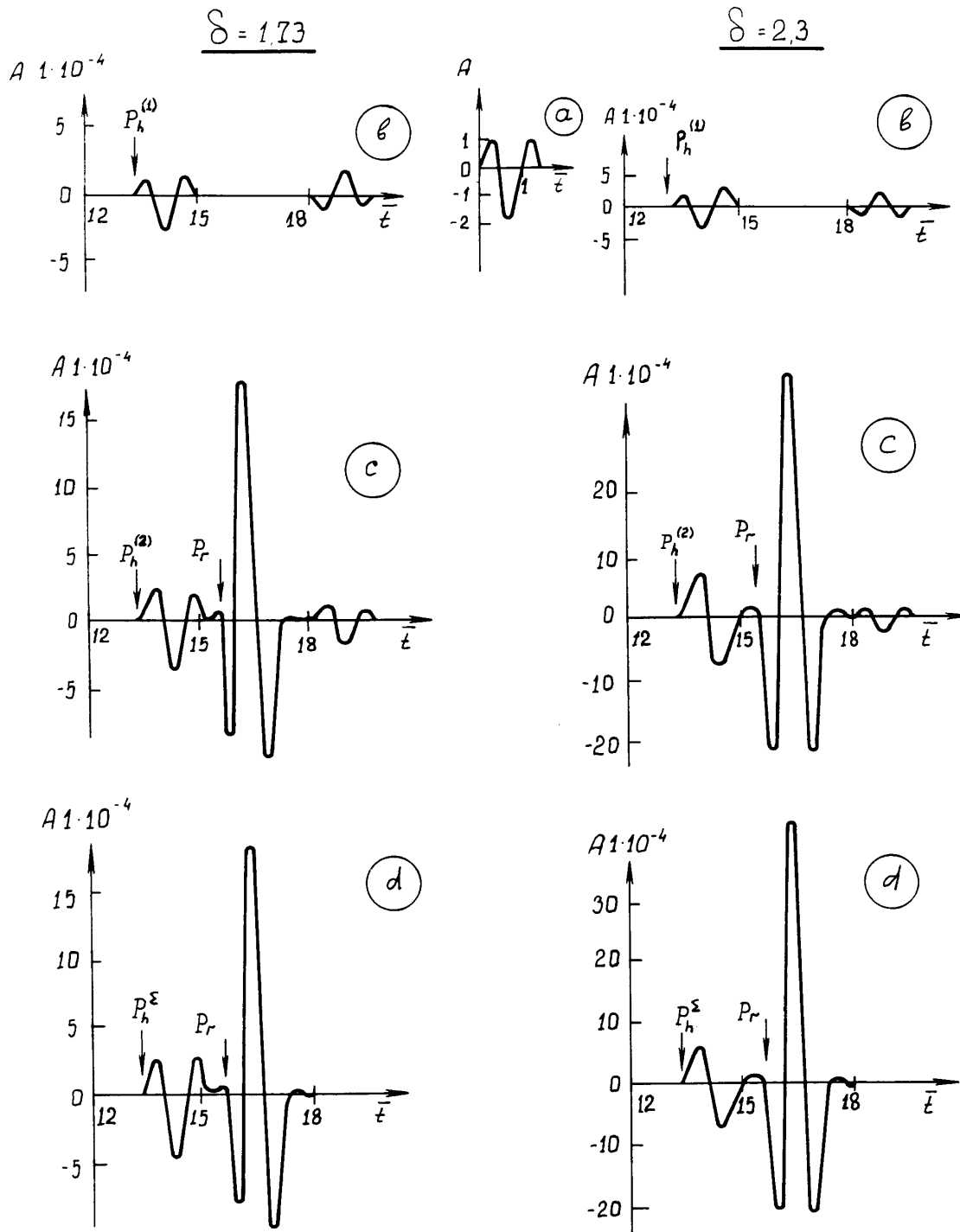


Figure 3.10: Exact synthetic seismograms of the P-wave reflected from a fluid/solid boundary. a - the incident pulse; b - the result of integration over sub-critical incidence angles; c - the result of integration over post-critical incidence angles; d - the total seismogram to be recorded by a real receiver. The model parameters are:  $n=0.7$ ,  $\sigma=2$ ,  $\bar{h} = z_0/\lambda = 2$  ( $z = z_0$ ,  $\lambda$  is the predominant wavelength),  $\bar{r} = r/\lambda = 15$ .  $\delta$  (shown on the plots) is the ratio of the P to S-velocity in the solid medium.

The splitting of the integration path made it possible to single out two components of the head wave, one due to sub-critical incidence angles ( $P_h^{(1)}$ ), and another - due to post-critical angles ( $P_h^{(2)}$ ). We recall that the stationary phase method failed to produce a stationary point for sub-critical angles. The distinction between the two components of the head wave is helpful in understanding the limitations of asymptotic methods and the properties of the head wave. However, since both components arrive practically at the same time and cannot be separated on experimental seismograms, we should be mostly concerned with the properties of the head wave as a whole.

The shape of the component  $P_h^{(1)}$  is close to the incident pulse, while the shape of the post-critical component  $P_h^{(2)}$  is more distorted. For relatively large values of  $\delta$  (the P/S velocity ratio in the reflecting medium), the post-critical component and the head wave as a whole are close to the integral of the incidence pulse, as we should expect from the asymptotic formula (3.4.37). Note that for large  $\delta$  a fluid/solid boundary approaches the model of a fluid/fluid boundary we studied above by means of analytic methods. It is interesting that for smaller  $\delta$  the shape of both components of the head wave is much closer to the incident wave than to the integral of it.

The distortion in the shape of the post-critical reflection is rather small, although the angle of incidence is far beyond the critical value. As shown in Aki and Richards (1980, Box 5.6), the shape of the post-critical reflection is determined by a linear combination of the incident pulse and its Hilbert transform with the coefficients  $\cos \epsilon$  and  $\sin \epsilon$  respectively, where  $\epsilon$  is the phase shift due to the reflection coefficient. At large incidence angles, close to  $90^\circ$ , the phase of the reflection coefficient (3.3.15) is close to  $180^\circ$  ( $\epsilon = \pi$ ), and the contribution of the Hilbert transform is small. Therefore, the shape of the post-critical reflection approaches the shape of the incidence pulse at grazing incidence angles close to  $90^\circ$ .

The character of the interference of the two components of the head wave is shown in more detail in Figure 3.11. The arrow shows the traveltime  $t_h$  given by the asymptotic expressions (3.3.25,3.3.26). Clearly, there is a small time delay between  $t_h$  and the first break, mostly due to the late arrival of the second component  $P_h^{(2)}$ . This delay is developed near the critical ray, and it does not change much with offset  $r$  once the receiver leaves the near-critical area. Therefore, the horizontal velocity of the head wave outside the critical region practically coincides with  $c_1$ , but its traveltime is slightly higher than the asymptotic value  $t_h$ . This time delay is relatively small and varies between  $0.05 T$  and  $0.15 T$ , where  $T$  is the period of the source pulse, depending on the velocity ratio and  $z + z_0$ . The shift of the first break of the head wave with respect to the ‘‘geometrical’’ time  $t_h$  was observed in physical modeling (Guha, 1965).

Figure 3.12 shows the amplitude curves of the head wave and its two components for two values of the P/S velocity ratio  $\delta$ . For both models, the first component  $P_h^{(1)}$  decays at large offsets as  $1/r^{1.5}$ , while the divergence factor for the component  $P_h^{(2)}$  and the total head wave is a function of  $\delta$ . For large  $r > (7 - 8) r_{cr}$  ( $r_{cr}$  is the critical distance) the total head wave decays approximately as  $1/r^\delta$  if  $1.7 < \delta < 2$ , and as  $1/r^2$  for  $\delta > 2$ .

The influence of the shear-wave velocity in the reflecting medium on the spectrum and the amplitude of the head wave is entirely associated with the post-critical component

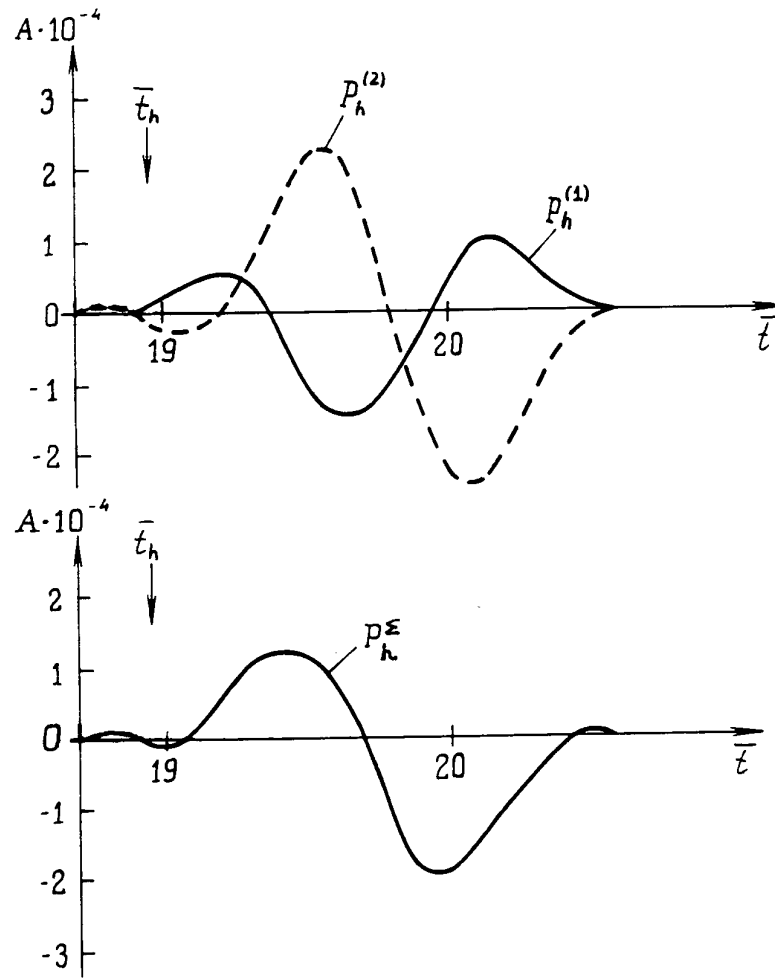


Figure 3.11: Interference of the two components of the head wave; the total head wave is shown below.  $n=0.7$ ,  $\delta = 2.1$ ,  $\sigma=1.9$ ,  $\bar{h} = 1$ ,  $\bar{r} = 25$ .  $t_h$  corresponds to the “geometrical” traveltime of the head wave;  $\bar{t} = t f_0$ ,  $f_0$  is the central frequency of the source pulse.

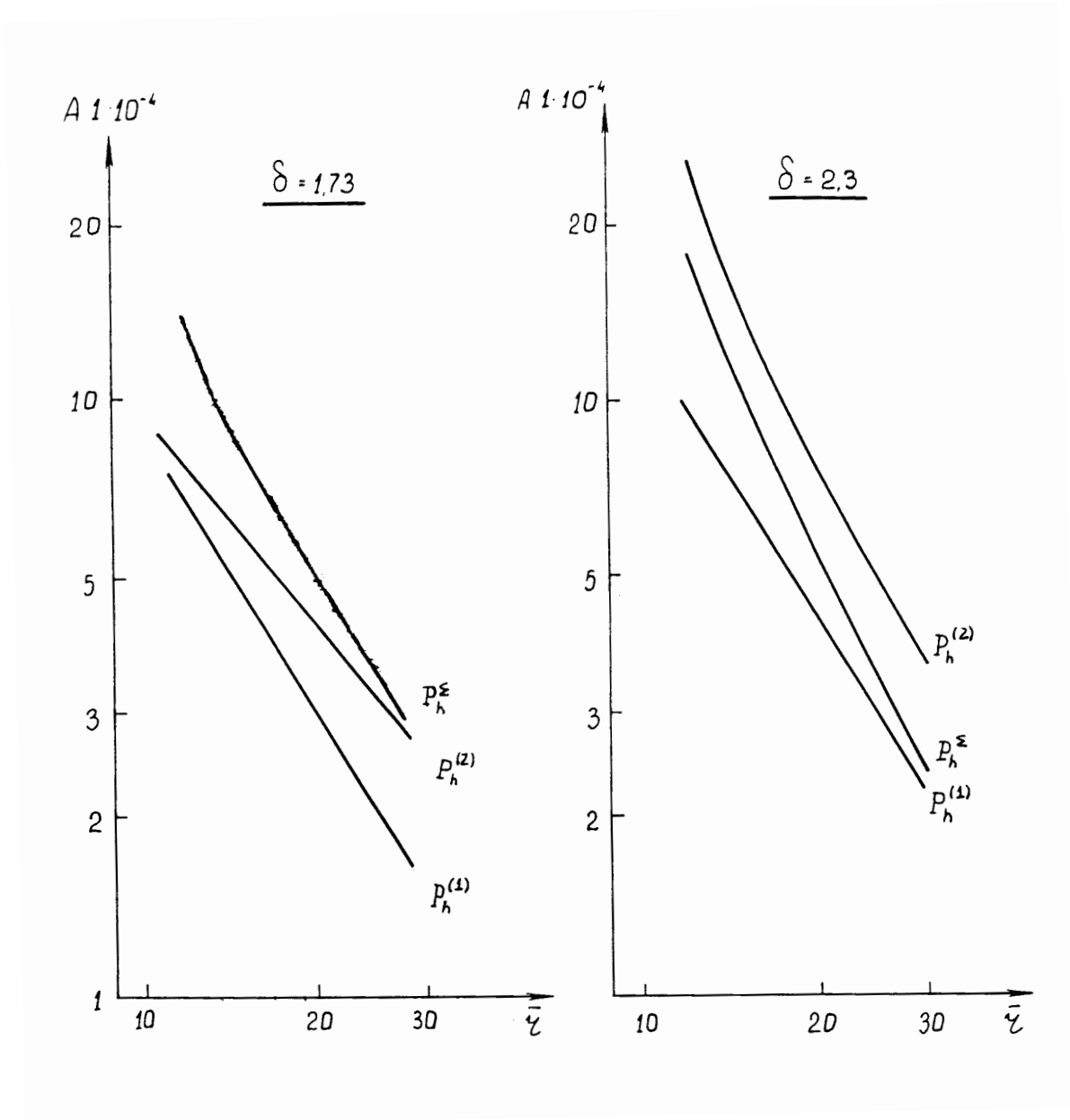


Figure 3.12: Amplitude curves of the head wave and its components for two different  $\delta$  (the scale is logarithmic).  $n=0.7$ ,  $\sigma=2$ ,  $\bar{h} = 2$ .

$P_h^{(2)}$  and can be explained by the shift of the stationary-phase point of  $P_h^{(2)}$  toward the critical angle at  $\delta < 2$ . As a result of this shift, the inhomogeneous wave excited by  $P_h^{(2)}$  in the high-velocity medium decays more slowly away from the boundary, and its frequency content becomes higher. Since the wave  $P_h^{(2)}$  is generated by a “skin layer” of a finite thickness below the boundary, the predominant frequency of  $P_h^{(2)}$  at small  $\delta$  becomes higher, and the shape of the head wave approaches the shape of the incident wave.

Also, at a fluid/solid boundary the stress component  $\tau_{zx}$  vanishes, and

$$\frac{\partial u_x}{\partial z} = -\frac{\partial u_z}{\partial x}.$$

Therefore, assuming that the particle motion is relatively stable, a slower decay in the vertical direction means a slower decay in the horizontal direction (with increasing  $r$ ). Summing up, a shift of the stationary-phase point of the component  $P_h^{(2)}$  towards the critical angle at  $\delta < 2$  leads to a higher predominant frequency and a slower decay with  $r$  of the head wave.

The shift of the stationary point discussed above is related to the contribution of  $\delta$  to the reflection coefficient. Physically, the influence of  $\delta$  is associated to the excitation of the transmitted  $PS$  wave and the  $PPS$  head wave in the high-velocity medium. The wave propagating along the boundary with the velocity close to  $c_1$  generates not only the pure P head wave in the incidence medium, but also a shear head wave ( $PPS$ ) of the same nature in the high-velocity medium.

Therefore, for a wide range of elastic parameters the head wave at a fluid/solid interface decays with distance more slowly than predicted by the term  $r^{-1/2}L^{-3/2}$ . However, for a fluid/fluid boundary the amplitude decay at large offsets ( $r > [7 - 8]r_{cr}$ ) is close to  $1/r^2$ . The rate of amplitude decay is much higher near the critical ray although, clearly, not as high as predicted by the asymptotic expression (3.4.37). In the vicinity of the critical ray the head wave interferes with the post-critical reflection, and it is not worthwhile to study any of the two waves as a separate arrival.

It should be also mentioned that except for the near-critical area the head wave is much weaker than the post-critical reflection. The main factors contributing to this are a rapid decay in the head wave’s amplitude during its propagation along the boundary and a large reflection coefficient at post-critical angles ( $|V|=1$ ). However, it is very common to see intensive refracted arrivals on experimental seismograms which have much higher amplitudes compared to synthetic head waves. The reason for this discrepancy is the presence of vertical velocity gradient below the refracting boundary. Due to the gradient, the transmitted waves penetrate into the medium and turn back up at different depths rather than travel as pure head waves along the boundary. As a result, refracted waves are formed by a larger part of the incident wavefront than pure head waves, and carry more energy.

## 3.6 Asymptotic analysis of the transmitted wavefield

### 3.6.1 Geometrical transmitted wave

The methods of the stationary phase (SPM) and saddle-point integration discussed above can be applied in the same fashion to the integral (3.2.5) for the transmitted wave. First, we will obtain the geometrical-seismics solution by using the zero-order approximation of the SPM.

Substituting an asymptotic representation of Bessel function  $J_0$  (3.3.1) into the integral (3.2.5) yields

$$\begin{aligned} \phi_{tr} = & i \sqrt{\frac{k}{2\pi}} \int_0^{\pi/2-i\infty} \frac{W(\theta)}{\sqrt{r \sin \theta}} \{ e^{i[kz_0 \cos \theta + k_1 d \cos \theta_1 + kr \sin \theta - \pi/4]} \\ & + e^{i[kz_0 \cos \theta + k_1 d \cos \theta_1 - kr \sin \theta + \pi/4]} \} \sin \theta d\theta, \end{aligned} \quad (3.6.1)$$

$d = -z$  is the distance between the receiver and the boundary.

Taking the derivative of the phase of the first exponential function

$$\Phi(\theta) = kz_0 \cos \theta + k_1 d \cos \theta_1 + kr \sin \theta - \pi/4,$$

we find the stationary-phase condition to be

$$\frac{d\Phi(\theta)}{d\theta} = -kz_0 \sin \theta + k_1 d \frac{d \cos \theta_1}{d\theta} + kr \cos \theta = 0. \quad (3.6.2)$$

Note that in this derivation we assume both angles ( $\theta$  and  $\theta_1$ ) to be real i.e., both the incident and reflected waves are homogeneous. Representing  $\cos \theta_1 = \sqrt{n^2 - \sin^2 \theta}/n$  ( $n = c/c_1$ ) gives

$$\frac{d \cos \theta_1}{d\theta} = -\frac{\sin \theta \cos \theta}{n \sqrt{n^2 - \sin^2 \theta}}.$$

Then the stationary-phase equation (3.6.2) becomes

$$-kz_0 \sin \theta - kd \frac{\sin \theta \cos \theta}{\sqrt{n^2 - \sin^2 \theta}} + kr \cos \theta = 0. \quad (3.6.3)$$

Taking into account that  $\theta$  and  $\theta_1$  are related by Snell's law  $\sin \theta/c = \sin \theta_1/c_1$ , we obtain from equation (3.6.3):

$$r = z_0 \tan \theta + d \tan \theta_1. \quad (3.6.4)$$

The geometrical meaning of the stationary-phase equation (3.6.4) is clear: the most prominent contribution to the transmitted wavefield is made by the ray from the source to the receiver refracted in accordance with Snell's law. This geometrical ray exists for all source-receiver positions and velocity ratios and corresponds to real  $\theta$  ( $0 < \theta < \pi/2$ ).

For the transmission into a high-velocity medium ( $n < 1$ ), the refracted geometrical ray is due to sub-critical incidence angles  $0 < \theta < \sin^{-1} n$ .

It can be shown in the same way as for the reflected wave that the second exponential function in equation (3.6.1), which corresponds to in-going waves in the horizontal direction, does not generate any stationary-phase points on the integration path.

To calculate the amplitude of the geometrical refraction, it is necessary to evaluate the contribution of the stationary point satisfying equation (3.6.4). This derivation is virtually identical to the stationary-phase analysis performed for the reflected wave. Expanding the phase of the first exponential function into a Taylor series at the stationary point, taking the slowly varying terms out of the integral, and using the expression for the Fresnel integral (3.3.11), we find

$$\phi_{tr} = \sqrt{\frac{k \sin \theta_{st}}{r}} W(\theta_{st}) \frac{e^{i\pi/4}}{\sqrt{\left| \frac{d^2\Phi}{d\theta^2} \right|}} e^{i\Phi(\theta_{st})}, \quad (3.6.5)$$

where  $\theta_{st}$  is the angle that satisfies the stationary-phase equation (3.6.4).

The phase  $\Phi$  at the stationary point is given by

$$\Phi(\theta_{st}) = kz_0/\cos\theta + k_1d/\cos\theta_1 - \pi/4 = kR + k_1R_1 - \pi/4, \quad (3.6.6)$$

$R$  and  $R_1$  are the distances traveled by the geometrical ray in the source and receiver media, respectively.

After some algebra, the second derivative of  $\Phi$  at the stationary point can be shown to be

$$\frac{d^2\Phi}{d\theta^2}(\theta_{st}) = -\frac{kz_0}{\cos\theta} - \frac{kd \cos^2\theta}{n \cos^3\theta_1}. \quad (3.6.7)$$

Substituting equations (3.6.6,3.6.7) into (3.6.5) yields (the subscript ‘‘st’’ is omitted)

$$\phi_{tr} = \frac{W(\theta)}{\cos\theta \sqrt{\frac{r}{\sin\theta} \left( \frac{z_0}{\cos^3\theta} + \frac{d}{n \cos^3\theta_1} \right)}} e^{i(kR+k_1R_1)}. \quad (3.6.8)$$

Although it is not as obvious as it was in the case of the reflected wave, the result in the zero-order approximation of the SPM (3.6.8) is equivalent to the geometrical-seismics solution. Indeed, the travelttime of the transmitted wave is calculated along the geometrical ray and the amplitude depends on the transmission coefficient for the plane wave incident on the boundary at the ‘‘geometrical’’ angle. The denominator, as shown in Brekhovskikh (1980), describes the divergence of energy along the geometrical ray; this term is just more complicated than the simple spherical divergence factor for the reflected wave.

Using formula (2.4.12) for the transmission coefficient, we obtain the transmitted wave as an explicit function of the model parameters and incidence angle:

$$\phi_{tr} = \frac{2}{(\sigma \cos\theta + n \cos\theta_1) \sqrt{\frac{r}{\sin\theta} \left( \frac{z_0}{\cos^3\theta} + \frac{d}{n \cos^3\theta_1} \right)}} e^{i(kR+k_1R_1)}, \quad (3.6.9)$$



$$\sigma = \rho_1/\rho.$$

### 3.6.2 Inhomogeneous transmitted waves

In the above derivation, we searched for stationary points on the part of the integration path corresponding to homogeneous incident and transmitted waves. This means that the angle  $\theta$  was assumed to belong to the interval  $0 < \theta < \pi/2$  for transmission into a low-velocity medium ( $n > 1$ ) or to an even shorter interval  $0 < \theta < \sin^{-1} n$  for transmission into a high-velocity medium. Outside of these intervals, the incident and/or transmitted wave become inhomogeneous thus changing the stationary-phase equation.

We continue the discussion of the transmitted wavefield assuming that the incidence medium has a lower velocity:  $c < c_1$ ,  $n < 1$ . First we apply the zero-order approximation of the stationary-phase method and ignore the phase of the transmission coefficient. For the part of the integration path corresponding to real post-critical angles  $\sin^{-1} n < \theta < \pi/2$ , the phase of the integrand is given by

$$\Phi(\theta) = kz_0 \cos \theta + kr \sin \theta - \pi/4.$$

The term  $k_1 d \cos \theta_1$  becomes imaginary and drops out of the phase function. Differentiating  $\Phi(\theta)$ , we find the stationary point to be

$$\theta_{st} = \tan^{-1}(r/z_0). \quad (3.6.10)$$

In order for the stationary point to belong to the interval  $\sin^{-1} n < \theta < \pi/2$ , the projection of the receiver on the boundary should be in the post-critical domain:

$$\theta_{st} = \tan^{-1}(r/z_0) > \sin^{-1} n.$$

The corresponding refraction angle is given by

$$\sin \theta_1 = \sin \theta_{st}/n = \frac{r}{nR} \quad (\sin \theta_1 > 1), \quad (3.6.11)$$

where  $R = \sqrt{r^2 + z_0^2}$  is the distance between the source and the projection of the receiver on the boundary.

Without performing a complete stationary-phase derivation, we can represent the inhomogeneous transmitted wave as

$$\phi_{tr}^{in} = A e^{ikR} e^{-k_1 d |\cos \theta_1|}, \quad (3.6.12)$$

where  $A$  is the amplitude coefficient, and

$$\cos \theta_1 = i \frac{\sqrt{\sin^2 \theta_{st} - n^2}}{n}. \quad (3.6.13)$$

We have obtained the inhomogeneous transmitted wave that was mentioned during the analysis of the reflected wave in the post-critical region (see Figure 3.9). The traveltime

of this transmitted wave is determined by the ray from the source to the boundary, while the amplitude exponentially decays from the boundary into the high-velocity medium. The rate of decay that can be deduced from equations (3.6.13,3.6.12) becomes higher with increasing incidence angle  $\theta$ .

As we have seen before, when an incident and/or transmitted wave becomes inhomogeneous, the reflection/transmission coefficients become complex and introduce additional terms into the stationary-phase equations. The transmission coefficient (2.4.12) for  $\theta > \sin^{-1} n$  is

$$W(\theta) = \frac{2 \cos \theta}{\sigma \cos \theta + i \sqrt{\sin^2 \theta - n^2}}. \quad (3.6.14)$$

Next we apply the first-order approximation of the SPM taking the phase of  $W(\theta)$  into account. The full phase of the integrand for the transmitted wave at post-critical incidence angles is

$$\Phi(\theta) = kz_0 \cos \theta + kr \sin \theta - \tan^{-1} \left( \frac{\sqrt{\sin^2 \theta - n^2}}{\sigma \cos \theta} \right) - \pi/4. \quad (3.6.15)$$

This phase function can be represented as

$$\Phi(\theta) = \frac{1}{2} \Phi_{refl}(\theta) - \pi/8, \quad (3.6.16)$$

where  $\Phi_{refl}$  is the phase of the reflected wave (3.3.17) for a receiver located at the point  $[z_0, 2r]$  in the post-critical region in the incidence medium. From equation (3.6.16) it is clear that the stationary points for the reflected and transmitted waves in the post-critical region are identical. One of the stationary points corresponds to the head wave that slides along the boundary. More precisely, the receiver near the boundary records the post-critical (inhomogeneous in the high-velocity medium) component of the head wave. The second stationary point corresponds to the inhomogeneous transmitted wave discussed above. In the first-order approximation of the SPM (equation [3.6.15]), this stationary point is shifted with respect to its position obtained in equation (3.6.10) in the zero-order approximation.

What do these results tell us about the physical picture of the transmitted wavefield? For any receiver position in the high-velocity medium, we can always find a geometrical ray from the source to the receiver refracted in accordance with Snell's law. Therefore, the only transmitted wave that exists for all source and receiver positions is the geometrical arrival described by equations (3.6.8,3.6.9). When the projection of the receiver on the boundary is in the post-critical region ( $\tan^{-1}(r/z_0) = \theta_{st} > \sin^{-1} n$ ), the transmitted wavefield also contains two inhomogeneous (evanescent) waves: the post-critical component of the head wave and the inhomogeneous transmitted wave generated at the projection of the receiver on the boundary. These waves correspond to the same incidence angles as the head and reflected waves (respectively) in the incidence medium (Figure 3.9). Physically, a receiver located in the high-velocity medium near the boundary picks up the transmitted components of both wave groups propagating along the interface. As we

have shown above, the faster group is formed by the head wave and homogeneous transmitted wave, while the slower group contains the incident, reflected, and inhomogeneous transmitted waves.

In order to record both inhomogeneous waves, the receiver should be close to the boundary. When the distance between the receiver and the boundary exceeds the wavelength (the predominant wavelength in the case of a transient pulse), the inhomogeneous waves vanish, and the transmitted wavefield contains only the geometrical arrival. Note that the rate of amplitude decay is higher for the inhomogeneous transmitted wave than for the post-critical component of the head wave, because the transmitted wave corresponds to larger incidence angles.

Since both inhomogeneous wave can exist only close to the boundary, they are similar to surface waves. However, if we replace the high-velocity halfspace with a thin high-velocity layer, the inhomogeneous waves can be transformed back into homogeneous waves upon leaving the layer and be recorded far from the source. Effects of this type are usually referred to as “*tunneling*” of energy.

The last part of the integration path that we have not examined yet is the one containing inhomogeneous waves from point-source radiation (complex values of  $\theta$ ). For  $n < 1$ , these waves remain inhomogeneous after the transmission, and both  $\cos \theta$  and  $\cos \theta_1$  are imaginary. Thus, the transmission coefficient becomes real again, and the phase of the integrand contains just  $kr \sin \theta - \pi/4$ . This phase is exactly the same as the phase of the reflected wave for the same incidence angles. As we have shown in the section devoted to the reflected wavefield, there are no stationary phase points corresponding to inhomogeneous waves in this case. This concludes our analysis for the acoustic transmission into a high-velocity medium ( $n < 1$ ).

### 3.6.3 Transmission into a low-velocity medium: nongeometrical waves

Now we consider the transmitted wave for the case when the incidence medium has a higher velocity:  $c > c_1$ ,  $n > 1$ . Applying the zero-order approximation of the stationary phase method to the interval corresponding to homogeneous incident waves ( $0 < \theta < \pi/2$ ), we get the same geometrical-seismics expression (3.6.9) as for  $n < 1$ . Since  $n > 1$ , elementary transmitted waves corresponding to  $\theta < \pi/2$  are also homogeneous, and the transmission coefficient is real. Therefore, the first-order SPM approximation will not produce any more stationary points on the interval corresponding to homogeneous incident waves.

Next we examine the part of the integration path from  $\theta = \pi/2$  to  $\theta = \pi/2 - i\infty$  that contains inhomogeneous incident waves. Since  $n > 1$ , inhomogeneous waves may be converted into homogeneous, non-decaying transmitted waves. Indeed, for the part of the integration path below the point  $\theta = \pi/2$  where  $1 < \sin \theta < n$ , the refraction angle is real ( $\sin \theta_1 = \sin \theta/n < 1$ ), and transmitted waves are homogeneous. The phase of the exponential function in the integral for the transmitted wave (3.6.1) can be written on the interval  $1 < \sin \theta < n$  as follows (the second, nonphysical, exponent in equation [3.6.1] is

ignored):

$$\Phi(\theta) = k_1 d \cos \theta_1 + kr \sin \theta - \pi/4.$$

Note that the term  $kz_0 \cos \theta$  is imaginary and does not contribute to the stationary-phase equation. Replacing  $kr \sin \theta$  with  $k_1 r \sin \theta_1$  and taking the derivative of  $\Phi$  with respect to  $\theta_1$ , we find the stationary point to satisfy

$$\theta_1 = \tan^{-1}(r/d). \quad (3.6.17)$$

The refraction angle from equation (3.6.17) corresponds to the transmitted wave propagating from the projection of the source on the boundary. This wave is usually called “pseudospherical” because its wavefront, like the wavefront of the incident wave, has a spherical shape but with the center moved from the source to its projection on the interface. For the pseudospherical wave to exist, the stationary point (3.6.17) should lie on the interval  $1 < \sin \theta < n$  or  $1/n < \sin \theta_1 < 1$ . Therefore, in order to record the pseudospherical wave, the receiver should be located between the interface ( $\sin \theta_1 = 1$ ) and the critical ray in the refracting medium ( $\sin \theta_1 = 1/n$ ). Calculation of the amplitude of the pseudospherical wave in the zero-order approximation of the SPM is suggested as an exercise for the students. The discussion of the properties of the transmitted wavefield will be continued after application of the first-order approximation of the SPM.

Since  $\cos \theta_1$  on the interval  $1 < \sin \theta < n$  is real while  $\cos \theta$  is imaginary, the transmission coefficient is given by

$$W = \frac{2i|\cos \theta|}{i\sigma|\cos \theta| + n \cos \theta_1}, \quad (3.6.18)$$

$$\sigma = \rho_1/\rho, \quad n = c/c_1.$$

The phase of the transmission coefficient is

$$\Phi_w = \pi/2 - \tan^{-1} \left( \frac{\sigma|\cos \theta|}{n \cos \theta_1} \right). \quad (3.6.19)$$

Using  $\theta_1$  as the variable,  $\Phi_w$  can be represented as

$$\Phi_w = \pi/2 - \tan^{-1} \left( \frac{\sigma \sqrt{n^2 \sin^2 \theta_1 - 1}}{n \cos \theta_1} \right)$$

or, introducing  $n_1 = 1/n = c_1/c$  and  $\sigma_1 = 1/\sigma = \rho/\rho_1$ ,

$$\Phi_w = \pi/2 - \tan^{-1} \left( \frac{\sqrt{\sin^2 \theta_1 - n_1^2}}{\sigma_1 \cos \theta_1} \right). \quad (3.6.20)$$

The total phase of the integrand in the expression for the transmitted wave (3.6.1) for  $1 < \sin \theta < n$  ( $1/n < \sin \theta_1 < 1$ ) becomes (only the first exponent is taken into account)

$$\Phi_{tr} = k_1 d \cos \theta_1 + k_1 r \sin \theta_1 + \pi/4 - \tan^{-1} \left( \frac{\sqrt{\sin^2 \theta_1 - n_1^2}}{\sigma_1 \cos \theta_1} \right). \quad (3.6.21)$$

In principle, we can proceed with the stationary-phase analysis by taking the derivative of the phase function and solving the equation for the stationary points. However, instead of doing this we can notice that the phase (3.6.21) virtually coincides with the phase of the integrand for the post-critical transmission into a high-velocity medium given by equation (3.6.15).

Let us switch the source and receiver positions and put the source at point  $R$  and receiver at point  $S$  (Figure 3.13). Rewriting the phase function (3.6.15) for the transmission from  $R$  to  $S$  at post-critical incidence angles yields

$$\Phi_{tr}(R \rightarrow S) = k_1 d \cos \theta_1 + k_1 r \sin \theta_1 - \pi/4 - \tan^{-1} \left( \frac{\sqrt{\sin^2 \theta_1 - n_1^2}}{\sigma_1 \cos \theta_1} \right). \quad (3.6.22)$$

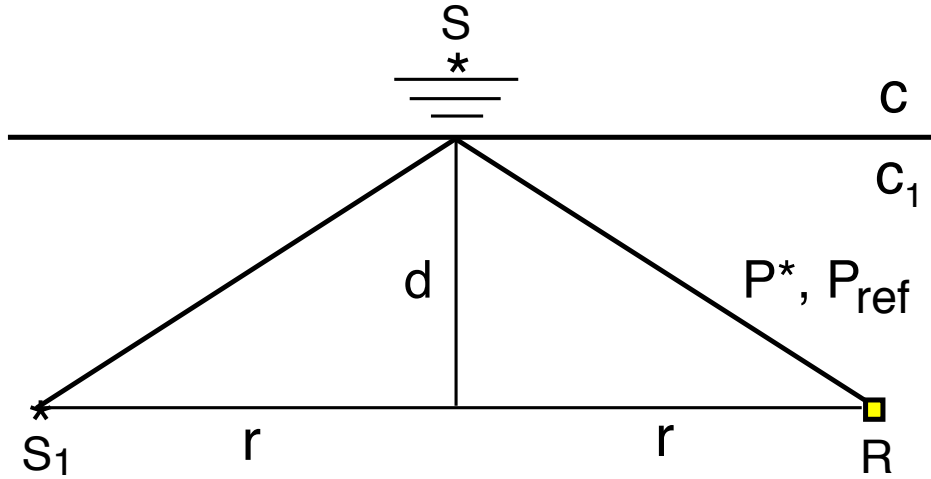


Figure 3.13: To the discussion of the kinematic equivalence of the transmitted wavefields from point  $S$  to  $R$ , from  $R$  to  $S$ , and the reflected wavefield from  $S_1$  to  $R$ .

The difference between the two phase functions (3.6.21, 3.6.22) is just a constant ( $\pi/2$ ), and the stationary-phase points would be identical. Essentially, this conclusion follows from the principle of reciprocity: the traveltimes (and, consequently, the stationary points) should remain the same when we exchange the positions of the source and receiver.

Therefore, it was not necessary to do the full-scale stationary-phase analysis for the transmitted wave on the interval  $1/n < \sin \theta_1 < 1$ . The stationary points  $\theta_1$  for the transmitted homogeneous waves formed by incident inhomogeneous waves (Figure 3.14) are the same as the stationary points  $\theta_1$  for the wavefield transmitted into the high-velocity medium at post-critical incidence angles.

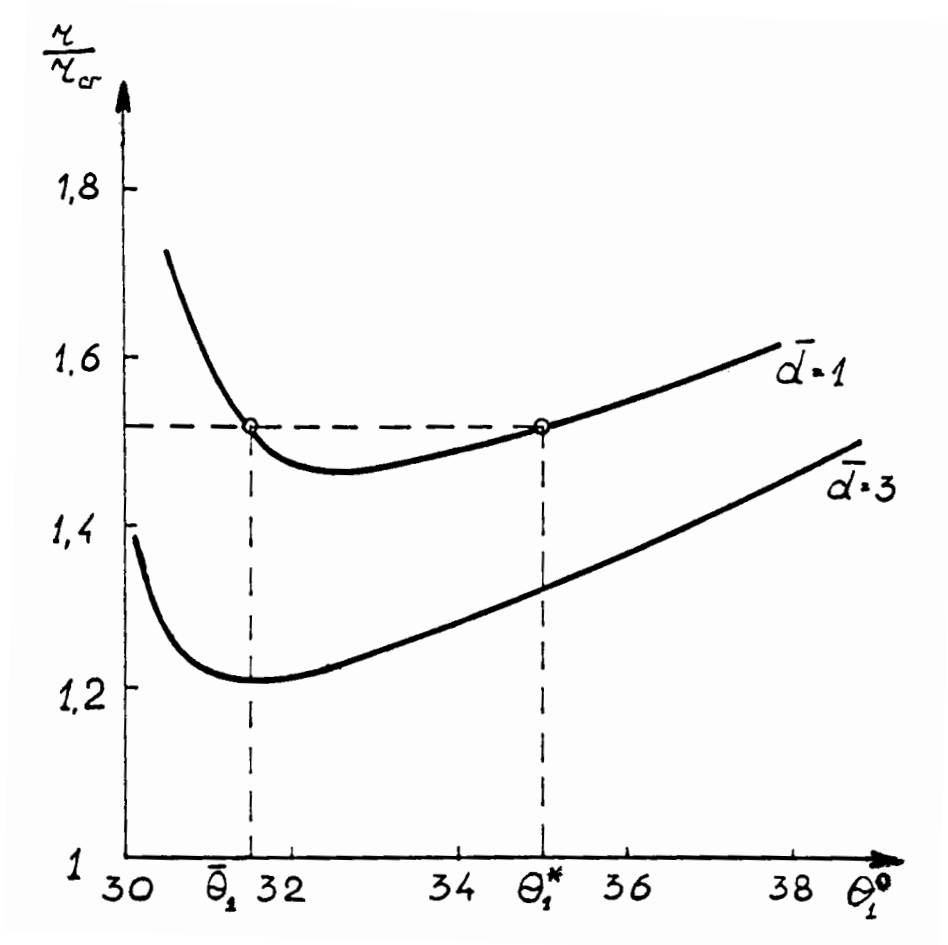


Figure 3.14: Stationary phase points corresponding to nongeometrical waves generated at a fluid/fluid boundary during the transmission into the low-velocity medium.  $\bar{\theta}_1$  - leaking wave;  $\theta_1^*$  - pseudospherical wave. Model parameters are  $n = 2$  ( $\theta_{1cr} = 30^\circ$ ),  $\sigma=0.8$ . Geometrical parameters are normalized by the wavelength:  $\bar{r} = r/\lambda$ ,  $\bar{d} = d/\lambda$ .

Below we discuss the physical nature of the transmitted waves associated with the stationary points in Figure 3.14. We will call these waves “nongeometrical” because they cannot be described within the framework of the standard ray theory. Both nongeometrical waves exist only in the post-critical domain in the low-velocity medium; the condition to be satisfied by the receiver coordinates is  $\tan^{-1}(r/d) > \theta_{1cr} = \sin^{-1}(c_1/c)$ . Since the value of  $\sin \theta$  for the nongeometrical waves is greater than unity, they are inhomogeneous in the incidence medium and decay exponentially when the source moves away from the boundary. This feature of nongeometrical waves makes them similar to surface waves. However, in the low-velocity medium both nongeometrical waves become homogeneous ( $\sin \theta_1 < 1$ ) and can be recorded far from the boundary. By their nature, nongeometrical waves can be classified as being somewhere in between conventional body waves and surface waves.

The pseudospherical wave associated with point  $\theta_1^*$  in Figure 3.14 has been briefly discussed above; it is kinematically analogous to the inhomogeneous wave transmitted at post-critical angles. The stationary point  $\theta_1^* \approx \tan^{-1}(r/d)$  for this wave is close to its position in the zero-order approximation of the SPM.

The second nongeometrical wave, analogous to the post-critical component of the head wave (point  $\bar{\theta}_1$  in Figure 3.14), is usually called “leaking” because it “leaks” energy into the low-velocity medium while propagating along the boundary. The stationary point for this wave is close to the critical angle:  $\bar{\theta}_1 \approx \sin^{-1}(1/n)$ .

Application of reciprocity is helpful in developing a better understanding of the physical nature of the nongeometrical waves. The stationary points in the case of the post-critical transmission into the high-velocity medium (from  $R$  to  $S$ , Figure 3.13) represent inhomogeneous waves formed due to the refraction of homogeneous waves incident on the boundary at post-critical angles. When the wavefield is transmitted in the opposite direction, into the low-velocity medium (from  $S$  to  $R$ ), this situation is reversed: inhomogeneous waves excited by the source are transformed into homogeneous waves propagating at post-critical refraction angles.

Nongeometrical waves can exist only when the source-boundary distance  $z_0$  is relatively small. When the source is moved away from the boundary, the amplitude of nongeometrical waves exponentially decreases and the predominant frequency becomes lower. We may say that source-generated inhomogeneous waves “tunnel” through the boundary, become homogeneous in the low-velocity medium, and give rise to nongeometrical wave components.

Further generalizing our discussion of the kinematic relations between the wavefields excited in both halfspaces, it is possible to show that the transmitted wavefield at point  $R$  formed by inhomogeneous incident waves excited at  $S$  is kinematically equivalent to the post-critical reflected wavefield in the low-velocity medium. In order to illustrate this, we move the source  $S$  into the halfspace with the receiver and put it at point  $S_1$  at the distance  $d$  from the boundary and  $2r$  from the receiver  $R$  (Figure 3.13). We have already proved that the stationary phase points are identical for the post-critical reflection from  $R$  to  $S_1$  (or  $S_1$  to  $R$ ) and post-critical transmission from  $R$  to  $S$ . Also, we have shown that the stationary phase points remain the same for the transmission from  $S$  to  $R$  or from  $R$

to  $S$ . Therefore, the head wave (post-critical component) and the post-critical reflection for the propagation from  $S_1$  to  $R$  should be kinematically equivalent to the leaking and pseudospherical waves respectively.

Indeed, let us write down the phase of the integrand in the expression for the post-critical reflected wavefield  $\Phi_{refl}$  when the source is located at point  $S_1$  and the receiver is at point  $R$  (Figure 3.13).  $\Phi_{refl}$  is given by equations (3.3.16),(3.3.17); the only change to be made is to assign index “1” to the incidence medium instead of the reflecting medium. Then for the interval  $1/n < \sin \theta_1 < 1$  we have

$$\Phi_{refl}(S_1 \rightarrow R) = 2k_1d \cos \theta_1 + 2k_1r \sin \theta_1 - \pi/4 - 2 \tan^{-1} \left( \frac{\sqrt{\sin^2 \theta_1 - n_1^2}}{\sigma_1 \cos \theta_1} \right). \quad (3.6.23)$$

Comparison with equations (3.6.20),(3.6.21) shows that

$$2\Phi_{tr}(S \rightarrow R) = \Phi_{refl}(S_1 \rightarrow R) + \frac{3}{4}\pi, \quad (3.6.24)$$

and the stationary-phase points at post-critical angles  $\theta_1 > \sin^{-1}(1/n)$  defined by  $\Phi' = 0$  are identical for the wavefields at point  $R$  from the sources at  $S$  and  $S_1$ . Equation (3.6.24) proves that for the geometry from Figure 3.13 the traveltimes of the post-critical reflected wave and the head wave (post-critical component) are twice the traveltimes of the pseudospherical and leaking waves respectively.

Let us now discuss the properties of the nongeometrical waves in greater detail. The pseudospherical wave kinematically analogous to the post-critical transmission into the high-velocity medium will be denoted as  $P^*$ . Ignoring the shift of the stationary point due to the transmission coefficient,  $P^*$  can be represented as

$$\phi^* = A^* e^{ik_1 R_1} e^{-kz_0 \sqrt{\sin^2 \theta^* - 1}}, \quad (3.6.25)$$

where  $R_1 = \sqrt{r^2 + d^2}$  is the distance traveled by the wave in the low-velocity medium,  $A^*$  is the amplitude coefficient, and

$$\sin \theta^* = n \sin \theta_1^* = \frac{n}{\sqrt{1 + (d/r)^2}}. \quad (3.6.26)$$

Equation (3.6.25) explicitly demonstrates one of the major features of the pseudospherical wave already mentioned above - its spherical wavefront with the center at the projection of the source on the boundary (Figure 3.15).

In the incidence medium,  $P^*$  is inhomogeneous with the rate of amplitude decay dependent on the receiver position in the refracting medium. For the receiver at the critical ray,  $\sin \theta^* = 1$ , and the decay factor in equation (3.6.25) is zero. With increasing refraction angle  $\theta_1^*$  the wave  $P^*$  decays faster due to larger  $\sin \theta^*$ . If the receiver is located close to the boundary,  $\theta_1^*$  approaches  $90^\circ$ ,  $\sin \theta^*$  is close to  $n$ , and the decay factor reaches its maximum value. Therefore, we may expect that the energy distribution along the spherical wavefront of  $P^*$  is very uneven with the highest amplitude near the critical ray



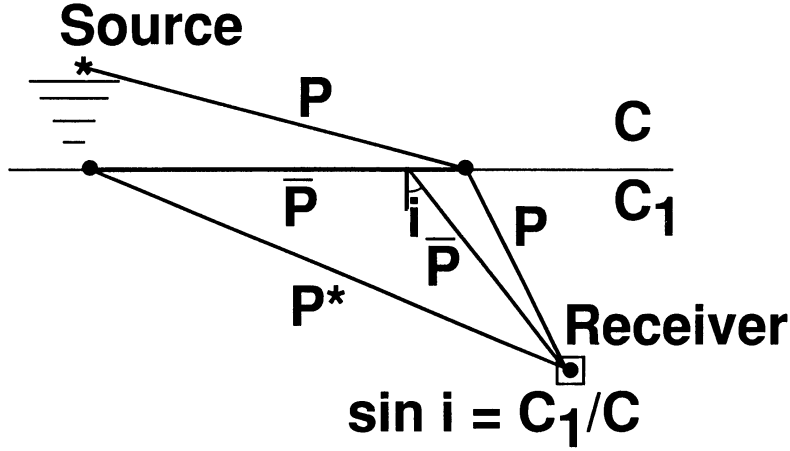


Figure 3.15: Asymptotic “raypaths” of the pseudospherical wave  $P^*$  and leaking wave  $\bar{P}$ .

and a minimum near the boundary. A more rigorous proof of this assertion requires the calculation of the amplitude factor  $A^*$ ; we have left it out as an exercise for the students.

It should be also mentioned that the frequency content of  $P^*$  changes along the wavefront because the decay factor contains the frequency as a multiplier. Essentially, for inhomogeneous waves the incidence medium acts as a low-pass filter with the parameters depending on the source-receiver geometry and elastic coefficients. From the analysis given above it follows that the wave  $P^*$  loses high frequencies as the receiver moves along the wavefront from the critical ray towards the boundary.

The nongeometrical arrival associated with the stationary point  $\bar{\theta}_1 \approx \sin^{-1}(1/n)$  is usually called the “leaking” wave and denoted as  $\bar{P}$ . In the stationary-phase approximation, the potential of the leaking wave is

$$\bar{\phi} = \bar{A} e^{i(kL+k_1 d/\cos \bar{\theta}_1)} e^{-kz_0 \sqrt{\sin^2 \bar{\theta}-1}}, \quad (3.6.27)$$

$L = r - d \tan \bar{\theta}_1$  is the distance traveled by the leaking wave along the boundary. Unlike the pseudospherical wave,  $\bar{P}$  has a fixed refraction angle  $\bar{\theta}_1$  close to the critical angle in the low-velocity medium. Therefore,  $\sin \bar{\theta}$  is close to unity, and the decay factor for  $\bar{P}$  is smaller than for  $P^*$  and does not depend on the receiver position.

Like a head wave, the leaking wave propagates along the boundary with the velocity close to the higher P-wave velocity ( $c$ ) and radiates (leaks) a conical wave into the low-velocity halfspace. The wavefront of the leaking wave in the incidence plane is a straight line that makes an angle of  $\theta_{1cr}$  with the boundary. However, while the head wave is generated by the refraction at the critical angle, the wave  $\bar{P}$  is excited directly in the high-velocity medium by inhomogeneous waves contained in the point-source radiation.

It should be emphasized that the “raypaths” of the nongeometrical waves have a different meaning than the raypaths of conventional body waves. The paths shown in Figure 3.15 represent a convenient way to explain analytic formulas for the nongeometrical waves rather than the actual directions of energy propagation. For instance, it is clear that there is no travelttime associated with the segment from the source to the boundary;

both nongeometrical waves experience an exponential decay in the incidence medium but there is no corresponding frequency-dependent phase shift. Since propagation of the nongeometrical waves cannot be described in terms of ray theory, there are no geometrical rays to be associated with waves like  $P^*$  and  $\bar{P}$ . We can say that nongeometrical waves “tunnel” through the boundary to give rise to homogeneous, non-decaying waves in the low-velocity halfspace.

Aki and Richards (1980) in their discussion of surface waves point out that since the amplitude and phase spectra of inhomogeneous waves are independent of each other, these waves are not causal and may in principle appear at negative times (if the source was initiated at  $t = 0$ ). The important point to make is that the waves  $P^*$  and  $\bar{P}$  do have some phase shift and an approximate “geometrical” traveltimes associated with the propagation along the boundary (for  $\bar{P}$ ) and in the low-velocity medium. These geometrical traveltimes should be computed along the solid lines in Figure 3.15). While the actual arrival times of both waves  $P^*$  and  $\bar{P}$  may be smaller than the geometrical values, the causality is not violated since  $P^*$  and  $\bar{P}$  do not appear at negative times.

From a practical point of view it is essential that at small source-boundary distances, when the exponential decay is relatively weak and the nongeometrical arrivals are still well-defined, the traveltimes of the nongeometrical waves are close to the values calculated along the “raypaths” in Figure 3.15. Although the traveltimes of the waves  $P^*$  and  $\bar{P}$  do not formally depend on the distance between the source and the boundary, the source elevation does affect the waveform and, therefore, may change the arrival time corresponding, for example, to the first peak.

We should also keep in mind that our analytic expressions have been derived in the high-frequency stationary-phase approximation. If the source moves away from the boundary, our asymptotics becomes less accurate due to a more rapid change in the decaying exponent that may shift the positions of the stationary points for the waves  $P^*$  and  $\bar{P}$ .

### 3.7 Numerical analysis of nongeometrical waves

The transmitted wavefield for a receiver located in the post-critical domain in the low-velocity medium is shown in Figure 3.16. The seismograms were calculated by numerical integration of the exact expression (3.2.5) for the transmitted wave. The contributions of homogeneous waves ( $0 \leq \theta \leq \pi/2$ , upper trace) and inhomogeneous waves (middle trace) from the point-source radiation were calculated separately and summed up in the bottom trace that represents the total response that would be recorded by a real receiver.

Since the source is close to the boundary, the leaking wave  $\bar{P}$  arrives almost at the same time as the conventional transmitted wave and substantially changes the amplitude and shape (but not the traveltimes) of the first arrival. Therefore, when the source is close to the boundary the first arrival (denoted as  $P_{\Sigma}$  in Figure 3.16) is made up of two wave components of different nature.

Near the critical angle the two nongeometrical waves interfere with each other like the head and reflected waves in the same area. Away from the critical ray in the low-

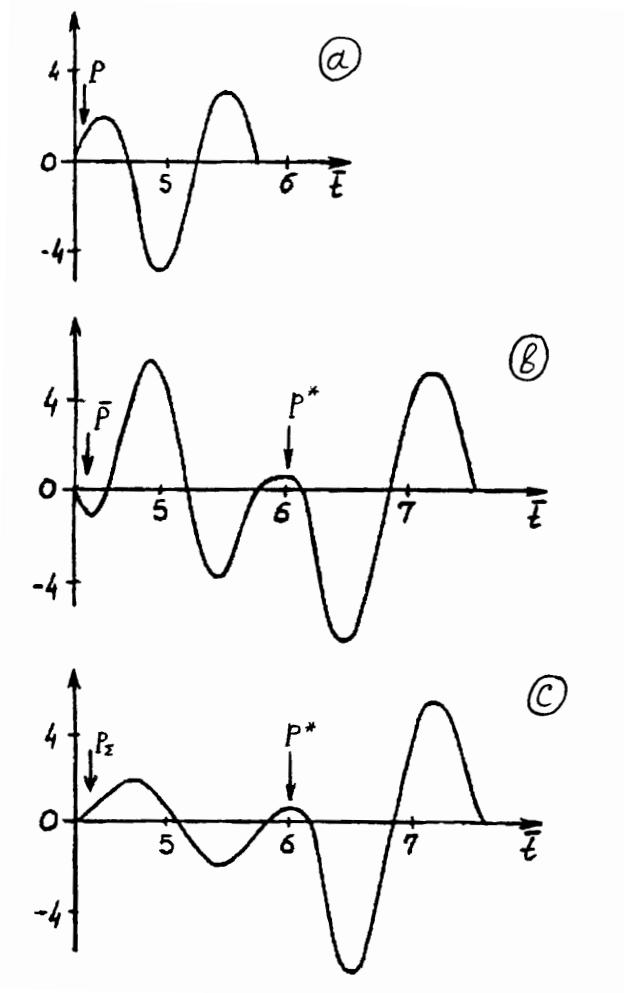


Figure 3.16: Exact synthetic seismograms of the wavefield transmitted into the low-velocity medium; the receiver is located in the post-critical region. The upper trace (a) is the contribution of homogeneous incident waves, the middle trace (b) is the contribution of inhomogeneous incident waves, the lower trace (c) is the total seismogram. Model parameters are  $n=1.5$ ,  $\sigma=0.8$ ,  $\bar{z}_0=0.1$ ,  $\bar{d}=0.25$ ,  $\bar{r}=4$ .  $\bar{z}_0$ ,  $\bar{d}$ ,  $\bar{r}$  are the distances normalized by the predominant wavelength in the high-velocity halfspace.

velocity medium the pseudospherical wave  $P^*$  forms a separate arrival that can dominate the seismogram if the distance between the source and the boundary is small compared to the predominant wavelength. Hence, unlike surface waves, nongeometrical waves span a wide range of traveltimes starting with the first arrival.

It is interesting to compare the transmitted wavefield in Figure 3.16 with the wavefield reflected from a high-velocity halfspace in the post-critical domain (Figure 3.10). We have already proved that for the geometry of Figure 3.13 the traveltimes of the leaking wave  $\bar{P}$  and the pseudospherical wave  $P^*$  are two times smaller than the traveltimes of the post-critical component of the head wave ( $P_h^{(2)}$ ) and the post-critical reflection respectively. Since the conventional transmitted wave for small  $z_0$  propagates practically along the interface, its traveltime is roughly a half of the traveltime of the sub-critical component of the head wave  $P_h^{(1)}$ . Therefore, from the kinematic standpoint the seismograms in Figure 3.16 represent scaled versions of the seismograms in Figure 3.10. We conclude that the wavefield transmitted into the post-critical domain of the low-velocity medium is kinematically equivalent to the reflected wavefield in the same region.

The critical model parameter for the nongeometrical waves is the distance between the source and the boundary ( $z_0$ ). The influence of  $z_0$  on the transmitted waves is shown in Figure 3.17. Since the receiver is far from the critical ray  $\bar{\theta}_{1cr} = \sin^{-1}(1/n)$ , the wave  $P^*$  decays with increasing  $\bar{z}_0$  much faster than  $\bar{P}$  and practically vanishes for  $\bar{z}_0 > 0.3$ . However, the dependence of the amplitude of  $P^*$  on the source elevation becomes much less pronounced when the receiver is closer to the critical ray.

It should be emphasized that the influence of  $\bar{z}_0$  on the amplitude of  $\bar{P}$  is relatively weak, and this nongeometrical wave affects the amplitude and the frequency content of the first arrival up to  $\bar{z}_0 = 0.5 - 0.8$ . While the nongeometrical waves decay when the source is moved away from the boundary, the amplitude of the geometrical transmitted wave and the first arrival  $P_\Sigma$  as a whole increases due to higher values of the transmission coefficient.

The distance between the receiver and the boundary ( $d$ ) also has a considerable influence on the dynamics of the nongeometrical waves, especially the pseudospherical wave  $P^*$  (Figure 3.18). The factors responsible for the increase in the amplitude of  $P^*$  with  $d$  are a weaker exponential decay in the incidence medium and larger values of the amplitude coefficient  $A^*$  in equation (3.6.25). The leaking wave, as a head wave, rapidly loses energy on its way along the boundary and, therefore, becomes more intensive with increasing  $d$ . However, the amplitude of  $\bar{P}$  is not as sensitive to  $d$  as the amplitude of the pseudospherical wave  $P^*$ .

The amplitude trends in Figure 3.18 continue within the area where the pseudospherical wave can be separated from the wave  $P_\Sigma$ . For relatively large  $d$  corresponding to a vicinity of the critical ray, the waves  $P^*$  and  $P_\Sigma$  begin to interfere with each other.

The dependence of the amplitudes on the horizontal offset  $r$  is well-approximated (far from the critical ray) by the law  $1/r^\alpha$ , with  $\alpha \approx 2 - 2.2$  for the waves  $P^*$  and  $P_\Sigma$ . It is interesting that both components of the interference wave  $P_\Sigma$  decay with  $r$  much slower, with  $\alpha \approx 1.5$ .

A rapid decrease in the amplitude of  $P^*$  with  $r$  is due to a lower energy level in the part

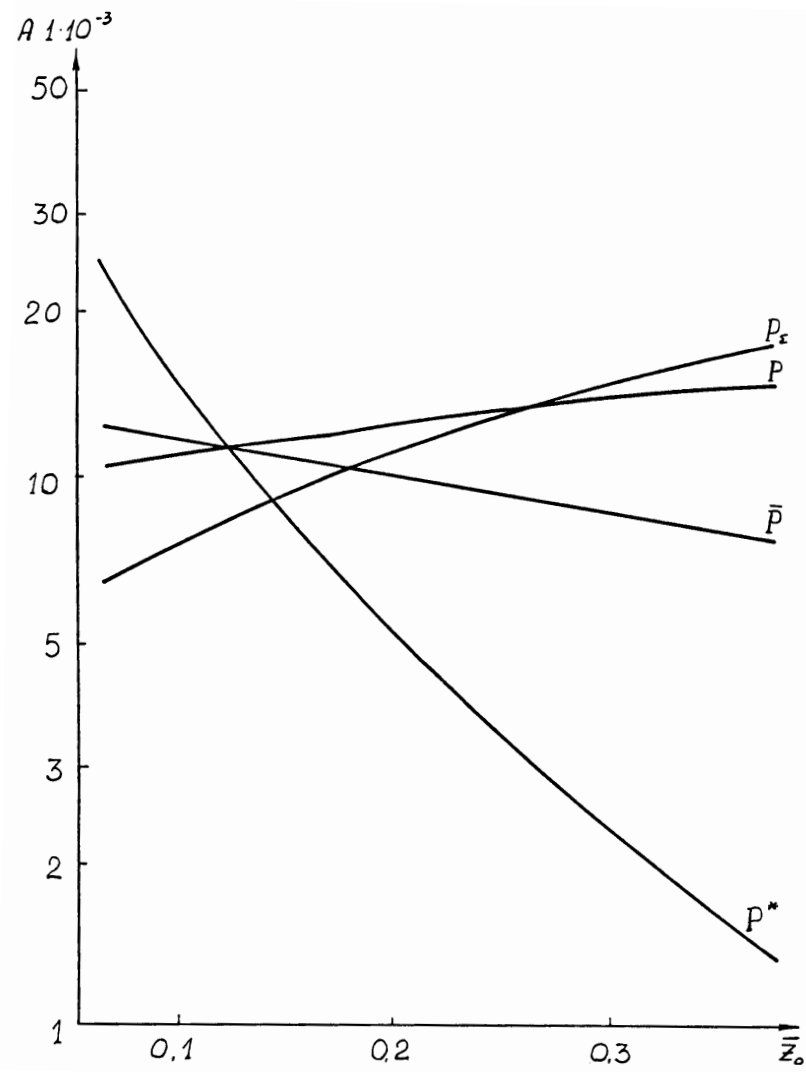


Figure 3.17: Dependence of the amplitudes of the transmitted waves on the normalized distance between the source and the boundary. Model parameters are  $n=3$ ,  $\sigma=1.4$ ,  $\bar{d}=0.66$ ,  $\bar{r}=1.8$ .

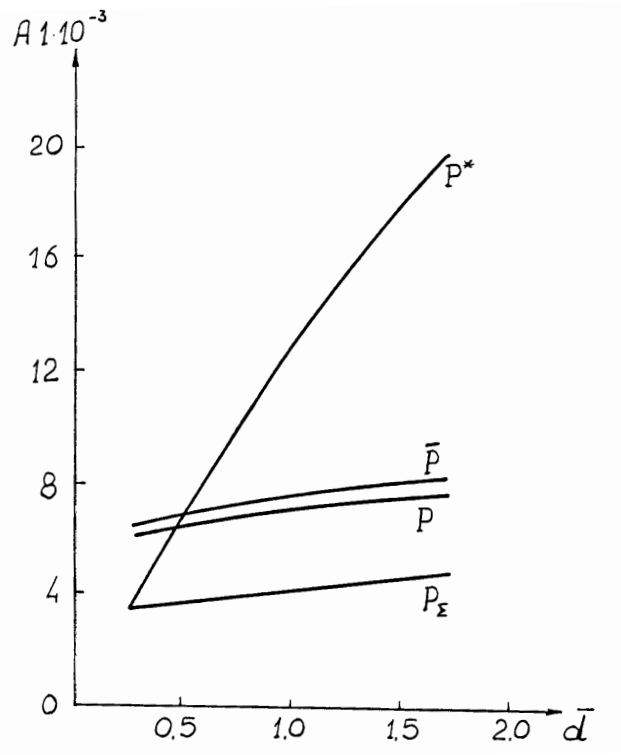


Figure 3.18: Dependence of the amplitudes of the transmitted waves on the normalized distance between the receiver and the boundary. Model parameters are  $n=3$ ,  $\sigma=1.4$ ,  $\bar{z}_0=0.1$ ,  $\bar{r}=2.5$ .

of the wavefront corresponding to larger refraction angles  $\theta_1^*$ . Note that the amplitude of  $P^*$  has a spherical divergence factor  $(1/\sqrt{r^2 + d^2})$  at a fixed refraction angle. Therefore, the peculiar dependence on  $r$  is explained by a sharply uneven distribution of energy along the wavefront of the pseudospherical wave.

In practice, we are mostly interested in the relative amplitudes of the waves  $P^*$  and  $P_\Sigma$ . From the analysis above it follows that the amplitude ratio  $P^*/P_\Sigma$  increases when the source is moved closer to the boundary and/or the receiver is moved away from the boundary (within the post-critical domain). The presence of attenuation in the low-velocity medium leads to smaller relative amplitudes of the wave  $P^*$  but does not change the wavefield drastically unless the attenuation coefficient is very large.

After having studied the transmitted wavefield we can finish our analysis of the reflected wavefield formed by incident inhomogeneous waves. While there are no stationary-phase points at complex  $\theta$  when  $n < 1$ , the situation changes for the case  $n > 1$ . If we apply the first-order approximation of the SPM on the interval  $1 < \sin \theta < n$ , we obtain two stationary points with  $\sin \theta$  slightly larger than unity and slightly smaller than  $n$ . The corresponding waves are inhomogeneous and propagate along the boundary with horizontal velocities close to  $c$  and  $c_1$  respectively. The first wave is excited by the leaking wave  $\bar{P}$  that travels along the boundary with the velocity a little bit smaller than  $c$  and generates an exponentially decaying wave in the incidence medium. The second wave is due to the horizontally propagating “ray” of the pseudospherical wave  $P^*$  that travels along the boundary in the reflecting medium with the velocity  $c_1$  and also generates an inhomogeneous wave in the incidence medium. Both reflected inhomogeneous waves exist only in the immediate vicinity of the boundary and decay exponentially with increasing source-boundary and/or receiver-boundary distance. In the saddle-point integration these waves should be taken into account when the saddle point approaches the branch point  $p = 1/c$  at large incidence angles.

We have discussed the properties of the nongeometrical waves for the simplest model - a fluid/fluid boundary. In the following chapter we will analyze complete wavefields including nongeometrical waves for more complicated elastic media.





# Chapter 4

## Point-source radiation in elastic media

### 4.1 Reflection/transmission of a spherical wave at a solid/solid boundary

After having treated the acoustic reflection/transmission problem, we continue the discussion of point-source radiation by considering reflection/transmission of spherical waves at a boundary between two elastic halfspaces.

As before, a point explosive source is located at distance  $z_0$  above a plane interface  $z = 0$ . The P-wave velocity, S-wave velocity and density in the incidence medium are denoted as  $c$ ,  $b$ , and  $\rho$  respectively; the same parameters of the second medium will have subscript “1.” The potential of the spherical wave radiated by the source is still given by equation (3.1.2) and may be decomposed into plane or cylindrical waves exactly as in a fluid medium. We will represent the potential of the incident wave as the Weyl integral over plane waves (3.1.10):

$$\phi_{inc} = \frac{1}{R} e^{i(kR - \omega t)} = \frac{ik}{2\pi} e^{-i\omega t} \int_0^{\pi/2 - i\infty} \int_0^{2\pi} e^{i[k_x x + k_y y + k_z(z_0 - z)]} \sin \theta d\theta d\phi. \quad (4.1.1)$$

The factor  $e^{-i\omega t}$  will be omitted in the following. The derivation of the integral expressions for the reflected/transmitted wavefield at a solid/solid interface is in principle similar to the acoustic case; the differences are associated with the treatment of shear waves. Below we will obtain integral expressions for the transmitted wavefield; the corresponding expressions for the reflected wavefield can be derived in the same fashion.

We begin with the potential of the transmitted P-wave. Taking into account the vertical phase shift and the transmission coefficient, an elementary transmitted P-wave from the decomposition (4.1.1) can be written as

$$\phi_{tr}^{pl} = W_{pp}(\theta) e^{i(k_x x + k_y y + k_z z_0 - k_{1z} z)}. \quad (4.1.2)$$

The value of the transmission coefficient  $W_{pp}$  is known from the solution of the plane-wave problem. Integrating over the transmitted plane waves, we get

$$\phi_{tr} = \frac{ik}{2\pi} \int_0^{\pi/2-i\infty} \int_0^{2\pi} W_{pp}(\theta) e^{i(k_x x + k_y y + k_z z_0 - k_{1z} z)} \sin \theta d\theta d\phi. \quad (4.1.3)$$

Applying formula (3.1.12) for the Bessel function, we find the potential of the transmitted P-wave to be

$$\phi_{tr} = ik \int_0^{\pi/2-i\infty} W_{pp} e^{i(k z_0 \cos \theta - k_1 z \cos \theta_1)} J_0(kr \sin \theta) \sin \theta d\theta. \quad (4.1.4)$$

We have obtained a Sommerfeld-type integral identical to the expression (3.2.5) for the wavefield transmitted through a fluid/fluid boundary; the difference is only in the value of the transmission coefficient.

Since the model is now elastic, each incident plane P-wave also generates a transmitted SV-wave with the potential  $\psi$  given by

$$\psi_{tr, \vec{y}}^{pl} = W_{ps}(\theta) e^{i(k_x x + k_y y + k_z z_0 \cos \theta - k_{s1} z \cos \gamma_1)}, \quad (4.1.5)$$

where  $k_{s1}$  and  $\gamma_1$  are the S-wave's wavenumber and the refraction angle in the second (refracting) medium. SH-waves are not excited because an explosive source generates only P-waves and there is no coupling between P and SH-waves at the boundary.

Unlike the P-wave potential, the S-wave potential  $\vec{\psi}_{tr}^{pl}$  is a vector that lies in the horizontal plane perpendicular to the wave vectors of the incident and transmitted plane waves. This property of  $\vec{\psi}_{tr}^{pl}$  was established when we discussed the potentials of P and S plane waves in 1-D layered models (see equations [2.2.3 - 2.2.5]). Formula (4.1.5) gives the scalar value of the S-wave's potential along the horizontal  $\vec{y}$ -axis perpendicular to the wave vectors  $\vec{k}$  and  $\vec{k}_{s1}$ . Therefore, when we sum up the elementary transmitted S-waves, we have to perform a vector summation of the potentials instead of the scalar summation we have just done for the P-wave.

It is convenient to find the projections of the S-wave potential on the directions parallel and perpendicular to the receiver azimuth  $\alpha$  ( $x = r \cos \alpha$ ,  $y = r \sin \alpha$ ). Since the horizontal component of the wave vector  $\vec{k}_{s1}$  makes the angle  $\phi$  with the  $x$ -axis, the angle between the corresponding S-wave potential  $\vec{\psi}_{tr}^{pl}$  and the  $x$ -axis is  $\phi + 90^\circ$ . The angle between  $\vec{\psi}_{tr}^{pl}$  and the receiver azimuth is then  $\phi + 90^\circ - \alpha$ , and the projection of the S-wave potential on the source-receiver direction is

$$\psi_{\parallel}^{pl} = \psi_{tr}^{pl} \cos(\phi - \alpha + 90^\circ) = -\psi_{tr}^{pl} \sin(\phi - \alpha). \quad (4.1.6)$$

The projection of  $\vec{\psi}_{tr}^{pl}$  on the normal to the source-receiver direction is (the positive direction of the normal is counterclockwise from the  $x$ -axis):

$$\psi_{\perp}^{pl} = \psi_{tr}^{pl} \cos(\phi - \alpha). \quad (4.1.7)$$

In order to find the total S-wave potential in the refracting medium due to the incident spherical wave, we perform the summation over the plane waves' potentials projected on the above two directions. Using equations (4.1.5, 4.1.6), we get for the S-wave potential in the source-receiver direction

$$\psi_{\parallel} = -\frac{ik}{2\pi} \int_0^{\pi/2-i\infty} \int_0^{2\pi} W_{ps}(\theta) e^{i(k_x x + k_y y + k_z z \cos \theta - k_{s1} z \cos \gamma_1)} \sin(\phi - \alpha) \sin \theta d\theta d\phi. \quad (4.1.8)$$

Representing  $k_x x + k_y y = kr \sin \theta \cos(\phi - \alpha)$ , the integral over  $\phi$  can be written as

$$I_{\parallel}^{\phi} = \int_0^{2\pi} e^{ikr \sin \theta \cos(\phi - \alpha)} \sin(\phi - \alpha) d\phi. \quad (4.1.9)$$

Due to the combination of the even and uneven functions (the exponent and the term  $\sin(\phi - \alpha)$ ), the integral (4.1.9) is zero and, consequently, the whole component  $\psi_{\parallel}$  vanishes.

Similarly, from equation (4.1.7) the S-wave potential projected on the normal to the source-receiver direction is

$$\psi_{\perp} = \frac{ik}{2\pi} \int_0^{\pi/2-i\infty} \int_0^{2\pi} W_{ps}(\theta) e^{i(k_x x + k_y y + k_z z \cos \theta - k_{s1} z \cos \gamma_1)} \cos(\phi - \alpha) \sin \theta d\theta d\phi. \quad (4.1.10)$$

The integral over  $\phi$  in this case takes the form

$$I_{\perp}^{\phi} = \int_0^{2\pi} e^{ikr \sin \theta \cos(\phi - \alpha)} \cos(\phi - \alpha) d\phi. \quad (4.1.11)$$

Using the expression for the first-order Bessel function

$$J_1(x) = \frac{-i}{2\pi} \int_0^{2\pi} e^{ix \cos t} \cos t dt, \quad (4.1.12)$$

we obtain

$$I_{\perp}^{\phi} = 2\pi i J_1(kr \sin \theta). \quad (4.1.13)$$

The integral for the S-wave's potential becomes

$$\psi_{\perp} = -k \int_0^{\pi/2-i\infty} W_{ps}(\theta) e^{i(k_z z \cos \theta - k_{s1} z \cos \gamma_1)} J_1(kr \sin \theta) \sin \theta d\theta. \quad (4.1.14)$$

Thus, the potential of the transmitted S-wave lies in the horizontal plane normal to the source-receiver direction.

From this point on it is more convenient to use a cylindrical coordinate system  $[r, \alpha, z]$ . This choice of the coordinate system is natural since our problem is axially symmetric, and there should be no dependence on the angle  $\alpha$ . Also, equation (4.1.14) that we have just derived gives the  $\alpha$ -component of the S-wave potential ( $\psi_{\perp} = \psi_{\alpha}$ ). Although we have obtained this result without explicitly applying any symmetry considerations, it is obvious that the SV-wave motion is confined to the incidence plane (the vertical plane through the source and receiver) and, therefore, the corresponding shear-wave potential should be perpendicular to this plane. In other words, the SV-wave motion has only  $r$  and  $z$ -components, so the potential should point in the  $\alpha$ -direction.

While in the acoustic problem we studied the P-wave potential (or pressure) only, in elastic media we are dealing both with P- and S-waves, and it is necessary to obtain

the displacement  $\vec{u} = \text{grad } \phi + \text{curl } \vec{\psi}$ . Due to the symmetry of the problem the displacement vector has only the horizontal radial ( $u_r$ ) and vertical components ( $u_z$ ); the horizontal transverse component ( $u_\alpha$ ) is zero. Using the expressions for gradient and curl in cylindrical coordinates yields

$$u_r = \frac{\partial \phi}{\partial r} - \frac{\partial \psi_\alpha}{\partial z}, \quad (4.1.15)$$

$$u_z = \frac{\partial \phi}{\partial z} + \frac{\partial \psi_\alpha}{\partial r} + \frac{\psi_\alpha}{r}. \quad (4.1.16)$$

Substituting the expressions for the potentials (4.1.4,4.1.14) into equations (4.1.15,4.1.16) and using the relations between the Bessel functions

$$J_0'(x) = -J_1(x),$$

$$J_1'(x) = J_0(x) - \frac{J_1(x)}{x},$$

we obtain the final formulas for the displacement of the transmitted wave:

$$u_r = -ik \int_0^{\pi/2-i\infty} P_r e^{ikh \cos \theta} J_1(kr \sin \theta) \sin \theta d\theta, \quad (4.1.17)$$

$$P_r = k \sin \theta W_{pp} e^{ik_1 d \cos \theta_1} + k_{s1} \cos \gamma_1 W_{ps} e^{ik_{s1} d \cos \gamma_1},$$

$$u_z = k \int_0^{\pi/2-i\infty} P_z e^{ikh \cos \theta} J_0(kr \sin \theta) \sin \theta d\theta, \quad (4.1.18)$$

$$P_z = k_1 \cos \theta_1 W_{pp} e^{ik_1 d \cos \theta_1} - k \sin \theta W_{ps} e^{ik_{s1} d \cos \gamma_1},$$

where  $h = z_0$ ,  $d = -z$ .

The integrals for the displacement components have essentially the same structure as the expressions for the wavefields reflected and transmitted at a fluid/fluid boundary. Clearly, the main difference between the solid and fluid models is the presence of the *PS* component in integrals (4.1.17,4.1.18). One of the advantages of the plane-wave decomposition technique is the ability to separate wavefields of different types e.g., *PP* and *PS*-waves.

It should be emphasized that the integral solutions for any layered elastic model (including the reflection of a spherical wave from a free surface) are very similar to formulas (4.1.17,4.1.18). This point will be developed in more detail below, in the discussion of the reflectivity method.

## 4.2 Analysis of the reflected/transmitted wavefield

The similarity between the integral solutions for a solid/solid and fluid/fluid boundaries makes it easier for us to understand the basic features of the transmitted wavefield hidden in formulas (4.1.17,4.1.18). Any displacement component for each of the waves has practically the same structure as the integrals for the reflected/transmitted P-wave at a fluid/fluid boundary. The first-order Bessel function  $J_1$  can be represented for large arguments as

$$J_1(x) \approx \sqrt{\frac{2}{\pi x}} \cos(x - 3\pi/4) = \sqrt{\frac{1}{2\pi x}} [e^{i(x-3\pi/4)} + e^{-i(x-3\pi/4)}]. \quad (4.2.1)$$

The difference between this expression and a similar asymptotic formula for the zero-order Bessel function  $J_0$  (3.3.1) is just a constant ( $\pi/2$ ). Therefore, the phases of the integrands (not including the reflection/transmission coefficients) in formulas (4.1.17-4.1.18) are identical to the phase functions we have considered for the acoustic reflection/transmission problem. For instance, the phase of the integrand in the expression for the transmitted PS-wave for large  $kr \sin \theta$  is

$$\Phi_{ps} = kh \cos \theta + k_{s1}d \cos \gamma_1 + kr \sin \theta + const. \quad (4.2.2)$$

Clearly,  $\Phi_{ps}$  virtually coincides with the phase function for the P-wave transmitted across a fluid/fluid boundary in formula (3.6.1); the only difference is in the value of the wavenumber in the refracting medium.

Therefore, there are many similarities between the contour integration for the waves scattered by a solid/solid and a fluid/fluid boundary. The saddle points and the steepest-descent paths are determined by the same equations with the appropriate wavenumbers and reflection/refraction angles. As in our analysis for the acoustic case, the saddle points for a solid model correspond to the geometrical arrivals reflected and transmitted in accordance with Snell's law. The contour integration for a solid/solid boundary is much more involved technically due to more complicated reflection/transmission coefficients and the presence of four radicals (instead of two in the acoustic case) for the vertical slownesses of P- and S-waves in both media. However, the principal features of the analysis performed above for the acoustic case remain valid in elastic media. For example, integration along the branch cuts yields asymptotic expressions for the head waves; more branch cuts just mean that the solid model generates more head waves.

Our analysis for the acoustic model has shown that there are no surface waves at an interface between two fluid halfspaces. One of the important properties of a solid/solid boundary is the potential existence of a surface wave (the so-called Stoneley wave). For certain velocity and density ratios the denominator of the reflection/transmission coefficients can become zero, and this pole is responsible for the generation of the Stoneley wave. Aki and Richards (1980) show how the contribution of the surface-wave pole can be picked up by an appropriate deformation of the integration path. It should be emphasized, however, that the conditions necessary for the excitation of the Stoneley wave are not typically encountered in the Earth (Sezawa and Kanai, 1939; Ginzburg and Strick,

1958). By contrast, the surface wave at a free surface of a solid halfspace (the Rayleigh wave) does exist for any combination of elastic parameters.

The other high-frequency asymptotic technique we have used - the stationary phase method (SPM) - also works for a solid/solid interface essentially in the same way as in the acoustic problem. Since the phases of the integrands in the expressions for the reflected/transmitted waves have the same structure for the two boundaries, there is no substantial difference between the application of the zero-order approximation of the SPM in the acoustic and elastic case. For instance, if we take the derivative of the expression (4.2.2) to find the stationary phase points for the transmitted PS-wave, we will obtain the equation for the geometrically transmitted ray.

If the S-wave velocity in the refracting medium is smaller than the P-wave velocity in the incidence medium, the zero-order approximation of the SPM would also yield the stationary point for the pseudospherical wave ( $S_1^*$ ). Indeed, the phase function (4.2.2) for inhomogeneous incident P-waves and homogeneous transmitted S-waves becomes

$$\Phi_{ps} = k_{s1}d \cos \gamma_1 + kr \sin \theta + const = k_{s1}d \cos \gamma_1 + k_{s1}r \sin \gamma_1 + const, \quad (4.2.3)$$

and for the stationary point we get  $\gamma_1 = \tan^{-1}(r/d)$ .

It seems that the difference between the acoustic and elastic problems should be more pronounced if the first-order approximation of the stationary phase method is applied. Indeed, the expressions for the reflection/transmission coefficients and, therefore, the corresponding phase functions are much more complicated in the elastic case. However, the “big picture” of the stationary points in the first-order approximation of the SPM remains essentially the same. Actually, Figure 3.3, which we used to illustrate the solution of the stationary-phase equation for a fluid/fluid boundary, corresponds to a boundary between two solids. Our analysis for the fluid model has shown that the phase functions of the reflection/transmission coefficients generate stationary points only near the critical angles. This conclusion remains valid for the elastic model as well. When the vertical slownesses of the reflected/transmitted waves go to zero, the derivative of the phase functions of the reflection/transmission coefficients becomes infinite leading to stationary phase points in the vicinity of the critical angles. Depending on the velocity ratios and the type of the incident wave, these stationary points correspond either to head waves or to leaking waves. The physical properties of the head and leaking waves at a fluid/fluid and solid/solid boundaries are also similar.

For instance, if the P-wave is reflected from a high-velocity medium and  $b < b_1 < c < c_1$ , the only possible head wave has the horizontal velocity  $c_1$ . Propagating along the boundary, this wave generates conical P ( $PP_1P$ ) and S ( $PP_1S$ )-waves in the incidence medium and a shear conical wave ( $PP_1S_1$ ) in the reflecting medium. Physically, the generation of the head waves has exactly the same character as at a fluid/fluid boundary. The leaking and pseudospherical waves at a solid/solid boundary are discussed in more detail in the next section.

### 4.3 Nongeometrical waves in elastic media

We begin with the case of a single boundary between two solids and then outline some implications of our results for stratified models. As we have proved for the acoustic model, nongeometrical waves are generated by the transition of inhomogeneous waves contained in point-source radiation into homogeneous, non-decaying waves during the reflection/transmission at a boundary. In order to understand what types of nongeometrical waves are excited for a specific model, we recall that this transition requires a decrease in velocity. For instance, for nongeometrical transmitted PS-waves to occur, the S-wave velocity in the refracting medium should be smaller than the P-wave velocity in the incidence medium.

Let us consider in more detail the case of a point source located in the high-velocity medium close to the boundary; the velocities in the model satisfy  $c > b > c_1 > b_1$ . Excitation from the high-velocity halfspace allows us to observe all nongeometrical waves that can be generated at an interface between two solids.

The horizontal velocity of the inhomogeneous waves from the plane-wave (or cylindrical-wave) decomposition of point-source radiation decreases from  $c$  to zero along the integration path. The inhomogeneous waves with the horizontal velocity  $V_h$  greater than  $b$  ( $c > V_h > b$ ) are transformed into homogeneous reflected S-waves and, therefore, give rise to the leaking wave  $\bar{P}S$  with the horizontal velocity slightly smaller than  $c$  and the pseudospherical wave  $S^*$ . These nongeometrical waves are excited in the incidence medium and have essentially the same properties as the nongeometrical waves at a fluid/fluid boundary.

Several more nongeometrical arrivals are generated in the refracting (low-velocity) medium (Figure 4.1). The leaking wave propagating along the boundary with the velocity close to  $c$  radiates two conical transmitted waves: the P-wave  $\bar{P}P_1$  with the refraction angle close to  $\sin^{-1}(c_1/c)$  and the S-wave  $\bar{P}S_1$  with the angle close to  $\sin^{-1}(b_1/c)$ . Since the horizontal velocities of the incident inhomogeneous waves cover the whole range  $V_h < c$ , two more leaking waves are excited. One of them, with the horizontal velocity slightly smaller than  $b$ , “leaks” two conical waves into the low-velocity medium:  $\bar{S}P_1$  and  $\bar{S}S_1$ . The horizontal velocity of the third leaking wave is close to  $c_1$ ; therefore, it excites only one (transmitted) conical wave  $\bar{P}_1S_1$ .

Since  $c > c_1$  and  $c > b_1$ , a point source located in the high-velocity halfspace also generates two pseudospherical waves (P and S) in the low-velocity medium denoted as  $P_1^*$  and  $S_1^*$ . The resulting transmitted wavefield is very complicated due to the interference of many nongeometrical arrivals with different waveforms and polarizations.

Figure 4.1 shows the vertical component of the displacement vector near the boundary, where the refraction angles of both pseudospherical waves are relatively large. Since the nongeometrical waves have almost linear polarization, the wave  $P_1^*$  is much more intensive for this geometry on the horizontal displacement component. Being one of the most intensive waves even on the vertical component,  $P_1^*$  virtually dominates the horizontal displacement. Computations for a wide range of elastic models have shown that the pseudospherical wave  $P_1^*$  is usually the most prominent nongeometrical arrival in the

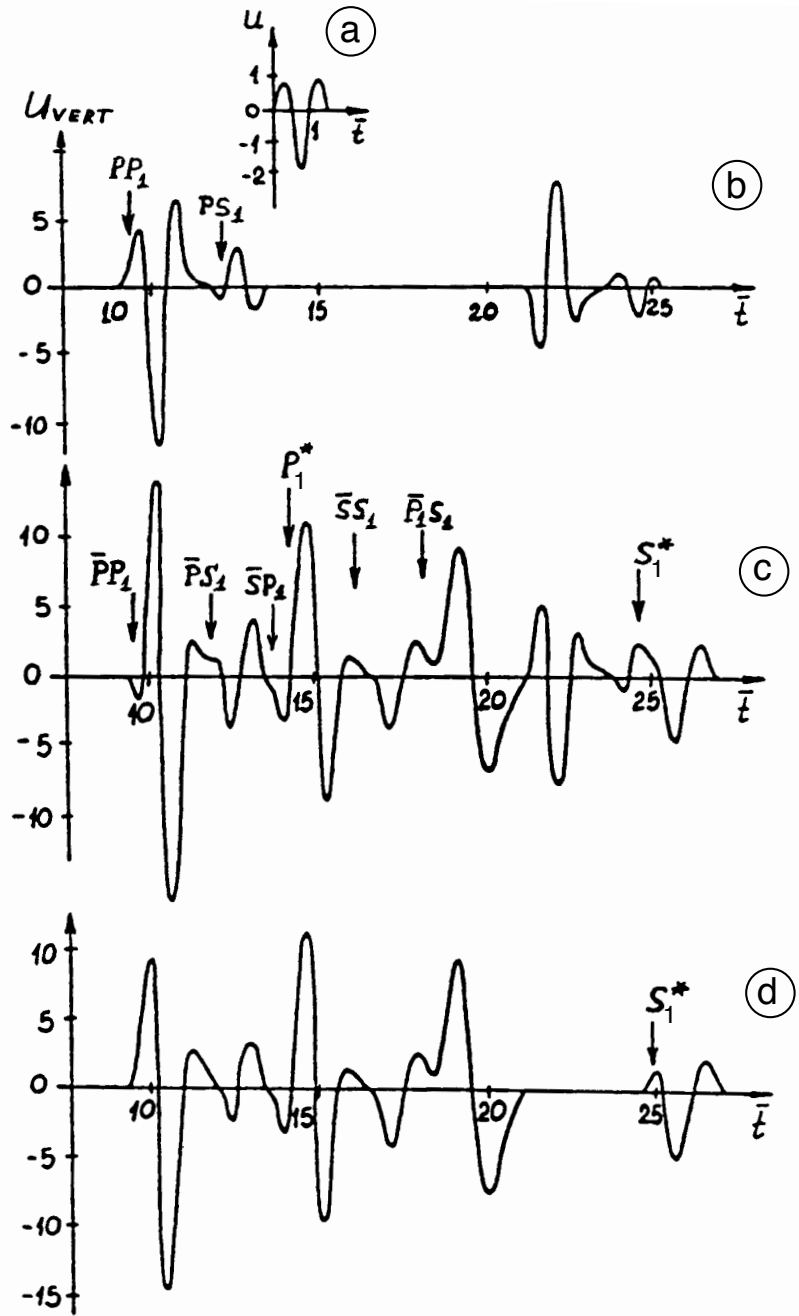


Figure 4.1: Exact synthetic seismograms of the wavefield transmitted through a solid/solid boundary (vertical displacement). a - source pulse, b - the contribution of homogeneous incident waves, c - the contribution of inhomogeneous incident waves (nongeometrical waves), d - the total seismogram. Note false arrivals at  $\bar{t} > 20$  that vanish on the total seismogram. Model parameters are  $n = c/c_1=2$ ,  $\sigma = \rho_1/\rho=0.8$ ,  $c/b = c_1/b_1 = 1.73$ ,  $\bar{h}=0.1$ ,  $\bar{d}=1.5$ ,  $\bar{r}=7$ .  $\bar{h}$ ,  $\bar{d}$ ,  $\bar{r}$  are the distances normalized by the predominant wavelength in the high-velocity halfspace.



transmitted wavefield.

The nongeometrical waves vanish if the source is moved away from the boundary with the degree of decay becoming higher with decreasing horizontal velocity. For instance, the fastest-decaying leaking wave is  $\bar{P}_1$ , followed by  $\bar{S}$  and  $\bar{P}$ . The distribution of energy along the wavefronts of the pseudospherical waves is essentially the same as in the acoustic model, with much higher amplitudes near the critical ray and almost no energy propagating along the boundary.

It should be emphasized that the geometrical seismics predicts only two ( $PP_1$  and  $PS_1$ ) conventional transmitted waves on trace b in Figure 4.1. A large number of intensive nongeometrical arrivals in a very simple model suggests that nongeometrical waves may be often misinterpreted on real data. If a seismogram like the one in Figure 4.1 were recorded in a cross-hole experiment, it would be natural for the interpreter to attribute the complexities of the observed wavefield to the influence of non-existent boundaries.

An important feature of the wavefield in Figure 4.1 is a significant amount of shear energy generated by a pure explosive source due to the nongeometrical effects. For instance, note that one of the leaking waves propagates along the boundary with the shear velocity in the incidence medium. By contrast, there are no conventional S-waves excited directly by the source in the high-velocity medium (although, of course, the reflected  $PS$ -wave does exist).

The experimental example below shows how we can take advantage of nongeometrical shear waves in cross-hole surveys. Cross-borehole geometry is especially favorable for nongeometrical waves to be generated because a downhole source is often located close to one of the internal boundaries. The experiment has been carried out by Moscow University in Crimea, former USSR (now a disputed territory between Russia and Ukraine). A source (electrical sparker) and a receiver (pressure recorder) were placed in two water-filled boreholes near the boundary between sandstone and clay layers (Figure 4.2).

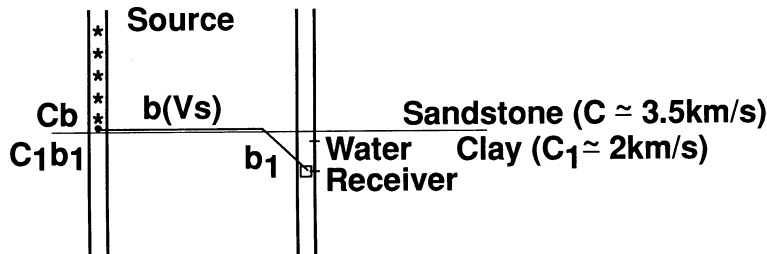


Figure 4.2: Scheme of the experiment in Crimea. The source is located in sandstone, the receiver is in clay. The distance between the boreholes is 18.5 m, the receiver is 1 m under the boundary. The leaking wave  $\bar{S}$  propagates along the boundary with the shear-wave velocity in the sandstone ( $b$ ).

The wavefield for this model (Figure 4.3) is much simpler than the one displayed in Figure 4.1. Since the borehole has not been included in the model, it was assumed that the horizontal displacement for this geometry gives the closest approximation to the pressure

inside the hole. Numerical modeling shows that the only intensive nongeometrical wave that forms a separate arrival is the leaking wave propagating along the boundary with the shear-wave velocity in the sandstone ( $b$ ). The nature of this wave can be identified by the rapid amplitude decay with the increasing distance between the source and the boundary. Note that a small distance between the receiver and the boundary makes the contribution of the pseudospherical waves negligible.

The overall match between the experimental and synthetic data is satisfactory. Some differences in the waveforms and amplitudes are most possibly caused by the influence of the borehole ignored in the modeling. This experiment made it possible to determine the value of the shear-wave velocity in the sandstone (1960 m/s) that was confirmed later by tube-wave measurements.

In the marine environment, pronounced nongeometrical effects can be expected in shallow water, when a source and a receiver are close to the sea bottom. The model in Figure 4.4 has been encountered by an expedition of Moscow University in one of the shallow Baltic Sea bays. An underwater layer composed of low-velocity tough silt ( $c_1=300-800$  m/s) overlaid a relatively thick layer of sand with the velocity  $c_2=1800-2200$  m/s.

In this model, the pseudospherical wave  $P_1^*$  formed at the sea bottom excites a very strong head wave in the sand ( $P_1^*S_2P_1^*$ ) that propagates with the horizontal velocity  $b_2$  and generates a P-wave back into the silt layer. Reverberations of the pseudospherical wave  $P_1^*$  inside the layer produce a number of multiples with the amplitudes far exceeding the amplitude of the primary  $P_1^*$ -reflection. Such high amplitudes of head waves and multiple reflections are quite unusual for conventional body waves but very typical for nongeometrical waves. The reason for this effect is the uneven distribution of energy along the wavefront of the pseudospherical wave  $P_1^*$  incident on the top of the sand layer. While the “secondary” head wave and the multiples are formed by the most intensive part of the wavefront that is close to the critical ray  $\theta_{1cr} = \sin^{-1}(c_1/c)$ , the primary reflection  $P_1^*$  at relatively large horizontal offsets is due to the low-amplitude section of the wavefront adjacent to the sea bottom. It is interesting that the multiples in the underwater layer are very intensive in spite of a very large value of the attenuation coefficient.

When the source is close to the sea bottom, the seismograms are almost entirely composed of the nongeometrical waves (Figure 4.5). The most prominent arrival in a wide range of offsets is the secondary head wave  $P_1^*S_2P_1^*$ . These synthetic traces closely match the experimental data. The traveltimes of nongeometrical waves made it possible not only to map the thickness and the P-wave velocity of the silt layer, but also to estimate the shear-wave velocity in the sand.

Possible applications of nongeometrical waves are not limited to the examples discussed above. Explosive sources often produce shear waves of uncertain nature (Lash, 1985), which are likely to be caused by nongeometrical effects at the free surface or shallow boundaries. With the advent of multicomponent seismology, these waves will definitely attract more attention.

Nongeometrical waves also make a prominent contribution to seismological earthquake records because the wave propagation from buried sources toward the surface usually in-

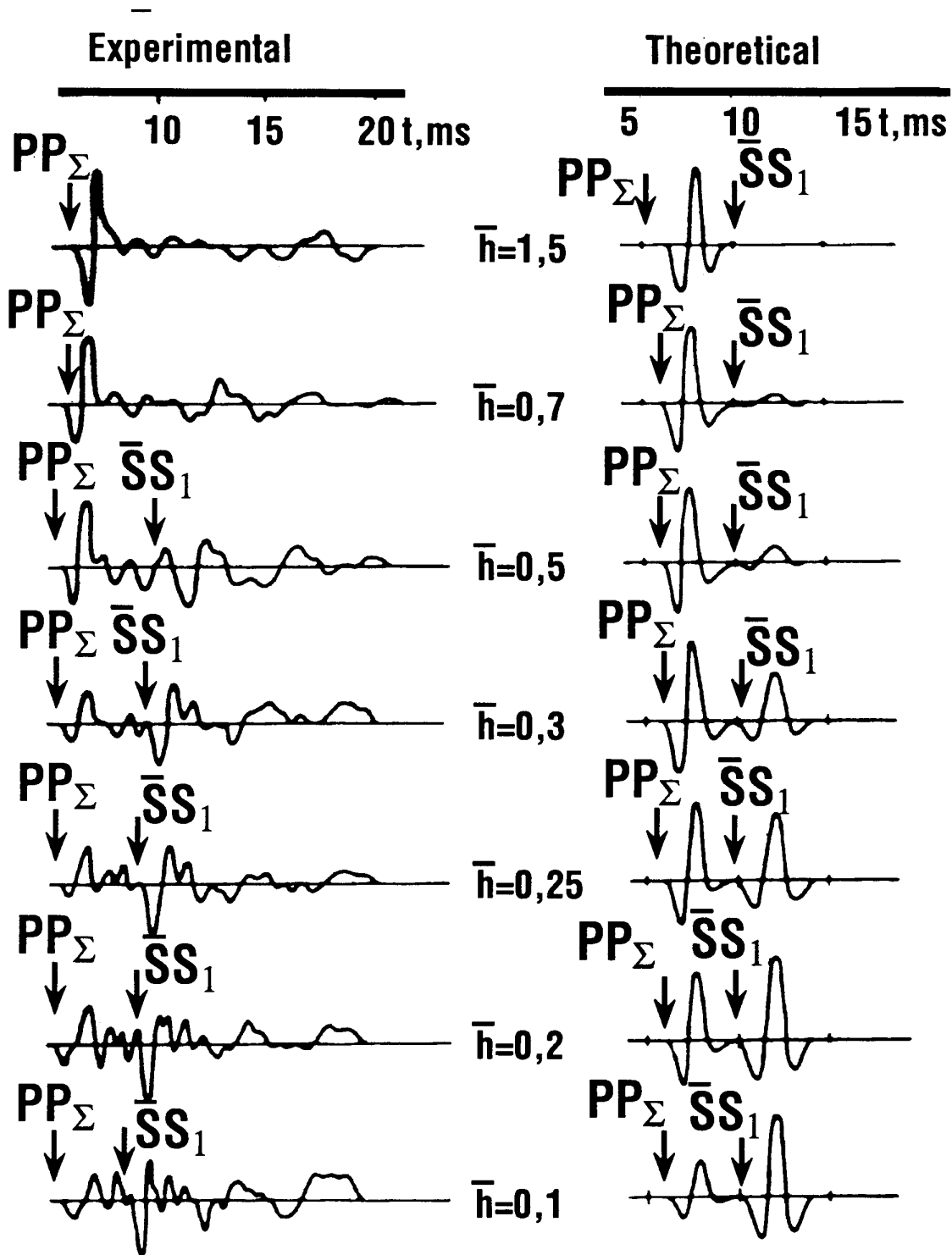


Figure 4.3: Field data (pressure) and synthetic seismograms (horizontal displacement) for the Crimea experiment. The synthetic traces are scaled to match the experimental seismograms, which do not give the correct absolute amplitudes.  $\bar{h} = h/\lambda$  is the normalized source-boundary distance,  $\lambda = 5$  m is the predominant wavelength.

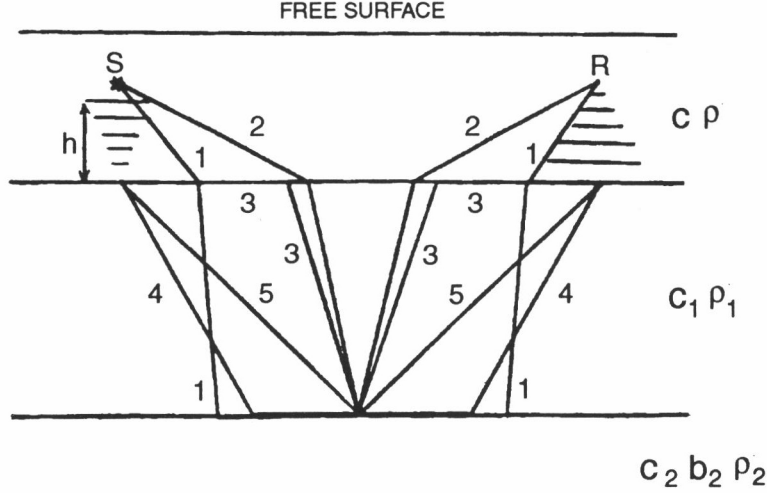


Figure 4.4: Reflection from a low-velocity underwater layer. The velocities in the model satisfy  $c_1 < b_2 < c < c_2$ . Conventional P-waves: 1 - head wave; 2 - reflected wave. Nongeometrical waves: 3 - leaking wave ( $\bar{P}$ ); 4 - secondary head wave ( $P_1^* S_2 P_1^*$ ); 5 - reflected pseudospherical wave ( $P_1^*$ ).

volves transmission from high-velocity into low-velocity layers with generation of a considerable amount of nongeometrical energy. For instance, the presence of nongeometrical waves may seriously affect the recovery of the source moment tensor.

#### 4.4 Wave phenomena due to additional terms of the ray series

It is important to make a distinction between geometrical seismics and a general ray theory. The geometrical seismics approximation represents just the leading term of the ray series expansion. Therefore, some effects incompatible with geometrical seismics can still be explained by ray theory if additional terms of the ray series expansion are taken into account. By contrast, the nongeometrical waves discussed above cannot be described within the framework of the ray theory as a whole.

In the so-called “space-time” version of the ray method the displacement is represented as follows:

$$\vec{U}(\vec{R}, t) = \vec{U}^{(0)}(\vec{R}) f^{(0)}(t - \tau) + \vec{U}^{(1)}(\vec{R}) f^{(1)}(t - \tau) + \dots, \quad (4.4.1)$$

where  $\tau(\vec{R})$  is the travelttime along the geometrical ray, and

$$f^{(1)}(t) = \int_0^t f^{(0)}(y) dy. \quad (4.4.2)$$

$\vec{U}^{(0)}$  is the displacement vector in the geometrical seismics approximation,  $\vec{U}^{(1)}$  determines the displacement of the first additional term of the ray series. While the leading

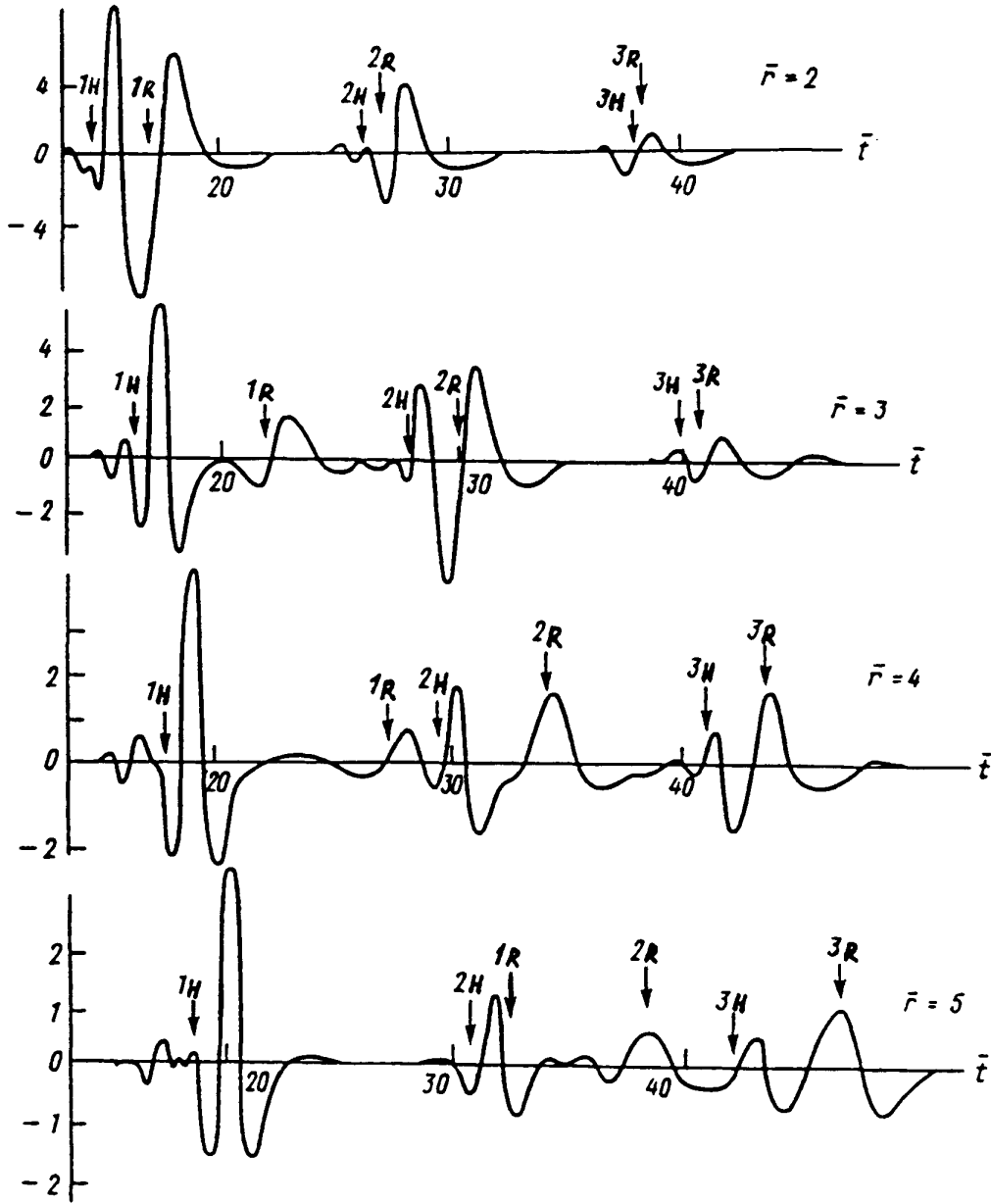


Figure 4.5: Synthetic traces (potential) at different offsets for the model from Figure 4.4. High-frequency reverberations in the water have been filtered out. 1 - primary arrivals, 2,3 - multiples inside the layer. The subscript “H” denotes the secondary head wave ( $P_1^*S_2P_1^*$ ), “R” stands for the reflected pseudospherical wave ( $P_1^*$ ). Model parameters are  $c/c_1=5$ ,  $c_1/c_2=0.15$ ,  $c_2/b_2=2$ ,  $\rho_1/\rho=1.4$ ,  $\rho_2/\rho_1=1.3$ ,  $\bar{h}=0.1$ ,  $\bar{d}=1$  ( $d$  is the thickness of the layer),  $\bar{H}=0.375$  ( $H$  is the thickness of the water). Attenuation coefficients are  $\alpha_{P1} = 5 \cdot 10^{-6}$  s/m (underwater layer),  $\alpha_{P2} = 10^{-4}$  s/m (P-waves in the lower halfspace),  $\alpha_{S2} = 10^{-5}$  s/m (S-waves in the lower halfspace).

term is rather easy to derive, the first-order one has a complicated structure specific to each particular problem. Among the general properties of the first-order term is its lower frequency content compared with the leading term (this is evident from formula [4.4.2]) and a more rapid amplitude decay along the ray.

The polarization of the first-order term is generally different from the polarization in the geometrical-seismics approximation. Therefore, if the contribution of the first-order term is significant, the particle motion becomes nonlinear due to the differences in polarization and waveform between the two leading terms of the series.

In general, deviations from the geometrical seismics are substantial in the areas where the leading term of the ray series is small or rapidly varies with spatial coordinates (due to the dependence of  $\vec{U}^{(1)}$  on the spatial derivatives of  $\vec{U}^{(0)}$ ). For instance, in a homogeneous medium the influence of the first-order term is most significant near minima of radiation patterns.

As an example of a wave phenomenon that needs at least two terms of the ray series expansion to be adequately described, we consider the PS arrival generated by a spherical P-wave at a solid/solid boundary (Figure 4.6).

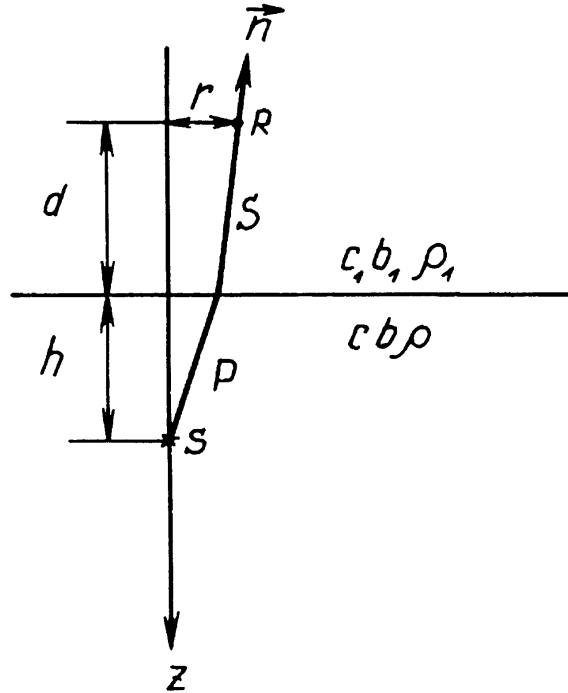


Figure 4.6: Source-receiver geometry in the analysis of the anomalous PS-wave.  $\vec{n}$  is the ray direction for the transmitted PS arrival.

Geometrical seismics predicts no PS converted wave at normal incidence since the plane-wave PS-conversion coefficient is zero. However, exact modeling shows that zero-offset seismograms of the *vertical* displacement contain (in addition to the PP reflected/transmitted waves) a wave that propagates with the shear-wave velocity after the

reflection or transmission (Figure 4.7). Note that the amplitude of this anomalous wave may reach 50% of the amplitude of the PP-reflection.

The anomalous PS arrival, although being formally denoted as a shear wave, has a pure longitudinal polarization. In fact, from the symmetry of the problem it is clear that the particle motion at zero offset should be strictly vertical. Indeed, the horizontal component of the displacement vector given by equation (4.1.17) vanish at  $r = 0$  because  $J_1(0) = 0$ .

In order to explain the properties of the PS-wave with the anomalous polarization, we have to take into account the first additional term of the ray series ( $\vec{U}^{(1)}(\vec{R}) f^{(1)}(t - \tau)$ ). At the vertical the leading (geometrical) term for the PS-wave is identically zero, and the anomalous PS arrival is entirely formed by the next, first-order term. While  $\vec{U}^{(0)}$  for the PS-wave is polarized like a conventional SV-wave (perpendicular to the ray direction in the incidence plane), the first-order term  $\vec{U}^{(1)}$  has a component polarized like a P-wave, parallel to the ray. At normal incidence this “longitudinal” component forms the first-order term and, consequently, the PS-wave as a whole.

In principle, the PS-wave at the vertical can be influenced by several higher-order terms of the ray series. However, it can be proved that the first two terms are usually sufficient to describe the anomalous PS-wave formed at a solid/solid boundary or at a free surface of an elastic halfspace. The dominant contribution of the first-order term manifests itself in the shape of the anomalous PS-wave: it is close to the integral of the source pulse, as predicted by formulas (4.4.1,4.4.2).

Physically, the generation of the anomalous PS-wave is related to the high curvature of the wavefront of the incident P-wave. If the source is located far from the boundary, the incident wavefront at any point is well-approximated by a plane wave, and the reflected and transmitted waves can be accurately described by geometrical seismics (the leading term of the ray series). In this case, the PS-wave at the vertical is very weak compared to the PP-wave. However, if the source-boundary distance is relatively small, the wavefront curvature at the reflection/transmission point is large, and the influence of the first-order term may be substantial.

Evidently, the PS/PP amplitude ratio at the vertical decreases if the source is moved away from the boundary (Figure 4.7). However, it should be emphasized that the anomalous PS-wave does not decay with increasing distance between the source and the boundary as rapidly as “pure” nongeometrical waves. Since the PS-wave is not related to the inhomogeneous waves contained in the point-source radiation, its amplitude decay is not exponential. From Figure 4.7 it is clear that the contribution of the PS-wave remains significant even if the distance between the source and the boundary exceeds the predominant wavelength. Another difference between the PS-wave and “pure” nongeometrical waves is in the dependence of the PS amplitude on the distance between the receiver and the boundary: the PS-wave decays as the receiver moves away from the boundary.

While at the vertical the PS-wave is entirely described by the first-order term of the ray series, the influence of the leading (zero-order) term rapidly increases with the horizontal offset (Figure 4.8). From the shape of the horizontal displacement it is clear that it is mostly formed by the geometrical-seismics term. However, the contribution of the first-

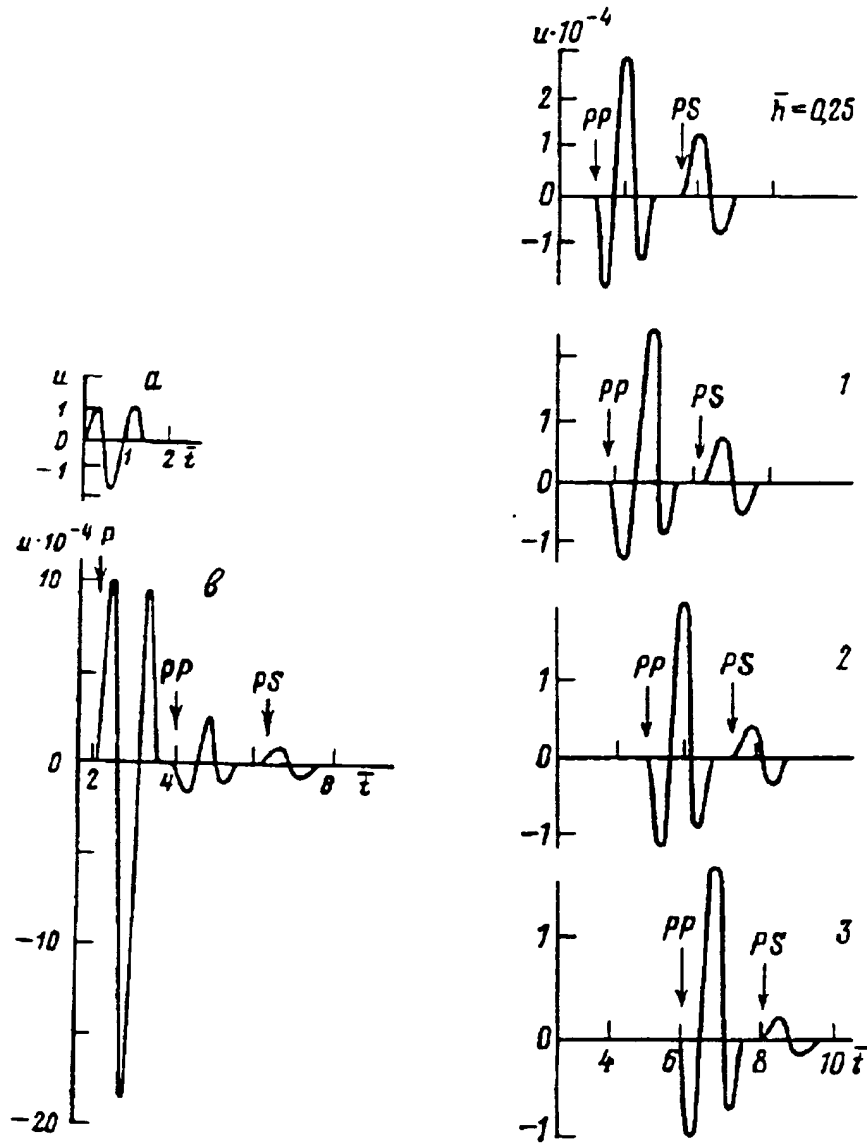


Figure 4.7: Zero-offset reflected wavefield (vertical displacement) excited by a point explosive source located near a solid/solid boundary. The horizontal displacement at  $r = 0$  is zero. On the left: a - the incident pulse; b - the wavefield at the vertical including the direct wave (P), PP-reflection, and PS-conversion. Model parameters are  $n = c/c_1 = 0.71$ ,  $\delta = c/b = 1.73$ ,  $\delta_1 = c_1/b_1 = 1.73$ ,  $\sigma = \rho_1/\rho = 1.25$ ,  $\bar{h}=1$ ,  $\bar{d}=3$ ,  $\bar{r}=0$ . On the right: seismograms of the reflected wave for different distances  $h$  between the source and the boundary. All the parameters except for  $h$  are the same as on the left.



order term to the vertical displacement and to the PS-wave as a whole remains substantial up to  $r \approx d/2$ . From Figure 4.8 it is clear that even away from the vertical the first-order term of the ray series is polarized virtually like a compressional wave.

A detailed discussion of the area of validity of ray theory in the description of the anomalous PS-wave can be found in Kiselev and Tsvankin (1989). Unless both the source and the receiver are very close to the boundary, the accuracy of the double-term ray series (consisting of the first two terms) is sufficiently high. Ray theory breaks down only at relatively large horizontal offsets beyond the critical point of the pure nongeometrical waves (Figure 4.9). Even an infinite ray series expansion (4.4.1) is based on the geometrical raypath and, therefore, cannot account for leaking or pseudospherical waves. It is interesting that by changing one geometrical parameter (the horizontal offset) in Figure 4.9, we move through three areas with a completely different character of the PS-wave. While in the area near the vertical ( $r \approx 0$ ) the PS-wave is described by the first additional term of the ray series, at intermediate offsets both the leading and the first-order terms are needed and, finally, at larger offsets the wavefield becomes purely nongeometrical and cannot be described by ray theory at all.

## 4.5 Comparison of modeling methods for stratified isotropic media

The Sommerfeld-type integrals for point-source radiation derived above provide the basis for a popular modeling technique for horizontally homogeneous media called the “reflectivity” method. This method has been widely used in global seismology and seismic exploration, especially in crustal studies in the interpretation of long (regional) reflection profiles.

Suppose we are interested in the exact response of a stack of horizontal homogeneous isotropic layers to an incident spherical P-wave. Then, repeating the derivation of formulas (3.2.4,4.1.4), we find the potential of the reflected P-wave to be

$$\phi_{refl} = ik \int_0^{\pi/2 - i\infty} V_{pp}(\theta) e^{ik(z+z_0)\cos\theta} J_0(kr \sin\theta) \sin\theta d\theta, \quad (4.5.1)$$

where  $z$  and  $z_0$  are the distances from the source and receiver respectively to the top of the first layer,  $V_{pp}$  is the response of the layered medium to an incident plane P-wave.

The form of  $V_{pp}$  depends on whether we would like to compute the total wavefield generated by the layered medium or just one or several wave components. In the former case we should use the matrix propagator for the reflected plane P-wave that takes all multiples and conversions into account. This matrix expression can be derived in a straightforward fashion from formula (2.7.18). If only a particular wave component (say, PSP conversion in the top layer) is desired,  $V_{pp}$  should be composed of the reflection/transmission coefficients and the vertical phase shifts for the corresponding plane wave. Also, it is possible to decompose the wavefield even further by calculating the contributions of different parts of the integration path separately. Therefore, the reflectivity method provides a sufficient

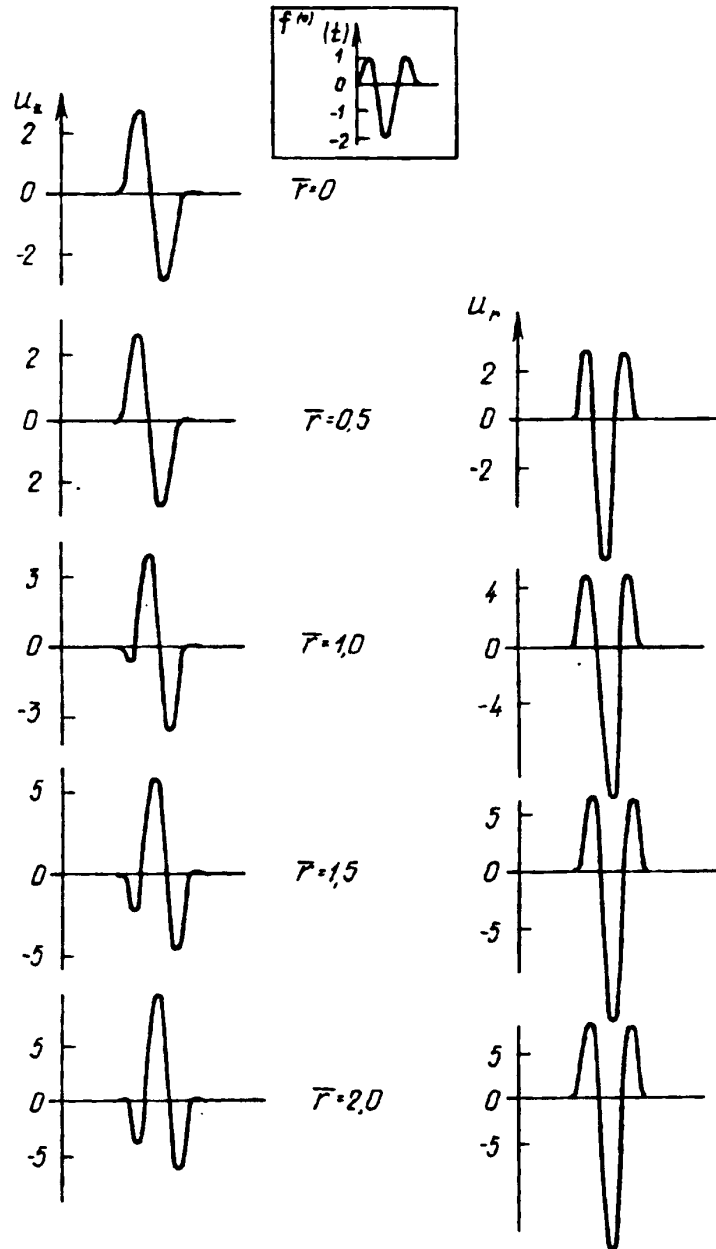


Figure 4.8: Synthetic seismograms of the transmitted PS-wave for different source-receiver offsets. The left column is the vertical displacement, the right column is the horizontal one (the horizontal component at  $r = 0$  is zero). Elastic parameters are the same as in Figure 4.7;  $\bar{h}=0.25$ ,  $\bar{d}=3$ .

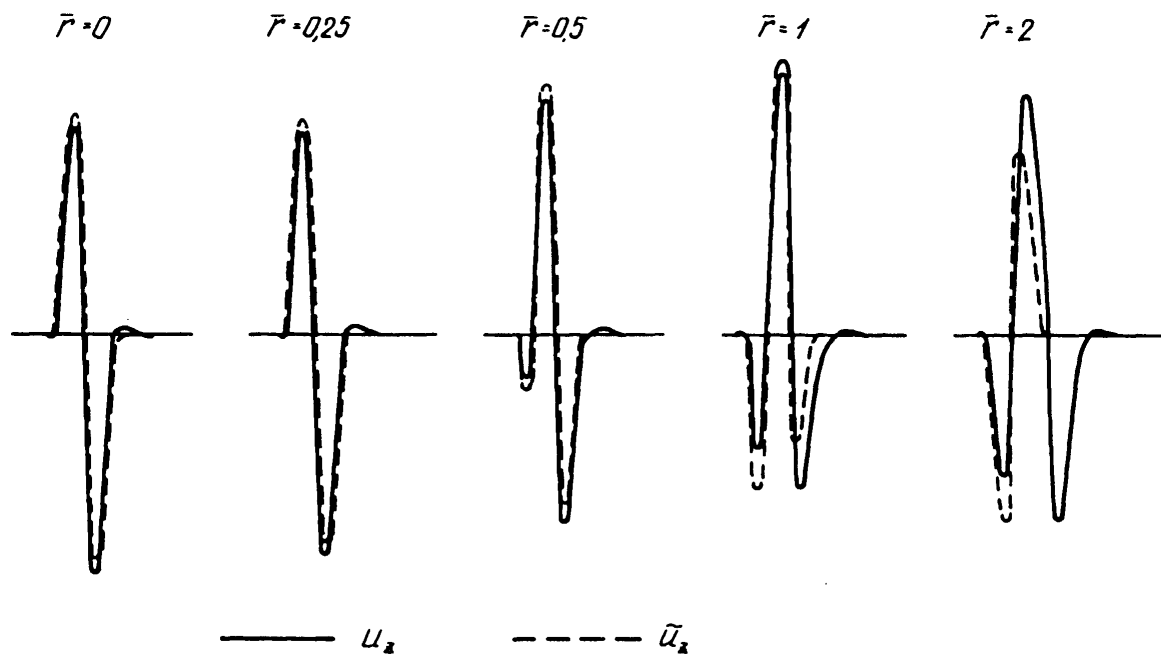


Figure 4.9: Comparison between the exact PS-waveform (solid line) and the first two terms of the ray series (dashed line). The traces represent the vertical component of the transmitted PS-wave for  $\bar{h}=0.25$ ,  $\bar{d}=0.25$ . Elastic parameters are the same as in the previous plots.

flexibility in decomposing the wavefield and selecting only the components of interest in any particular problem.

To generate synthetic seismograms, integral (4.5.1) is evaluated numerically for a set of frequencies with the subsequent application of the inverse Fourier Transform (Fuchs and Mueller, 1971). Since for realistic multilayered models the method is time-consuming, the practical implementation of the reflectivity modeling usually involves several simplifications. The full matrix propagator for an elementary plane wave is often calculated only in the lower part of the section, called the “reflection zone,” while the wave propagation in the overburden is described using the “generalized” ray method. Here by generalized ray method we mean a simplified version of the reflectivity integral in which  $V_{pp}$  for the overburden contains the expression for the plane P-wave propagating down to the reflection zone and then back up to the surface, with no allowance for multiples or PS conversions.

Another common simplification is to restrict the integration in formula (4.5.1) to real incidence angles which correspond to homogeneous incident waves ( $0 < \theta < \pi/2$ ) and, in some cases, integrate over an even more narrow range of angles that corresponds to the range of horizontal slownesses believed to be of interest in the problem at hand. A combination of the generalized ray theory for the overburden with the slowness windowing makes it possible to consider different structures of the overburden beneath the source and receiver (Kennett, 1983). This trick makes the upper part of the model “quasi-two-dimensional” although, clearly, there should be no lateral changes in the reflectivity zone where the full matrix propagator is computed.

While the reflectivity method can generate the complete wavefield in 1-D media and provide enough flexibility in choosing particular wave types, it experiences difficulties in treating vertical velocity gradients. In reflectivity modeling gradient zones are usually approximated by step-wise velocity functions containing many thin layers. If the gradient is pronounced, the number of layers becomes very large, making the calculation of the matrix propagator extremely time-consuming. One of the ways to get around this problem is to replace the standard reflectivity technique in the gradient zones by the WKBJ approximation (Mallick and Frazer, 1987).

The computational speed of the reflectivity modeling is mostly determined by the number of layers, the frequency band and the range of offsets. For complicated models that contain dozens of layers it is often more economical to use finite-difference or finite-element methods. One especially efficient modeling technique based on a combination of partial separation of variables and finite-difference methods was developed by Alekseev and Mikhailenko (1980). The main disadvantages of finite-difference methods are the high computational cost and the inability to decompose the wavefield into the individual wave components.

Another modeling approach that has certain advantages for simple models is the Cagniard-de-Hoop method. Unlike the reflectivity method that uses the Fourier transform over time and Fourier-Bessel integrals in the frequency domain, the approach developed by Cagniard and de-Hoop is based on a Laplace transform. In the Cagniard-de-Hoop method, the possibility to get a relatively simple solution in the time domain is ensured

by a particular choice of the integration path in the complex ray-parameter plane (the so-called *Cagniard* path). While providing concise time-domain solutions for line sources and simple, one- or two-layer models, the Cagniard-de-Hoop method is much less efficient for realistic multilayered media. First of all, the Cagniard path has to be found for each generalized ray separately which is not practical when it is necessary to sum up a large number of different waves. Second, the analytic advantages of the Cagniard-de-Hoop method cannot be exploited in attenuative media and in models with a combination of velocity gradients and discontinuities.

A computationally cheap alternative to the methods discussed above is ray tracing. Most ray-theory modeling algorithms use the geometrical-seismics approximation i.e., the leading term of the ray series expansion. Therefore, ray tracing becomes inaccurate in the areas where additional terms of the ray series cannot be ignored. An improvement over the conventional ray tracing in these areas can be achieved by applying more accurate high-frequency approximations, such as Gaussian beam modeling or Maslov asymptotic theory. Still, all versions of ray theory do not produce reliable amplitudes if deviations from geometrical seismics are pronounced. Another principal problem in the application of ray-theory algorithms is the difficulty in accounting for all individual waves in complicated layered models.

## 4.6 Acknowledgments

I am grateful to Anatoly Levshin (CU, Boulder) for sharing his insights into wave-propagation problems and to my colleagues at the Colorado School of Mines (Norm Bleistein, Jack Cohen, Alex Kaufman, Ken Lerner, John Scales, John Stockwell) for their support and helpful discussions. Some of the results in this book were obtained with support of the Army Research Office, grant number DAAH04-95-1-0173. The suggestion by John Scales to submit this manuscript to Samizdat Press is greatly appreciated. Many complicated plots in this book have been drawn by Barbara McLenon of the Center for Wave Phenomena.



# Bibliography

- [1] Aki, K., and Richards, P.G., 1980, Quantitative seismology: theory and methods: W.N. Freeman & Co., San Francisco.
- [2] Alekseev, A.S., and Mikhailenko, B.G., 1980, The solution of dynamic problems of elastic wave propagation in inhomogeneous media by a combination of partial separation of variables and finite-difference methods: *J. of Geophysics*, **48**, 161-172.
- [3] Bleistein, N., 1984, *Mathematical methods for wave phenomena*: Academic Press.
- [4] Brekhovskikh, L.M., 1980, *Waves in layered media*: Academic Press, New York.
- [5] Fuchs, K., 1971, The method of stationary phase applied to the reflection of spherical waves from the transition zones with arbitrary depth-dependent elastic moduli and density: *J. Geophys.*, **37**, 89-117.
- [6] Fuchs, K., and Mueller, G., 1971, Computation of synthetic seismograms with the reflectivity method and comparison with observations: *Geophys. J. R. astr. Soc.*, **23**, 417-433.
- [7] Ginzburg, A.S., and Strick, E., 1958, Stoneley wave velocities for a solid/solid interface: *Bull Seismol. Soc. Am.*, **48**, 51.
- [8] Guha, S., 1965, Model seismic investigation of refracted waves: *Geophys. Prosp*, **13**, 659-664.
- [9] Gutowski, P.R., Hron, F., Wagner, D.E., and Treitel, S., 1984, S\*: *Bull. Seism. Soc. Am.*, **74**, 61-78.
- [10] Hron, F., and Mikhailenko, B.G., 1981, Numerical modeling of nongeometrical effects by the Alekseev-Mikhailenko method: *Bull. Seismol. Soc. Am.*, **71**, 1011-1029.
- [11] Kennett, B.L.N., 1983, *Seismic wave propagation in stratified media*: Cambridge Univ. Press.
- [12] Kind, R., 1976, Computation of reflection coefficients for layered media: *Journal of Geophys.*, **42**, 191-200.
- [13] Kiselev, A.P., and Tsvankin, I.D., 1989, A method of comparison of exact and asymptotic wave field computations: *Geophys. J. International*, **96**, 253-258.

- [14] Lash, C.C., 1985, Shear waves produced by explosive sources: *Geophysics*, **50**, 1399-1409.
- [15] Mallick, S., and Frazer, L.N., 1987, Practical aspects of reflectivity modeling: *Geophysics*, **52**, 1355-1364.
- [16] Sezawa, K., and Kanai, K., 1939, The range of possible existence of Stoneley wave and some related problems: *Bull. Earthquake Res. Inst. (Tokyo)* 17, 1.
- [17] Thomson, W.T., 1950, Transmission of elastic waves through a stratified solid material: *J. Appl. Phys.*, **21**, 1215.
- [18] Tsvankin, I.D., Kalinin, A.V., Pivovarov, B.L., and Litvin, A.L., 1981, Reflection of an acoustic spherical wave from a low-velocity layer: *Herald of Moscow University, Geology*, **5**, 85-91 (in Russian).
- [19] Tsvankin, I.D., and Chesnokov, E.M., 1990, Synthesis of body-wave seismograms from point sources in anisotropic media: *J. Geophys. Res.*, **95**(B7), 11317-11331.
- [20] Tsvankin, I.D., 1991, Determination of shear-wave velocities using nongeometrical waves: 61 SEG Annual Meeting, Expanded Abstracts, 1587-1590.



# Acknowledgments

Samizdat Press gratefully acknowledges the generous support of the Institute for Resource and Environmental Geosciences at the Colorado School of Mines, Unocal, and the Society of Exploration Geophysicists (SEG).

